2011

Algebraic Aspects of (Bio) Nano-chemical Reaction Networks and Bifurcations in Various Dynamical Systems

Teng Chen
University of Central Florida

ALGEBRAIC ASPECTS OF (BIO) NANO-CHEMICAL REACTION NETWORKS AND BIFURCATIONS IN VARIOUS DYNAMICAL SYSTEMS

by

Teng Chen
B.S. University of Science and Technology of China, 2006
M.S. University of Central Florida, 2008

A dissertation submitted in partial fulfillment of the requirements
for the degree of Doctor of Philosophy
in the Department of Mathematics
in the College of Sciences
at the University of Central Florida
Orlando, Florida

Summer Term
2011

Major Professor:
Joseph P. Brennan

Abstract

The dynamics of (bio) chemical reaction networks have been studied by different methods. Among these methods, the chemical reaction network theory has been proven to successfully predicate important qualitative properties, such as the existence of the steady state and the asymptotic behavior of the steady state. However, a constructive approach to the steady state locus has not been presented. In this thesis, with the help of toric geometry, we propose a generic strategy towards this question. This theory is applied to (bio)nano particle configurations. We also investigate Hopf bifurcation surfaces of various dynamical systems.

To my wife Lei

Acknowledgments

I would like to thank my advisor, Joseph Brennan, for his support and patience. I would like to thank Roy Choudhury for permission to include co-authored material: Chapter 6. I would also like to thank Qun Huo, for her data support and help on my thesis. The theoretical results of Chapter 5 are based on the experimental results provided by Qun's Lab. I also want to thank Jiongmin Yong for his advice on my graduate study. I learned convex polytopes and optimization from his class, which is employed in Chapter 3. The author wishes in addition to thank Grady Webb-Wood and Haimei Shao for their support with my writing.

TABLE OF CONTENTS

LIST OF FIGURES

LIST OF TABLES

CHAPTER 1
INTRODUCTION

There have been increasingly demands for chemists and biologists to understand the underlying mechanism of complex (bio) chemical reactions. By breaking down the reaction into a set of elementary reactions, most particularly unimolecular and bimolecular elementary reactions, the study the resulting (bio) chemical reaction networks leads to an understanding of the system properties.

The pioneer study on the chemical reaction network was first conducted by Horn and Jackson in the 1970s. Between 1970 and late 1980s, a lot of interesting results were developed. Among these results (The Chemical Reaction Network Theory (CRNT)), the *deficiency zero theorem* and the *deficiency one theorem* are the biggest results. These are concerned with the dynamics of a large class of chemical reaction networks. During 1990s, Feinberg and Ellison also suggested algorithmic results on the CRNT. The *deficiency one algorithm* and *advanced deficiency algorithm* concerning the qualitative properties of the dynamics of a reaction network [31,40]. Craciun developed a different approach to study the multistationarity [4,28], which is different from the *deficiency algorithm*. The connection between the CRNT and the algebraic study of the sparse polynomial systems was first developed by Gatermann [47–50]. This bridge also inspired Craciun et al. to use the saturation ideal to build toric dynamic systems [27]. Another research direction (the Stoichiometric Network Analysis (SNA)) has been also developed by Clarke et al. which is driven by the particular needs to calculate the bifurcation set for steady states of an unstable chemical reaction networks [16, 82, 85, 86].

The framework of CRNT has been proved successful to determine the dynamical behaviors like monostationarity, multistationarity and oscillations for a family of reaction networks [21, 32, 34, 36, 39, 42, 42, 91].

Theoretical results arising in the study the CRNT using toric geometry are made in this thesis, while the first application of the CRNT to a nanoparticle reaction is also discussed. Other algebraic tools are also employed to discover the bifurcations behavior of dynamical system arising from chemical reaction networks.

Now we give the outline of this thesis. Chapter 2 is concerned with the fundamentals of the CRNT. We review the basic setting of the CRNT using the rigorous language of graphs and matrix algebra. The decoupling of the dynamical systems is performed by the decomposition of the linear transformation. Some results of the CRNT are proved in this setting. Several convex cones are introduced for the study in the next chapter. Their relations are also discussed. In section 2.3, the fundamental theorems (*deficiency one theorem* and *deficiency zero theorem*) are formulated using the rank conditions.

Chapter 3 is devoted to develop a straightforward method to calculate the equilibrium of a chemical reaction network. In section 3.1, some algebraic basics are covered so as to make the chapter to be self-contained. A general computation strategy is proposed and two toric varieties are introduced in section 3.2. In section 3.3, theoretical results concerned with the intersections of the toric varieties introduced in section 3.2 and convex polytopes introduced in the previous chapter are formulated. In section 3.4, the application of the theoretical re-

sults to deficiency zero theorems is discussed. Algorithmic results and computation examples are included in section 3.5.

Chapter 4 is concerned with the Belousov-Zhabotinsky (BZ) reaction, which is a special family of chemical reactions that has the capacity to exhibit complex dynamical behaviors. The applicability of the CRNT to the BZ reaction is discussed in section 4.1. In the rest of the chapter, several algebraic tools are utilized to investigate the bifurcations of the BZ reaction. On the other hand, the norm form of the BZ reaction is calculated to determine the singularity classification of the BZ reaction.

Chapter 5 is devoted to study (bio)nano particle configurations. A deterministic model is proposed to study the process of nanoparticle clusters using the tools of *mass action kinetics*. The assumptions of the model are explained while the existence and uniqueness of the steady state are confirmed. The application of the CRNT to this particular model is examined.

Chapter 6 is concerned with the Hopf and double Hopf bifurcation of a modified Chens system. Analytical expressions for the periodic orbits resulting from the Hopf bifurcation are derived in section 6.4. In section 6.5, normal form is verified by the numerical simulations and the various types of post-bifurcation dynamics are investigated.

CHAPTER 2
THE MATHEMATICAL MODEL OF (BIO)CHEMICAL REACTION NETWORKS

During the early 1970s, the chemical reaction network theory (CRNT) was first developed by Horn and Jackson in a series of papers [41, 42, 63–66] using a set of assumptions that they called the "Quasi-Thermodynamic" hypothesis. Feinberg and others have continued to develop the CRNT model, establishing a systematic framework to extend the application of the theory to a more generalized set of reaction networks. [34–41].

There has been a strong motivation to study the CRNT: instead of solving each different chemical reaction network individually, it is possible to make inference of the dynamics for some classes of reaction networks, solely based on the topological structure of the model. Mathematically, the reaction networks can be described as a system of ordinary differential equations (ODEs) and partial different equations (PDEs). To study the dynamics of these networks, these equations need to be understood first. However, it is a significant challenge to find the equilibrium (the zero of the equations) due to the nonlinearity of the equations. Horn and others realized that the system of rate equations governing the reaction kinetics can be simplified and linearized by assuming that *mass action kinetics* are as reasonable approximations to the true rate equations.

The study of CRNT has been particularly driven by the challenges of systems biology recently (for example, see [2,5,30,95]). The fact that the conclusion of CRNT does not depend on the kinetic constants input is the key feature which can be utilized in these biological

models, for example, modeling selection [20]. The deficiency one theorem is particularly concerned with the multistationarity in a large class of networks, the deficiency one algorithm and the advanced deficiency one algorithm are concerned with the study of multistationarity within a class of so-called "regular" reaction networks. The solvability of a system of inequalities is used to determine the possibility of multistationarity of the reaction network. With the increasing size of the network, the inequality system becomes more complex and its solvability becomes more and more difficulty to determine. Conradi [19, 21] argues that it is possible to study the multistationarity of the parent network by examining some special subnetwork of the system. This work can be traced back to the *stoichiometric network analysis* (SNA) by Clarke [16]. The SNA is also an important approach to investigate the complex reaction network, especially in the study of the instability behavior of the networks via numerical study, for example, see [13,14,84–86]. The SNA will not be discussed in detail; however, a comparison between the SNA and the CRNT is made in the next chapter with the help of algebraic geometry.

In this chapter, the basic framework of CRNT is reviewed. Since the goal of this chapter is to provide self-contained introduction of CRNT to a more general audience, including mathematicians, chemists and biologists, the fundamentals of the CRNT are reviewed in the language of matrix and combinatorics. To be rigorous and consistence, some concepts in the CRNT has been rephrased, while new proofs are also given to some results in the CRNT.

2.1 Chemical Reaction Networks and Mass Action Kinetics

2.1.1 The Fundamental Graphs and Matrices of Chemical Reaction Network

The goal of this section is to introduce some basics of CRNT and the assumption underlying it, the hypothesis of *mass action kinetics*. First, we will make some simplifying assumptions about the environment where a reaction takes place. For a reaction taking place in solution, assuming:

1. Perfect mixing: the reaction vessel is constantly stirred such that the contents of the vessel is spatially *homogeneous*;
2. Isothermal: the temperature is fixed;
3. The volume of the vessel is also fixed;
4. The system can be either closed or open, referred as *constant stirred tank reactor (CSTR)*. Figures 2.1 illustrate the closed and open chemical model respectively.

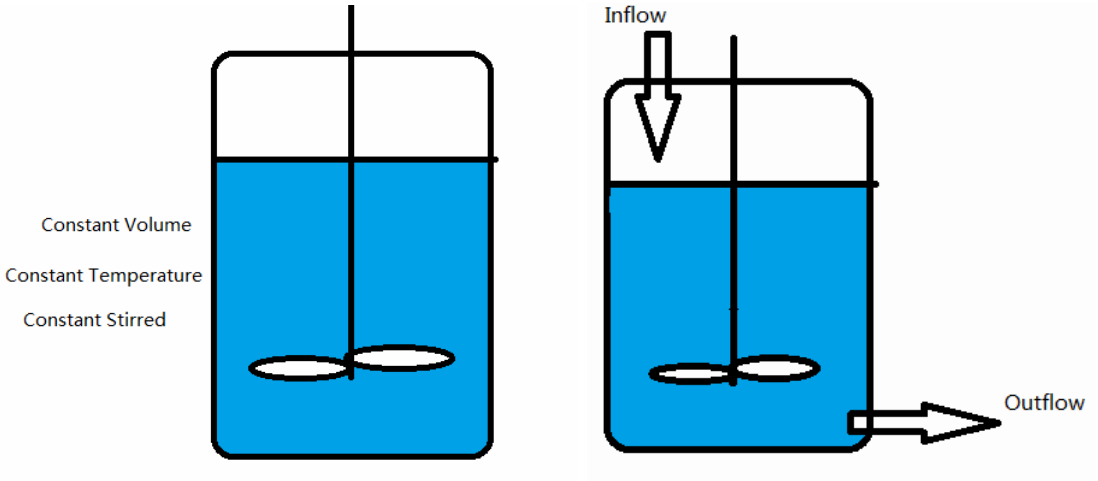

(a) Closed system (b) Open system

Figure 2.1: The reactors

These assumptions simplify our mathematical model of a chemical reaction network. In order to see how a dynamical system could arise from such a chemical reaction network, it is helpful to consider the following reaction system:

Example 2.1.1.

$$2A \underset{k_{B\to 2A}}{\overset{k_{2A\to B}}{\rightleftharpoons}} B \tag{2.1.1.1}$$

Notice that this is a *reversible* reaction, where molecule A represents the reactants, and molecule B is the product in the forward reaction $2A \xrightarrow{k_{2A\to B}} B$. In the backward reaction $B \xrightarrow{k_{B\to 2A}} 2A$, A becomes the product and B is the reactant. Chemically, in the forward reaction, the arrow indicates that two units of chemical species A can react together to form one units of chemical species B. Suppose that the concentration of the species A and B are c_A and c_B, respectively. The concentration vector is denoted by $\mathbf{c} = (c_A, c_B)$. In the

chemical literature, $2A$ and B are also known as complexes. $k_{B\to 2A}, k_{2A\to B}$ are the rate constants which describe the thermodynamics of the reaction.

We will explore the dynamics of this reaction network. Assume that the forward reaction rate is $r_{2A\to B}(\mathbf{c})$, and the backward reaction rate is $r_{B\to 2A}(\mathbf{c})$. The reaction rates are functions of the concentrations of different species and other thermodynamic factors, such as temperature, pressure, etc. In this chemical reaction network, the rate of producing the species A is $2r_{B\to 2A}$, while the rate of annihilating the species A is $2r_{2A\to B}(\mathbf{c})$, and the net production rate of species A is $-2r_{2A\to B}(\mathbf{c}) + 2r_{B\to 2A}(\mathbf{c})$. The production rate of species B can be obtained similarly, $r_{2A\to B}(\mathbf{c}) - r_{B\to 2A}(\mathbf{c})$; thus, the reaction network gives rise to the following dynamic systems.

$$\begin{aligned} \frac{dc_A}{dt} &= -2r_{2A\to B}(\mathbf{c}) + 2r_{B\to 2A}(\mathbf{c}) \\ \frac{dc_B}{dt} &= r_{2A\to B}(\mathbf{c}) - r_{B\to 2A}(\mathbf{c}) \end{aligned} \tag{2.1.1.2}$$

A natural question to ask regarding this dynamical system is whether the system has the capacity to admit a positive equilibrium; and if it does, whether the equilibrium is unique or it could admit multiple steady states. Furthermore, it would be interesting to know if any asymptotic behavior will arise from the system, and if the system could admit chaotic behavior.

These questions have be answered for a particular network, the *deficiency zero* chemical reaction network. The deficiency zero theorem [36] concludes the monostationarity of such network. However, for more general chemical reaction systems, these questions have not been fully addressed.

We now can establish the mathematical framework of our theory by generalizing the approach in this simple example. Following the notation of [36], a chemical reaction network can be understood as a triple $(\mathcal{S}, \mathcal{R}, \mathcal{C})$, where $\mathcal{S}$ represents the set of species, $\mathcal{C}$ is the set of the complexes, and $\mathcal{R} \subset \mathcal{C} \times \mathcal{C}$ is a relation. Hence, in our example (2.1.1)

$$\mathcal{S} = \{A, B\}, \mathcal{C} = \{2A, B\}, \mathcal{R} = \{2A \to B, B \to 2A\} \tag{2.1.1.3}$$

As the dynamics of the systems are of interest, it is useful to extend the definition of a chemical reaction system to a quadruple $(\mathcal{S}, \mathcal{R}, \mathcal{C}, \mathcal{K})$, in the above example (2.1.1), $\mathcal{K} = \{k_{B\to 2A}, k_{2A\to B}\}$. Previous works [49] suggested that the chemical reaction systems can be also interpreted as two graphs: a weighted directed graph and a weight directed bipartite graph. The advantage of this interpretation is that it connects graph theory and the chemical reaction network theory. It will be clear in the following that the better understanding of the graphs of a reaction network, especially the weight directed graph of the system, could help one to understand the dynamics of the reactions.

To better illustrate the graphical structure, consider another example

Example 2.1.2. Consider the following chemical reaction network

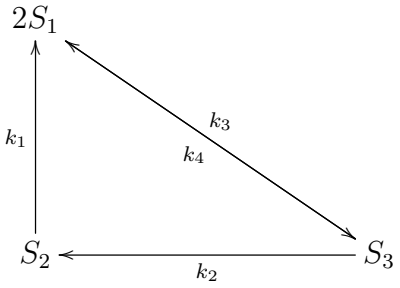

Figure 2.2: A simple chemical reaction network

This chemical reaction contains three complexes $\mathcal{C} = \{2S_1, S_2, S_3\}$ and three species $\mathcal{S} = \{S_1, S_2, S_3\}$, and $\mathcal{R} = \{2S_1 \to S_3, S_3 \to 2S_1, S_2 \to 2S_1, S_3 \to S_2\}$.

As we mentioned earlier, previous work [47] suggests studying the chemical reaction network by exploring two weighted graphs. The basic idea is that the all of the possible reaction states of the chemical reaction network will be encoded into these two graphs. The rigorous definition is given below.

Definition 2.1.3 (Complex Graph)**.** The *complex graph* is a weighted directed graph G. The vertex set $V(G)$ is composed of the complexes $\{C_i\}_{i=1}^n$ of the chemical reaction network; the edge set $E(G)$ is composed by the reaction $\{C_i \to C_j|$ where $C_i \to C_j \in \mathcal{R}\}$; the weight of the corresponding edge is represented by the rate constant of the reaction $k_{ij} = k_{C_j \to C_i}$

Definition 2.1.4 (Complex-Species Graph)**.** The *complex-species graph* is a weighted bipartite graph G. The vertex set $V(G)$ consists of the chemical species $\{S_i\}_{i=1}^m$ and the complexes $\{C_i\}_{i=1}^n$[1]; the edge set $E(G)$ is presented by $\{C_iS_j|\forall i = 1, ..., n$ and $j = 1, ..., m\}$; each edge C_jS_i has a weight y_{ij}, which is the stoichiometric coefficient of S_j in the complex C_i.

[1]Symbols m and n will continue to serve as the total numbers of the species and the complexes through this work.

Remark 2.1.5. $\{y_{ij}\}_{i=1,j=1}^{n,m}$ are known to chemists and kineticists as the stoichiometric coefficients, which are the relative numbers of the molecules participating in the complexes. To make it more clear, consider the complex $C_1 = S_1 + 3S_2$ in a pseudo reaction network, $y_{11} = 1, \quad y_{21} = 2.$

Example 2.1.2 (continued)

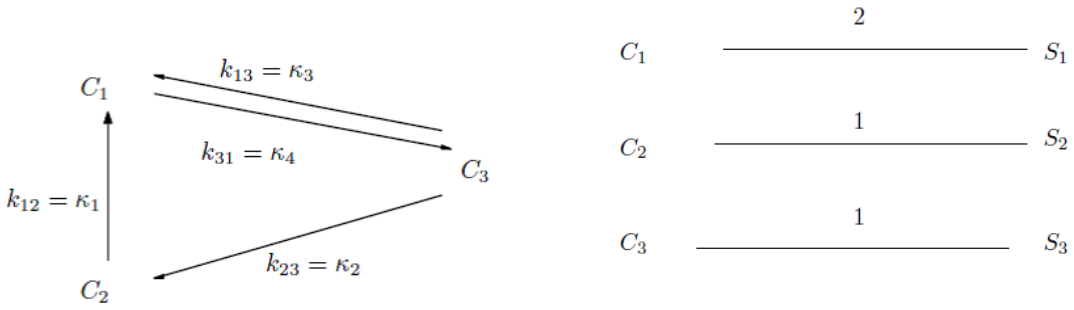

(a) Complexes Graph (b) Complex-Species Graph

Figure 2.3: Complexes Graph and Complex-Species Graph

Definition 2.1.6 (Adjacency Matrix K)**.** The weighted adjacency matrix of the weighted directed graph is an $n \times n$ matrix, where n is the number of complexes in the chemical reaction. To be more precise, the entries of the matrix are defined as follows:

$$K(i,j) = \begin{cases} k_{ij}, & \text{if } C_j \xrightarrow{k_{ij}} C_i \\ 0, & \text{otherwise} \end{cases} \tag{2.1.1.4}$$

Similar to the definition of the degree of the vertex in graph theory, it would be convenient to define the degrees of the complexes in the reaction network.

Definition 2.1.7 (Indegree and Outdegree of a complex)**.**

$$\text{outdegree } \deg^+ C_i = |\{C_j \in \mathcal{C} | C_i \to C_j \in \mathcal{R}\}| \tag{2.1.1.5}$$

$$\text{indegree } \deg^- C_i = |\{C_j \in \mathcal{C} | C_j \to C_i \in \mathcal{R}\}| \tag{2.1.1.6}$$

Definition 2.1.8 (Degree Matrix D)**.** The degree matrix of the weighted directed graph is an $n \times n$ matrix, where n is the number of complexes. The entries of the matrix are defined as follows.

$$D(i,j) = \begin{cases} \sum_{l=1}^{n} k_{il}, & \text{if } i = j, \\ 0, & \text{otherwise.} \end{cases} \tag{2.1.1.7}$$

Definition 2.1.9 (Laplacian Matrix L)**.** [9] The definition is essentially the negative of the classical definition of the laplacian matrix. It is an $n \times n$ matrix,

$$L(i,j) = \begin{cases} d_{ij} - k_{ij}, & i = j, \\ -k_{ij}, & i \neq j, \\ 0, & \text{otherwise.} \end{cases} \tag{2.1.1.8}$$

Clearly, $L = D - K$.

Example 2.1.2 (continued)

$$K = \begin{pmatrix} 0 & k_{12} & k_{13} \\ 0 & 0 & k_{23} \\ k_{31} & 0 & 0 \end{pmatrix} \qquad D = \begin{pmatrix} k_{12}+k_{13} & 0 & 0 \\ 0 & k_{23} & 0 \\ 0 & 0 & k_{31} \end{pmatrix}$$

$$L = D - K = \begin{pmatrix} k_{12}+k_{13} & -k_{12} & -k_{13} \\ 0 & k_{23} & -k23 \\ -k31 & 0 & k_{31} \end{pmatrix} \tag{2.1.1.9}$$

Definition 2.1.10 (Stoichiometric Matrix $\mathcal{Y}$)**.** The weighted adjacency matrix of the complex-species graph is an $n \times m$ matrix, where n is the number of complexes and m is the number of the species. The entries of the stoichiometric matrix $\mathcal{Y}(i,j)$ are y_{ij}

If all the edges (reactions) in the complex graph are relabeled from α_1 to α_r, where r is the number of arrows (reactions) in the reaction network, then we may define the following oriented incidence matrix.

Definition 2.1.11 (Oriented Incidence Matrix I_r)**.** The oriented incidence matrix of the complex graph is an $n \times r$ matrix. The entries of the matrix I_r are defined as follows:

$$I_r(i,j) = \begin{cases} -1, & \text{if } C_i \text{ is the reactant complex in } \alpha_j, \\ 1, & \text{if } C_i \text{ is the product complex in } \alpha_j, \\ 0, & \text{if } C_i \text{ otherwise.} \end{cases} \tag{2.1.1.10}$$

Remark 2.1.12. The number of columns of I_r is the number of the arrows, in another words, the number of the reactions in the reaction network. Clearly, this number should always be bounded above by the number of the complexes. The two numbers are equal when the reaction network is strongly connected, or strongly linked.

Remark 2.1.13. For each edge (reaction) $\alpha_p, p = 1, ..., r$ in the complex graph[1], there are only two corresponding complexes, say C_i and C_j, acting as reactant and product complexes, separately. Thus there are only two non-zero entries corresponding to each column of the *oriented incidence matrix* I_r, one is 1, the other one is -1. In particular, the row sum of I_r is zero.

Note the *adjacency matrix* K and the *oriented incidence matrix* $I_{\boldsymbol{\kappa}}$ both are matrices with rate constants as their entries. However, their size and structure are different.

On the other hand, there is exactly one rate constant $k_{i(p),j(p)}$ which corresponds to each reaction $\alpha_p, p = 1, ..., r$. Then the corresponding rate constant $k_{i(p),j(p)}$ can be denoted as κ_p. Therefore we have another matrix defined as follows:

Definition 2.1.14 (Rate Incidence Matrix $I_{\boldsymbol{\kappa}}$)**.** The rate incidence matrix of the complex graph is an $r \times n$. The entries of the matrix $I_{\boldsymbol{\kappa}}$ is defined as follows.

$$I_{\boldsymbol{\kappa}}(i,j) = \begin{cases} \kappa_i, & \text{if } C_j \text{ is the reactant complex in } \alpha_i, \\ 0, & \text{otherwise.} \end{cases} \tag{2.1.1.11}$$

[1]The symbol r will continue to serve as the total number of reactions in a reaction network through this work.

There exists only one reactant complex for each reaction α_p, hence there is only one non-zero entry for each row in $I_{\boldsymbol{\kappa}}$. Moreover, a complex is not necessarily a reactant complex, hence some columns of $I_{\boldsymbol{\kappa}}$ might be zero columns. One complex could serve as reactant complexes for several reactions, so for each column, it could have multiple non-zero entries. Based on these simple observations, we have a lemma concerning the relation between the structure of the network and the rank of the rate incidence matrix $I_{\boldsymbol{\kappa}}$.

Lemma 2.1.15. *The rate incidence matrix $I_{\boldsymbol{\kappa}}$ is of full (row) rank r if and only if in the reaction network, $\forall i$, $\deg^+ C_i \leq 1$, i.e. each complex serves as a reactant complex at most once.*

Proof. First, if for each complex, $\deg^+ C_i \leq 1$, then, for each non-zero column of $I_{\boldsymbol{\kappa}}$, there exists exactly one non-zero entry. Moreover, since each reaction only has one reactant complex, there exists exactly one non-zero element for each row. Therefore, $\mathbf{rank}\, I_{\boldsymbol{\kappa}} = r$. On the other hand, by contradiction, assuming $C_i \xrightarrow{k_a} C_j$ and $C_i \xrightarrow{k_b} C_p$ are both in the network, then $k_a\mathbf{e}_i$ and $k_b\mathbf{e}_i$ are the $a-$the row and $b-$th row in the rate incidence matrix $I_{\boldsymbol{\kappa}}$, where $\mathbf{e}_i$ is the unit vector in which i-th component equals one. Therefore, $\mathbf{rank}\, I_{\boldsymbol{\kappa}} < r$. Contradiction. □

The *stoichiometric matrix*, the *rate incidence matrix*, and the *oriented incidence matrix* of example 2.1.2 are computed as follows:

Example 2.1.2 (continued)

$$\mathcal{Y} = \begin{pmatrix} 2 & 0 & 0 \\ 0 & 1 & 0 \\ 0 & 0 & 1 \end{pmatrix}, \quad I_r = \begin{pmatrix} 1 & 0 & 1 & -1 \\ -1 & 1 & 0 & 0 \\ 0 & -1 & -1 & 1 \end{pmatrix}, \quad I_{\boldsymbol{\kappa}} = \begin{pmatrix} 0 & \kappa_1 & 0 \\ 0 & 0 & \kappa_2 \\ 0 & 0 & \kappa_3 \\ \kappa_4 & 0 & 0 \end{pmatrix} \tag{2.1.1.12}$$

2.1.2 Rate Function and Mass Action Kinetics

We have already introduced some mathematical preliminaries concerning the structure of reaction networks. Another important aspect of the reaction mechanism is the rate function of the elementary reactions. A complex chemical reaction can be decoupled by the linear part of the reaction, which represents the structure of the reaction networks, and the non-linear part (rate functions). This basic idea is extensively explained in section 2.1.3. The fundamental assumption on the rate function throughout this work is the the *law of mass action*. Before the introduction of the *law of mass action*, we should mention that in order to apply CRNT, the assumption of rate function can actually be generalized. Sontag [91] generalized the mass action condition to a local Lipchitz function with the property mimicking the mass action form and Chaves [10] studied the control application of this idea. However, for our purpose, we will focus on *mass action kinetics*.

The *law of mass action* was proposed by Guldberg and Waage [97] in 1864. There are two aspects of this law, namely the equilibrium aspect and the kinetic aspect. The kinetic aspect of the the *law of mass action* states that the rate of the elementary reaction is proportional to the product of the concentrations of the reactants. Statistical mechanics provides a physical interpretation of the law of mass action, realizing ideal reaction systems as ones of statistically independent molecules. In particular, the reaction rate is the product of the rate of collision among reactants and the probability of the collision. The law of mass action is not the only way to realize the reaction rate; however, it is widely accepted [32] as long as the detailed elementary steps forming the overall reaction can be found.

Definition 2.1.16 (Mass Action Law)**.** The rate function R_{ij} corresponding to reaction $C_j \overset{k_{ij}}{\to} C_i$, is equal to

$$R_{ij}(\mathbf{c}) = k_{ij}\mathbf{c}^{\mathbf{y_j}} = k_{ij}c_1^{y_{1j}}c_2^{y_{2j}}\cdots c_n^{y_{nj}} \tag{2.1.2.1}$$

If we define a non-linear function

$$\Phi(\mathbf{c}) = \mathbf{c}^{\mathcal{Y}} = (\mathbf{c}^{\mathbf{y_1}}, \mathbf{c}^{\mathbf{y_2}}, ..., \mathbf{c}^{\mathbf{y_n}}), \tag{2.1.2.2}$$

then the mass action law can be rewritten as $R_{ij}(\mathbf{c}) = k_{ij}\Phi_j(\mathbf{c})$. The rate constants k_{ij} have been introduced in the graphical structure of the reaction networks. It is a function of temperature, while independent of the concentration of the reactants. Typically, those constants are determined from the experiments, though in some particular cases, the rate constants might be derived from statistical mechanism. The inverse problem in the chemical reaction

literature concentrates mainly on how to determine these parameters from experiment data, such as from the equilibia concentration of the reactants and the products. Craciun, G and Pantea introduced the idea of the "Identifiability" of a chemical reaction network [29] to investigate which kinds of special structures of the reaction network would allow one to uniquely determine the kinetic constants from the experiment data.

2.1.3 The Decoupling of Chemical Reaction Network Dynamics

Let us formulate the following simple result which connects the system of differential equations and the structure of the graphs.

Lemma 2.1.17. *Let L denote the Laplacian matrix of the complex graph and let K denote the adjacency matrix of the complex graph, and $\mathcal{Y}$ denotes the stoichiometric matrix. Then,*

$$\frac{d\mathbf{c}}{dt} = \mathcal{Y} \cdot (-L) \cdot \Phi(\mathbf{c}) = \mathcal{Y} \cdot (K - D) \cdot \Phi(\mathbf{c}) \tag{2.1.3.1}$$

Proof.

$$\begin{aligned}
\frac{d\mathbf{c}}{dt} &= \sum_{i,j} R_{ij}(\mathbf{c})(\mathbf{y}_j - \mathbf{y}_i) \\
&= \sum_{i,j} k_{ij}\phi_i(\mathbf{c})(\mathbf{y}_j - \mathbf{y}_i) \\
&= \sum_{i,j} k_{ij}\phi_i(\mathbf{c})\mathbf{y}_j - \sum_{i,j} k_{ij}\phi_i(\mathbf{c})\mathbf{y}_i \\
&= \sum_{i} \phi_i(\mathbf{c}) \sum_{j} (k_{ij}\mathbf{y}_j) - \sum_{i} \phi_i(\mathbf{x})(\sum_{j} k_{ij})\mathbf{y}_i \\
&= \mathcal{Y} \cdot K \cdot \Phi(\mathbf{c}) - Y \cdot D \cdot \Phi(\mathbf{c}) \\
&= \mathcal{Y} \cdot (-L) \cdot \Phi(\mathbf{c}) \qquad (2.1.3.2)
\end{aligned}$$

□

This following important decomposition was suggested, but not proven, by Gatermann et al. in [49]. We believe that the following derivation represents the first proof of this result.

Theorem 2.1.18 (Dynamics Decoupling)**.** *[49] For a chemical reaction network, the dynamics of the reaction is determined by the following decomposition*

$$\frac{d\mathbf{c}}{dt} = \mathcal{Y} I_r I_{\boldsymbol{\kappa}} \Phi(\mathbf{c}). \qquad (2.1.3.3)$$

Proof. By the lemma 2.1.17, all we need is to show that $-L = I_r I_{\boldsymbol{\kappa}}$.

$$
\begin{aligned}
I_r I_{\boldsymbol{\kappa}}(i,j) &= \sum_{p=1}^{r} w_{ip}\kappa_{pj} \\
&= \sum_{\{p|w_{ip}=1\}} \kappa_{pj} - \sum_{\{p|w_{ip}=-1\}} \kappa_{pj} \\
&= \sum_{\{p|C_i \text{ is the reactant complex in } \alpha_p\}} 1\kappa_{pj} - \sum_{\{p|C_i \text{ is the product complex in } \alpha_p\}} 1\kappa_{pj} \\
&= \sum_{\{p|_{C_j \text{ is the reactant complex in } \alpha_p}^{C_i \text{ is the reactant complex in } \alpha_p}\}} 1k_p - \sum_{\{p|_{C_j \text{ is the reactant complex in } \alpha_p}^{C_i \text{ is the product complex in } \alpha_p}\}} 1k_p \\
&= \begin{cases} \sum\limits_{p:\ C_i \to C_p \in \mathcal{R}} k_{ip}, & \text{if } i = j \\ -k_{ij}, & \text{if } i \neq j \end{cases} \\
&= -L(i,j) \qquad (2.1.3.4)
\end{aligned}
$$

□

Consider the working example 2.1.2, under the assumption of the *mass action law*. It is easy to derive the ODEs of the system using Theorem 2.1.3.3.

Example 2.1.2 (continued)

$$\frac{d\hat{\mathbf{c}}}{dt} = \mathcal{Y} I_r I_{\boldsymbol{\kappa}} \Phi(\mathbf{c}) = \begin{pmatrix} -2\kappa_4 & 2\kappa_1 & 2\kappa_3 \\ 0 & -\kappa_1 & \kappa_2 \\ \kappa_4 & 0 & -\kappa_2 - \kappa_3 \end{pmatrix} \begin{pmatrix} c_1^2 \\ c_2 \\ c_3 \end{pmatrix}$$

$$= (-2\kappa_1 c_2 + 2\kappa_3 c_3 - 2\kappa_4 c_1^2, -\kappa_1 c_2 + \kappa_2 c_3, \kappa_4 c_1^2 + (-\kappa_2 - \kappa_3) c_3 + \kappa_4 c_1^2)^T \qquad (2.1.3.5)$$

The decomposition of the equation 2.1.3.3 implies the decomposition of the transformation of the mapping $\mathbf{f} : \mathbf{c} \mapsto \dot{\mathbf{c}}$. Consider the following three transformations:

$$\Phi : \mathbb{R}^m_{\geq 0} \longrightarrow \mathbb{R}^n_{\geq 0} : \quad \mathbf{c} \mapsto \Phi(\mathbf{c}) \qquad (2.1.3.6)$$

$$-\mathcal{L} : \mathbb{R}^n_{\geq 0} \longrightarrow \mathbb{R}^n_{\geq 0} : \quad \Phi(\mathbf{c}) \mapsto \mathcal{R}(\mathbf{c}) \qquad (2.1.3.7)$$

$$\mathcal{Y} : \mathbb{R}^m_{\geq 0} \longrightarrow \mathbb{R}^n_{\geq 0} : \quad \mathcal{R}(\mathbf{c}) \mapsto \frac{d\mathbf{c}}{dt} \qquad (2.1.3.8)$$

where, Φ is a non-linear map from the m-dimensional concentration vector space to a n-dimensional complexes space, $-\mathcal{L}$ is a linear transformation from the complexes space to the n-dimensional rate space of the reaction, and $\mathcal{Y}$ represents a linear mapping from the rate space of the reaction to the rate space of the species. The linearity of the mapping Φ and $-\mathcal{L}$ bring useful information which might simplify the dynamic of the chemical reaction

systems. In total, the dynamical system is decomposed into

$$\mathbf{f} = \mathcal{Y} \circ (-\mathcal{L}) \circ \Phi \tag{2.1.3.9}$$

Remark 2.1.19. Because of the *mass action kinetics*, the right hand side of the ODEs $\mathbf{f}(\mathbf{c})$ is polynomial type. In fact, if we also consider the rate constants as unknown, $\mathbf{f}(\mathbf{c})$ exists in the polynomial ring $\mathbb{Q}[\mathbf{c}, \mathbf{k}]$. Moreover, since tri-molecular (three species in a reactant complex) elementary reactions are very rare in reality, the structure of the monomials occurs in the reaction network is often composed of at most two variables (which corresponding to bimolecular reaction).

2.1.4 Practical Considerations with Pseudo-Reactions

As we mentioned earlier, chemical reaction network is just an approximation of the real reaction. The original work of CRNT was based on the closed reaction system. However, Continuous stirred-tank reactor (CSTR) may also modelled with this framework. Under the assumptions of CSTR, there is a continuous supply of fresh substrates (reactants) and continuous outflow of products. To better characterize the CSTR experiments, the species $\square$ was introduced to represent a continuous inflow of a substrate [33]. For example, consider this simple reaction, $B \to A$. If there is a continuous inflow of the species B to maintain the concentration of B, the reaction can be formulated as $\square \to A$. In the experimental

environment, if the concentration of some species is much higher than the others such that we could omit its change over time, we may also represent that species by the symbol $\square$. In fact, a lot of oscillatory reactions can be realized in CSTR environment, hence this special species $\square$ serves as an important tool to model this unstable dynamical behavior.

Another obstacle to overcome when modelling a chemical reaction using CRNT lies in a special family of reactions involving enzymes. Many biological reactions involve enzymes, which seems to be vary hard to describing using mass action kinetics. Indeed, biochemists usually characterize the kinetics of enzyme catalysed reactions by more complex formulas, for example, the following kinetics catalysed by enzyme E [22].

$$A \xrightarrow{E} B \tag{2.1.4.1}$$

$$\frac{dc_B}{dt} = \frac{Vc_A}{K + c_A} \tag{2.1.4.2}$$

which is a rational function of c_A. Michaelis-Menten proposed [77] the following mechanism:

$$A + E \underset{\kappa_1}{\overset{\kappa_2}{\rightleftharpoons}} AE \xrightarrow{\kappa_3} B + E \tag{2.1.4.3}$$

by realizing the chemical mechanics in this way, we may rewite Michaelis-Menten in mass action law fashion. Note the first reversible reactions are assumed to be fast compared to the second one, i.e. $\kappa_1, \kappa_2 >> \kappa_3$. There are also different variants of Michaelis-Menten mechanism, by assuming the different reversibility of the first and second reactions. On the

other hand, some results of CRNT are still valid without assumption of the *mass action kinetics*.

Therefore, by some technical modification of the reaction networks, the CRNT can be applied to a large family of chemical reactions.

Another practical problem of the CRNT is the question of how to derive the rate constants k_{ij}, which is related to the model validation problem. Note that the stoichiometric coefficients can be multiplied by any constant number without changing the real (experimental) reaction rate (because it is still the same reactions). This appears contrary to what the law of mass action implies. However, notice that *kinetic exponent*

$$\kappa_{ji} = \frac{\partial \log r_{ij}}{\partial \log c_i} \tag{2.1.4.4}$$

can be measured empirically. In most cases, the rate constants can be chosen such that they are equal to the *kinetic exponents*. In chemical engineering literature, kinetics exponents are also known as the *effective power function* [17].

2.2 Invariants and Stoichiometric Subspace in Chemical Reaction Networks

A simple question is: given a system of polynomial ODEs, can we construct an/the (if it is unique) underlying chemical reaction network. The answer is no. For example, consider the following Lorenz system:

Example 2.2.1.

$$\begin{aligned}\dot{c}_1 &= \alpha c_1 + \alpha c_2 \\ \dot{c}_2 &= \gamma c_1 - c_2 - c_1 c_3 \\ \dot{c}_3 &= c_1 c_2 - \beta c_3 \end{aligned} \tag{2.2.0.5}$$

Notice that the derivative of c_2 contains the term $-c_1 c_3$. This would mean that the there is a chemical reaction contributing to the decrease of the species S_2 that does not have the species S_2 as a reactant product. This is not compatible with the system being derived from a real chemical reaction system.

Lemma 2.2.2 (Negative Cross-Effects)**.** *Assume* $\mathbf{f} \in \mathbb{R}[\mathbf{c}, \mathbf{k}] = (f_1, f_2, ..., f_m)$*, then it could satisfy the dynamical system* $\frac{d\mathbf{c}}{dt} = \mathbf{f}(\mathbf{c}, \mathbf{k})$ *if and only if every negative monomial in* f_i *contains* c_i *as a factor.*

This fact was mentioned and proved in [32]; as also stated in [89] it is the defining characteristic of chemical network dynamical systems. This fact implies the forward-invariant property of the chemical reaction networks [91]. First, the invariant set is defined as follows. The definition is modified to meet the context of CRNT.

Definition 2.2.3 (Forward Invariant Set)**.** [94] A set $S \in \mathbb{R}^n$ is a invariant set for $\dot{\mathbf{c}} = \mathbf{f}(\mathbf{c})$, if for each $\mathbf{c}_0 \in S$, the solution $\mathbf{c}(t)$ with $\mathbf{c}(0) = \mathbf{c}_0$ lies in the set S for all $t > 0$.

The importance of the forward invariant property may not be obvious at first. For an general ODE system, the solution trajectories may span in the whole of the solution space. To be a compatible model for a chemical reaction system, one requires that the solution trajectories exist inside the non-negative quadrant of the space. The negative cross-effects guarantees this behavior, which is why it is the defining characteristic of our dynamical model.

For the complete proof, see [91]. The sketch of the proof of the following with the same proof idea is given below to see the direct effect of the non-negative effect of the chemical reaction network.

Lemma 2.2.4 (Forward Invariance)**.** *[91] Under the assumption of mass action kinetics,* $\mathbb{R}^m_{\geq}$ *and* $\mathbb{R}^m_{>}$ *are both forward invariant.*

Sketch of Proof: This argument is by contradiction. Suppose that there exists ξ such that $x_i(\xi) < 0$, then, by the continuity of $x_i(t)$, we know that the subset $A = \{0 < t < \xi | x_i(t) = 0\}$ is not an empty set. Therefore, let $\tilde{t} = \max A$ be the maximum number in A. Hence, $x_i(t) < 0$ for all $t > \tilde{t}$. Suppose $\epsilon > 0$, $x_i(\tilde{t}+\epsilon) = x_i(\tilde{t}) + \epsilon x_i'(\tilde{t}) + o(\epsilon^2) = \epsilon x_i'(\tilde{t}) + o(\epsilon^2)$. When ϵ is small enough, the sign of $x_i(\tilde{t}+\epsilon)$ is equal to the sign $x_i'(\tilde{t}) > 0$. Contradiction. ∎

In fact, we may even restrict the region where the trajectories exist further. First, we define the following subspace.

Definition 2.2.5 (Stoichiometric Subspace)**.** The stoichiometric subspace is generated by the difference of the column vectors of the stoichiometric matrix Y

$$\mathfrak{S} := \mathbf{span}\{\mathbf{y}_i - \mathbf{y}_j | k_{ij} > 0\}. \tag{2.2.0.6}$$

Due to the special structure of the oriented incidence matrix I_r, it is easy to see the following fact.

Lemma 2.2.6.

$$\mathfrak{S} = \mathrm{Im}(\mathcal{Y} I_r) \tag{2.2.0.7}$$

The time evolution of a chemical reaction network is given by equation 2.1.3.3. Considering the solution trajectories, we integrate both sides of the equation. The implicit solution form of this dynamic system is obtained as follows:

$$\mathbf{c}(t) = \int_0^t \mathcal{Y} I_r I_{\boldsymbol{\kappa}} \Phi(\mathbf{c}(u)) du = \mathcal{Y} I_r I_{\boldsymbol{\kappa}} \cdot \int_0^t \Phi(\mathbf{c}(u)) du + c_0 \subset \mathfrak{S} \tag{2.2.0.8}$$

Hence the the difference between $\mathbf{c}(t) - \mathbf{c}(0)$ must lie in the *stoichiometric subspace*.

Definition 2.2.7 (Stoichiometric Compatibility Class)**.**

$$\mathfrak{S}_{\mathbf{c}_0} := (\mathfrak{S} + \mathbf{c}_0) \cap \mathbb{R}^m_{\geq 0} \tag{2.2.0.9}$$

Since the difference $\mathbf{c}(t) - \mathbf{c}(0)$ is in the stoichiometric subspace, the solution trajectories $c(t)$ must be restricted in the stoichiometric compatibility class. The searching region of the equilibria of the system is significantly reduced. F. Horn and R. Jackson [42] realized the following fact.

Lemma 2.2.8. *The stoichiometric compatibility class is an invariant covex (unbounded)polytope.*

Proof. By equation 2.2.0.8, $\mathfrak{S} + \mathbf{c}_0$ is a forward invariant set; moreover, since the positive quadrant is also forward-invariant, $\mathfrak{S}_{\mathbf{c}_0}$ as an intersection of two invariant sets is also forward invariant. □

The stoichiometric compatibility classes of example 2.1.1 and example 2.1.2 are described as following:

Example 2.1.1 (continued)

,

$$\mathcal{Y} = \begin{pmatrix} 2 & 0 \\ 0 & 1 \end{pmatrix}, \quad I_r = \begin{pmatrix} 1 & -1 \\ -1 & 1 \end{pmatrix}, \quad \mathcal{Y}I_r = \begin{pmatrix} 2 & -2 \\ -1 & 1 \end{pmatrix} \tag{2.2.0.10}$$

hence $\mathfrak{S} = \mathbf{span}\{(2, -1)\}$

Example 2.1.1 (continued)

Three different stoichiometric compatibility classes are shown as following:

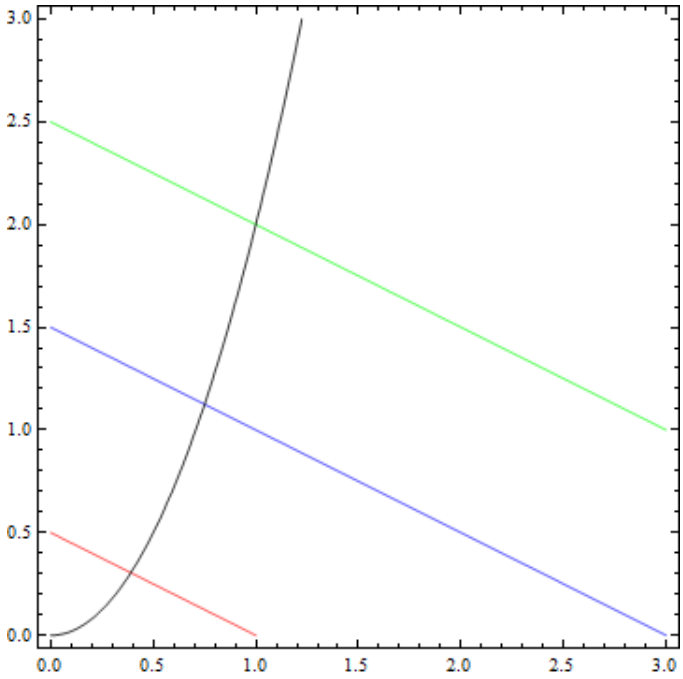

Figure 2.4: The green line represents the stoichiometric compatibility class $\mathfrak{S}+(1,2)$; the blue line represents the stoichiometric compatibility class $\mathfrak{S}+(1,1)$; the red line represents the stoichiometric compatibility class $\mathfrak{S}+(.5,.25)$; the parabola is the equilibria curve $c_1^2-c_2=0$. It is interesting to note that the parabola intersects each stoichiometric class exactly once.

Example 2.1.2 (continued)

$$\mathcal{Y}=\begin{pmatrix}2&0&0\\0&1&0\\0&0&1\end{pmatrix},\quad I_r=\begin{pmatrix}1&0&1&-1\\-1&1&0&0\\0&-1&-1&1\end{pmatrix},\quad \mathcal{Y}I_r=\begin{pmatrix}2&0&2&-2\\-1&1&0&0\\0&-1&-1&1\end{pmatrix}\tag{2.2.0.11}$$

hence $\mathfrak{S}=\mathbf{span}\{(2,-1,0),(0,1,-1)\}$

Example 2.1.2 (continued)

Three different stoichiometric compatibility classes are shown as following:

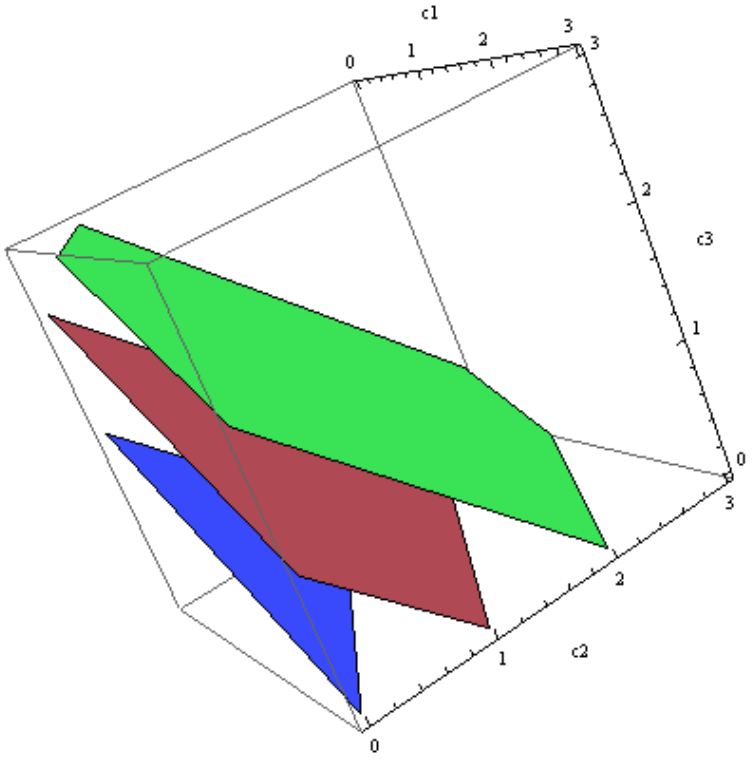

Figure 2.5: The green 2D area represents the stoichiometric compatibility class $\mathfrak{S} + (3, 1, 1)$; the blue 2D area represents the stoichiometric compatibility class $\mathfrak{S} + (1, .5, .5)$; the red 2D area represents the stoichiometric compatibility class $\mathfrak{S} + (1, 1, 1)$.

It is worthwhile to point out the close relation of the Stoichiometric Compatibility Class and the physical conservation law. In fact, we have the following result. We denote[1] $\dim \mathcal{S}$ as s

Lemma 2.2.9. *Assume that* $s < n$, *then* $\mathbf{c}(t) \in \mathfrak{S} + \mathbf{c}_0$ *is equivalent to the following conservation condition:*

H1: There exists independent vectors $\mathbf{v}_i$, *where* $i \in \{1, ..., n-s\}$, *such that* $\mathbf{v}_i \cdot (\mathbf{c} - \mathbf{c}_0) = 0$

[1]The symbol s will continue to serve as the dimension of the stoichiometric subspace through this work.

Proof. Since $\mathbf{c}(t) - \mathbf{c}(0) \in \mathfrak{S}$, for any vector $\mathbf{v} \in \mathfrak{S}^{\perp}$, $\mathbf{v} \cdot \mathbf{c}(t) - \mathbf{c}(0) = 0$, since $\dim \mathfrak{S} < n$, we could always find $n - \dim \mathfrak{S}$ bases $\mathbf{v}_i$, such that $\mathbf{v}_i \cdot (\mathbf{c}(t) - \mathbf{c}(0)) = 0$. On the other hand, if $\mathbf{span}\{\mathbf{v}_i\} \cdot (\mathbf{c}(t) - \mathbf{c}(0)) = 0$, $\mathbf{c}(t) - \mathbf{c}(0) \in \mathbf{span}\{\mathbf{v}_i\}^{\perp}$. □

The union of all of the *stoichiometric compatibility classes* covers $\mathbb{R}^n_{\geq 0}$. In fact, by realizing that any vector $\mathbf{c} \in \mathbb{R}^n_{\geq 0}$ lies naturally in the *stoichiometric compatibility class* $\mathfrak{S}_{\mathbf{c}}$, we have the following fact.

Lemma 2.2.10.

$$\bigcup_{\mathbf{c}_0 \in \mathbb{R}^n_{\geq 0}} \mathfrak{S}_{\mathbf{c}_0} = \mathbb{R}^n_{\geq 0}, \ \textit{and} \quad \mathfrak{S}_{\mathbf{c}_1} \cap \mathfrak{S}_{\mathbf{c}_2} = \emptyset, \ \textit{if } \mathbf{c}_1 - \mathbf{c}_2 \notin \mathcal{S}. \tag{2.2.0.12}$$

2.3 Connectivity, Deficiency, and Defect

Definition 2.3.1. [36] A network is called *reversible* if each reaction is accompanied by its " antireaction", if $C_i \to C_j$ is a reaction in the network, so is $C_j \to C_i$. A network is *weakly reversible* if, whenever there is a directed arrow path leading from complex $C_i \to C_j$,

$$C_i \to C_{i1} \to ... \to C_{is} \to C_j \tag{2.3.0.13}$$

there also exists a directed arrow path leading from $C_j \to C_i$. In this case, C_i is called *directed linked to* C_j.

$$C_j \to C_{j1} \to ... \to C_{jt} \to C_i \tag{2.3.0.14}$$

It is easy to see the fact that a *reversible* chemical reaction network is always a *weakly reversible* reaction network; however, the inverse is not true.

Remark 2.3.2. The definition coincides with the convention of *connected graph* and *strongly connected graph* in graph theory [9] when applied to the *complex graph*. It is also clear that the properties of *reversibility* and *weakly reversibility* are both reflexive, symmetric, and transitive.

Definition 2.3.3 (Linkage Class)**.** C_i is said to be linked to C_j if and only if there exist a chain of reactions such that the *weakly reversibility* defines an equivalent relation for the complexes set $\mathcal{C}$

$$[C_i] = \{C_j |\ \ C_j \textit{ is linked to } C_i\} \tag{2.3.0.15}$$

The weakly reversibility defines the complex set as a partially ordered set, in particularly, the extrema of this poset are called as *terminal strongly linkage classes*

Definition 2.3.4 (Terminal strongly linkage class)**.**

$$\bigcup_{L_i \text{ is weakly reversible}} \quad \bigcup_{L_i \subset L_j} L_i \tag{2.3.0.16}$$

Similarly, we may also define the *strongly linkage class* for the complexes set $\mathcal{C}$. Through this work, following the convention of [33], we will use l to denote the number of the *linkage classes*, and let t denotes the number of the *strongly linkage classes*. Moreover, the *weakly*

reversibility property yields a partition

$$[C_{i1}] \cup [C_{i2}] \cup [C_{i3}] ... \cup [C_{il}] = \mathcal{C}, \tag{2.3.0.17}$$

where $\{C_{ij}\}_{j=1}^{l}$ are not linked to each other.

Definition 2.3.5 (Defect of a reaction network, θ)**.**

$$\theta = \mathbf{rank}(I_r I_{\boldsymbol{\kappa}}) - \mathbf{rank}(Y \cdot I_r I_{\boldsymbol{\kappa}}) \tag{2.3.0.18}$$

By the *Rank-Nullity Theorem* of linear algebra, $\theta = \dim \ker Y|_{\mathrm{Im}(I_r I_{\boldsymbol{\kappa}})}$. As a matrix rank indicator, θ measures the defect of the matrix Y as a linear transformation. To be more precise, assume $\theta = 0$, which means Y is of full column rank(n) on the $\mathrm{Im}(I_r I_{\boldsymbol{\kappa}})$. Thus, the original task to solve the system of differential equations $Y I_r I_{\boldsymbol{\kappa}} \mathbf{z} = 0$ is reduced to solving $I_r I_{\boldsymbol{\kappa}} \mathbf{z} = 0$. Moreover, even if θ is not equal to zero, we will still manage to get some information when $\theta = 1$, in this case. As we will show later, the special structure of the $\ker I_r I_{\boldsymbol{\kappa}}$ makes the analysis of the CRNT possible, while it is the small value of θ which restricts our searching region of the CRNT system.

Martin Feinberg [36] suggests another indicator: the *deficiency* δ to study the chemical reaction networks.

Definition 2.3.6 (Deficiency, δ)**.** [36] Assume n is the number of the complexes, l is the number of the linkage class, s is the dimension of the stoichiometric subspace, the deficiency

of the chemical reaction network is defined as follows:

$$\delta = n - l - s. \tag{2.3.0.19}$$

The *deficiency* solely depends on the structure of the reaction network, because n, l, s are all combinatorial characteristics of the reaction network. The following lemma explains the connection between the combinatorial structure and and the dynamical equation of the reaction networks; it also guarantees that *deficiency* is always a non-negative integer. The proof presented here is more combinatorial-oriented, different from the original proof in [33].

Lemma 2.3.7.

$$\delta = \mathbf{rank}\, I_r - \mathbf{rank}(Y I_r) \tag{2.3.0.20}$$

Proof. Notice the $\mathbf{rank}(Y I_r)$ is equal to $\mathbf{rank}((\mathbf{y}_1, ..., \mathbf{y}_n) I_r)$. Since the column of I_r represents all the reactions (arrows) in the reaction networks, $\mathbf{rank}(Y I_r) = \mathbf{rank}\{\mathbf{y}_i - \mathbf{y}_j | C_j \to C_i\}$, which is exactly s, the dimension of the stoichiometric subspace. Then it is sufficient to show that $\mathbf{rank}(I_r) = n - l$. Because $\mathbf{C} = [C_{i1}] \cup [C_{i2}] \cup [C_{i3}] ... \cup [C_{il}]$, by relabeling the complexes of the reaction network, on has the matrix $I_r = I_{r1} \bigoplus I_{r2} \bigoplus I_{r3} ... \bigoplus I_{rl}$. Suppose that $|[C_{ij}]| = n_j \quad \forall j \in 1, 2, .., l$, if we could prove that $\mathbf{rank}(I_{rj}) = n_j - 1$, the proof would be completed. Since each column of I_{r1} contains only one element with value 1 and only one element with value -1, then $\mathbf{1}_{n_1} \cdot I_{r1} = \mathbf{0}$, where $\mathbf{1}_{n_1}$ is the size n_1 identity-vector. On the other hand, supposing $\mathbf{x} \cdot I_{r1} = \mathbf{0}$, where $\mathbf{x} \neq \mathbf{0}$, it is sufficient to show $\mathbf{x} = (1; 1; ...; 1) \in \mathbb{P}^4$. In fact, the support of $\mathbf{x}$, $\operatorname{supp} \mathbf{x} = \{1, 2, ..., r_1\} = \operatorname{supp}[C_{i1}]$, because for any $i \in \{1, 2, ..., r_1\}$,

there exists either j or k, such that in the reaction network, there exists a reaction $C_i \to C_j$ or $C_k \to C_i$. Due to the fact that $[C_{i1}]$ represents the first linkage class, no complex is isolated. Hence, either we have $x_i - x_j = 0$ or $x_k - x_i = 0$. This property not only confirms the cardinality of $\mathbf{x}$, it also shows that if C_i and C_j are linked, then the corresponding components x_i and x_j of $\mathbf{x}$ should be the same, i.e. the following set

$$[1] = \{j | x_1 = x_j, C_j \in [C_{i1}]\} \tag{2.3.0.21}$$

coincides with the support of $[C_{i1}]$. The proof is complete. □

Remark 2.3.8. The decomposition of the oriented incidence matrix is important in the analysis of the structure of the kernel of the I_r. In fact, when labeling the complexes $\{C_i\}_i^n$ and the reactions $\{\alpha\}_1^r$ to decompose I_r, $I_{\boldsymbol{\kappa}}$ is also decomposed in block form:

$$I_{\boldsymbol{\kappa}} = I_{\kappa 1} \bigoplus I_{\kappa 2} ... \bigoplus I_{\kappa l} \tag{2.3.0.22}$$

Let us denote by n_i, l_i the numbers of the complexes and reactions in the linkage class i, respectively. I_{ri} is a $n_i \times l_i$ matrix, while $I_{\kappa i}$ is a $l_i \times n_i$ matrix. In total, we have the following decomposition for $-L = I_r I_{\boldsymbol{\kappa}}$.

$$\begin{aligned} -L = I_r I_{\boldsymbol{\kappa}} &= (I_{r1} I_{\kappa 1}) \bigoplus (I_{r2} I_{\kappa 2}) \bigoplus ... \bigoplus (I_{rl} I_{\kappa l}) \\ &= -(L_1 \bigoplus L_2 \bigoplus ... \bigoplus L_l) \end{aligned} \tag{2.3.0.23}$$

As opposed to the defect θ, the *deficiency* is purely combinatorial concept. It is determined only by counting the number of linkage classes, the dimension of stoichiometric subspace, and the number of complexes in the reaction network. In fact, the *deficiency*, δ serves an upper bound of the *defect*, θ. We have the following lemma.

Lemma 2.3.9.

$$0 \leq \theta \leq \delta \tag{2.3.0.24}$$

Proof.

$$\begin{aligned} \theta &= \dim \ker Y|_{\mathrm{Im}(I_r I_{\boldsymbol{\kappa}})} \\ &\leq \dim \ker Y|_{\mathrm{Im}(I_r)} \\ &= \mathbf{rank}(I_r) - \mathbf{rank}(Y I_r) \\ &= \delta \end{aligned} \tag{2.3.0.25}$$

□

There will be no difference between θ and δ as long as $\mathbf{rank}(I_{\boldsymbol{\kappa}}) = r$, which is full row rank.

Corollary 2.3.10. *In a reaction network* $(\mathcal{C}, \mathcal{R}, \mathcal{S}, \kappa)$*, if* $\deg^+ C_i \leq 1, \forall i$*, i.e. each complex only serve as a reactant complex at most once, then*

$$\theta = \delta \tag{2.3.0.26}$$

Proof. Assume each complex only serve as a reactant complex at most once, then by 2.1.15, $\mathbf{rank}\, I_{\boldsymbol{\kappa}} = r$, hence $\mathrm{Im}(I_r I_{\boldsymbol{\kappa}}) = \mathrm{Im}(I_r)$. □

Remark 2.3.11. The idea of the *defect* of a reaction network θ and the *deficiency* can naturally be extended to the subnetworks of the entire chemical reaction network. In particular, we may define θ_i and δ_i for each reaction subnetwork (linkage class) i, using a similar approach. For example, if the number of the complexes in a reaction network is n_i, the dimension of the stoichiometric subspace corresponding to the subnetwork is s_i. We may define $\delta_i = n_i - s_i - 1$ and $\theta_i = \mathbf{rank}\, Y_i\mathcal{A}_i - \mathbf{rank}\, \mathcal{A}_i$, where Y_i is the first n_i columns of Y, i.e.

$$Y = (\underbrace{\mathbf{Y}_1}_{\text{The first } n_1 \text{ columns}}, \underbrace{\mathbf{Y}_2}_{\text{column } n_1+1 \text{ to column } n_2}, ..., \underbrace{\mathbf{Y}_l}_{\text{The last } n_l \text{ columns}}) \tag{2.3.0.27}$$

By a similar argument above, one can also prove the following analogous results without difficulty.

Lemma 2.3.12.

$$\delta_i = \mathbf{rank}\, I_{ri} - \mathbf{rank}(Y_i I_{ri}),\ \textit{and}\ 0 \leq \theta_i \leq \delta_i \tag{2.3.0.28}$$

Lemma 2.3.13.

$$s_i = \dim(\mathbf{Y}_i I_{r_i}) \tag{2.3.0.29}$$

$$:= \dim(\mathbf{Y}_i - \mathbf{y}_{n_i(1)}) \tag{2.3.0.30}$$

$$= \dim \mathbf{span}\{\mathbf{y}_{n_i(2)} - \mathbf{y}_{n_i(1)}, \mathbf{y}_{n_i(3)} - \mathbf{y}_{n_i(1)}, ..., \mathbf{y}_{n_i(n_i)} - \mathbf{y}_{n_i(1)}\} \tag{2.3.0.31}$$

2.4 Equilibrium and Convex Cones

Definition 2.4.1 (Equilibrium)**.** A vector $\mathbf{c}^* \in \mathbb{R}^n_{\geq 0}$ is an equilibrium of a chemical reaction network $\dot{\mathbf{c}}(t) = Y I_r I_{\boldsymbol{\kappa}} \Phi(\mathbf{c})$ if

$$Y I_r I_{\boldsymbol{\kappa}} \Phi(\mathbf{c}^*) = 0 \tag{2.4.0.32}$$

Remark 2.4.2. By lemma 2.2.10, each equilibrium $\mathbf{c}^*$ must exist in exactly one *stoichiometric compatibility class* $\mathfrak{S}_{\mathbf{c}_0}$ for some $\mathbf{c}_0$.

Remark 2.4.3. The question about the existence and uniqueness of the steady states of a chemical reaction network is a not easy task in general. *Monostationarity* refers to the uniqueness of the steady states in some (or all) *stoichiometric compatibility classes*; *Multistationarity* refers to the multiple steady states (at least two distinct steady states) in some (or all) *stoichiometric compatibility classes*.

Clarke [16] first suggested to study the intersection of the physical velocity space $\bar{\mathbb{R}}^r_+$ and $\ker \mathcal{Y} I_r$ (this matrix was defined as the *stoichiometric matrix* N in [16], though the decomposition was not realized), this was inspired by Kirchhoff's current law for electrical networks. Because of the decoupling of the chemical reaction network dynamics, this basic idea can be easily extended to other spaces. The explanation is as follows:

If a vector $\mathbf{c}^* \in \mathbb{R}^m_+$ is an equilibrium, satisfying the equation 2.4.0.32, then $\Phi(\mathbf{c}^*)$ must be an element in the kernel of the linear transformation $\mathcal{Y} I_r I_{\boldsymbol{\kappa}}$, hence it exists in the intersection of $\ker(\mathcal{Y} I_r I_{\boldsymbol{\kappa}})$ and the positive orthant. On the other hand, $I_{\boldsymbol{\kappa}} \Phi(\mathbf{c}^*) \in \mathbb{R}^r_+$ represents the

reaction rate of each reaction in the chemical reaction network, which must exist in the $\ker(\mathcal{Y}I_r)$. In general, given any element $\boldsymbol{\xi} \in \ker(\mathcal{Y}I_r I_{\boldsymbol{\kappa}})$, the existence and uniqueness of a positive concentration vector in $\mathbb{R}^n_+$ is not guaranteed. The non-linearity of $\Phi(\mathbf{c})$ not only gives rise the possibility that there exist multiple $\mathbf{c}$ corresponding to the same $\boldsymbol{\xi}$, but also defines the area of where such $\boldsymbol{\xi}$ exist.

Based on the observations above, we examine the following convex cones

Definition 2.4.4 (Current Cone)**.** [16]

$$Q_v = \{\mathbf{v} \in \bar{\mathbb{R}}^r_+ | \mathcal{Y} \cdot I_r \cdot \mathbf{v} = 0\} \tag{2.4.0.33}$$

Definition 2.4.5 (Feinberg's Cone)**.**

$$Q_f = \{\mathbf{g} \in \bar{\mathbb{R}}^n_+ | I_r \cdot I_\kappa \cdot \mathbf{g} = 0\} \tag{2.4.0.34}$$

Definition 2.4.6 (Complex Cone)**.**

$$Q_c = \{\mathbf{g} \in \bar{\mathbb{R}}^n_+ | \mathcal{Y} \cdot I_r \cdot I_\kappa \cdot \mathbf{g} = 0\} \tag{2.4.0.35}$$

Remark 2.4.7. By simple linear algebra, it is easy to see $Q_f \subset Q_c$. Moreover, Q_v, Q_f, and Q_c turns out to be convex polyhedrals. This is important since the convexity offers computational advantages. For example, the minimal generators of the these cones can be readily computed using linear programming. There are a lot of softwares which are designed

for this purpose, such as *polymake* [51], especially in large dimension cases. It is also easy to see that $Q_c \cong Q_v$ if $I_{\boldsymbol{\kappa}}$ is a non-singular square matrix.

The interior of the cones (we focus on the positive solutions, instead of the non-negative ones), Q_v°, Q_f°, and Q_f° have computational convenience during the study of the polynomial systems. This will be explained in the next chapter.

Example 2.1.1 (continued)

$$\begin{aligned} Q_f = Q_c &= \mathbf{span}\{(\frac{\kappa_2}{\kappa_1}, 1)\} \cap \mathbb{R}_+^2 \\ Q_v &= \mathbf{span}\{(1,1)\} \cap \mathbb{R}_+^2 \end{aligned} \tag{2.4.0.36}$$

In example 2.1.1, Q_f, Q_v and Q_c all degenerate to a one-dimensional ray.

Example 2.1.2 (continued)

$$\begin{aligned} Q_f = Q_c &= \mathbf{span}\{(\frac{\kappa_2+\kappa_3}{\kappa_4}, \frac{\kappa_2}{\kappa_1}, 1)\} \cap \mathbb{R}_+^3 \\ Q_v &= \mathbf{span}\{(1,1,0,1),(0,0,1,1)\} \cap \mathbb{R}_+^4 \end{aligned} \tag{2.4.0.37}$$

In example 2.1.2, Q_f degenerates to a one-dimensional ray while Q_c is two-dimensional.

These two examples both have the equality of the *Feinberg cone* and the *convex cone*. This situation is closely related to the defect, θ.

Corollary 2.4.8. *Consider a chemical reaction network* $\dot{\mathbf{c}}(t) = Y I_r I_{\boldsymbol{\kappa}} \Phi(\mathbf{c})$*, assuming that the defect of the reaction network is zero, i.e.* $\theta = 0$*, then*

$$Q_f = Q_c \tag{2.4.0.38}$$

Theorem 2.4.9 (Structure of the *Feinberg cone*)**.** *[33] Consider a chemical reaction network* $\dot{\mathbf{c}}(t) = Y I_r I_{\boldsymbol{\kappa}} \Phi(\mathbf{c})$*, there exist* $\sum_{\lambda=1}^{l} t_\lambda$ *independent vectors* $\{\boldsymbol{\xi}_{\lambda,\nu}\}_{\lambda=1,\nu=1}^{l,t_\lambda} \in \ker(I_r I_{\boldsymbol{\kappa}}) \cap \mathbb{R}^n_+$*, such that*

$$Q_f^\circ = \bigoplus_{\lambda=1}^{l} \bigoplus_{\nu=1}^{t_\lambda} (\mathbf{span}\{\boldsymbol{\xi}_{\lambda,\nu}\} \cap \mathbb{R}^n_+), \tag{2.4.0.39}$$

where l *is the number of the linkage classes, and* t_i *is the number of the strong linkage class in the linkage class* i

The complete proof of the theorem 2.4.9 can be found in [33], even though theorem 2.4.9 represents a variant of the original result. The basic idea of the proof is that with the help of the *weakly reversibility*, $I_{ri} I_{\boldsymbol{\kappa}_i}$, for all the *linkage classes* can be further decomposed, resulting invariant operators with corresponding invariant subspaces generated by single positive vectors.

Remark 2.4.10. This theorem gives a complete characterization of the simple structure of the interior of the *Feinberg Cone*. Moreover, when $t_\lambda = 1, \quad \forall \lambda = 1, ..., l$, the *Feinberg cone* can be simplified as $\bigoplus_{\lambda=1}^{l} (\mathbf{span}\{\boldsymbol{\xi}_\lambda\} \cap \mathbb{R}^n_+)$. The extreme case is for the reaction network with the single linkage class, the interior of the *Feinberg cone* is generated by single generator, i.e. $Q_f^\circ = \mathbf{span}\, \boldsymbol{\xi} \cap \mathbb{R}^n_+$, for some $\boldsymbol{\xi}$.

CHAPTER 3
ALGEBRAIC ASPECT OF CHEMICAL REACTION NETWORK THEORY

In the previous chapter, we described the fundamentals of the chemical reaction network theory (CRNT), with decoupled the reaction dynamics. The classical CRNT focuses on the qualitative behaviours of the reaction networks such as the existence and uniqueness of the chemical equilibria. However, certain quantitative aspects of the CRN (chemical reaction network) are not well demonstrated. For example, if the existence of the chemical equilibria are assumed to be exist, how can we calculate the equilibria inside a particular *stoichiometric compatibility class*. If there exists a bifurcation point, can this point be located? Questions like these arise naturally in the study of chemical reaction networks. The constructive results are especially desired. Throughout this chapter, we continue to examine chemical reaction networks, from an algebraic point of view. With the help of the concept of the *toric variety*, we offer an extensive investigation of the equilibria set of a chemical reaction network as a variety. By doing so, not only the classical CRNT results such as the *deficiency zero theorem* and *deficiency one theorem*, are confirmed, but also a constructive approach to locate equilibrium of the reaction is formulated.

For an arbitrary chemical reaction network $\dot{\mathbf{c}} = \mathcal{Y} I_r I_\kappa \Phi(\mathbf{c})$, locating the equilibria of the reaction system is reduced to solving the zeros a polynomial system, with the constraint of the mass action law. The zeros of the system of polynomials form a variety naturally, $V(\mathcal{Y} I_r I_\kappa \mathbf{c}^{\mathcal{Y}})$. For the general approaches to solving this system, see [26,93], in particular, the

resultants of multiple polynomials and Bernstein's Theorem provide computational tools to find the zeros of the polynomial systems. However, the calculation of the resultants and the mixed volume of the polytopes increases in computational complexity as our system becomes larger. This is especially true for the bio-chemical reaction networks, in which typically n is very large number.

The sparsity (fewnomials) of the polynomial system is a common scenario for the (bio)chemical reaction networks. This simple facts led to the early study of chemical reaction networks with Gröbner basis, see [76]. However, the Gröbner basis were employed without investigation of the network structure, leading to unexpected increasing computational complexity. Gatermann introduced the concept of using the "deformed toric variety" to investigate chemical reaction networks [49], while the number of the complex roots of the systems was discussed [47] with the polyhedral method [67].

In this chapter, a general constructive approach to finding the roots of the sparse polynomial which describes a chemical reaction network is proposed. Further simplification are offered due to the similarity among chemical reaction network problems. One projective toric variety and one usual toric variety are studied to find the equilibria set of a particular chemical reaction network. Algorithmic results under different combinatorial conditions are presented. We also give comparisons of some algebraic objects: a current cone and Feinberg's cone.

3.1 Some Algebraic Basics and Notations

In this section, some basics of algebraic techniques which are needed in the algebraic approach to solving CRN are introduced. To make this work self-contained and more readable to an audience besides mathematicians, some algebraic tools are introduced in the beginning of the chapter. A more thorough explanation of algebraic geometry, especially on the issue of toric varieties, can be found in [25, 26].

We will denote $\mathbb{K}$ as our working field[1]. Throughout this chapter, the variables $v_1, v_2, ..., v_r$ are used for the rate variables in the rate space $\mathbb{R}^r$, while $c_1, c_2, ...c_n$ are employed as the indeterminates of the concentration variables in the concentration space $\mathbb{R}^n$. Furthermore, we will use $\mathbb{C}^*$ to denote $\mathbb{C}/\{0\}$ and similarly, $\mathbb{R}^*$ to denote $\mathbb{R}/\{0\}$.

A monomial z in variables $c_1, c_2, .., c_n$ is of the form

$$z = \prod_{i=1}^{n} c_i^{\alpha_i} = \mathbf{c}^{\alpha} \tag{3.1.0.1}$$

where $\alpha_i \in \mathbb{Z}_{\geq 0}$. In this chapter, except where stated α_i will be $\{y_{ij}\}_{1 \leq i,j \leq n}$, which are the entries of the stoichiometric matrix (see definition 2.1.10) defined in chapter 2. $|\alpha| = \sum_{i=1}^{n} \alpha_i$ is the degree of the monomial z_j. A polynomial f in variables $c_1, c_2, ..., c_n$ with coefficients

[1]It will be specified as $\mathbb{R}$ or $\mathbb{C}$ later in this chapter, for the purpose of the computation or the algebraic arguments, separately.

in $\mathbb{K}$ is a finite linear combination of monomials.

$$f = \sum_{\alpha \in \mathbb{K}^n} a_\alpha \mathbf{c}^\alpha \tag{3.1.0.2}$$

where $a_{\alpha \in \mathbb{K}}$.

The set of all polynomials in $c_1, c_2, ..., c_n$ is denoted by

$$\mathbb{K}[c_1, c_2, ..., c_n] = \mathbb{K}[\mathbf{c}] \tag{3.1.0.3}$$

Given a set of polynomials $S \subset \mathbb{K}[\mathbf{c}]$, the basic geometric object will be defined as follows

$$V(S) = \{\mathbf{a} \in \mathbb{K}^n | f(\mathbf{a}) = 0 \ \ \forall f \in S\} \tag{3.1.0.4}$$

On the other hand, given a subset $X \subset \mathbb{K}^n$, the vanishing ideal of X is constructed by

$$I(X) = \{f \in \mathbb{K}(\mathbf{c}) | f(\mathbf{a}) = 0 \ \ \forall \mathbf{a} \in X\} \tag{3.1.0.5}$$

Hilbert basis theorem guarantees that each ideal is finitely generated.

Theorem 3.1.1 (*Hilbert Basis Theorem*)**.** *Every ideal $I \subset \mathbb{K}[\mathbf{c}]$ has a finite set of generators. That is, $I =< g_1, g_2, .., g_t >$ for some $g_1, g_2, ..., g_t \in I$*

For a constructive proof of this theorem, see [25].

Lemma 3.1.2. *[25] If $f_1, f_2, ..., f_s$ and $g_1, g_2, ..., g_t$ are the basis of the same ideal in $\mathbb{K}[\mathbf{c}]$, such that $< g_1, g_2, ..., g_s >=< f_1, f_2, ..., f_t >$, then*

$$V(f_1, f_2, ..., f_s) = V(g_1, g_2, ..., g_t) \tag{3.1.0.6}$$

Remark 3.1.3. It should be mentioned that it is the assumption of *mass action kinetics* that makes it possible to analyze the dynamical system of CRNT, $\dot{\mathbf{c}} = \mathbf{f}(\mathbf{c}(t))$, algebraically. Recall that by the definition of the *mass action law* 2.1.16 in the previous chapter, each rate function is defined as a monomial multiplied by the corresponding rate constant.

$$R_{ij}(\mathbf{c}) = k_{ij}\mathbf{c}^{\mathbf{y_j}} = k_{ij}c_1^{y_{1j}}c_2^{y_{2j}} \cdots c_n^{y_{nj}} \tag{3.1.0.7}$$

After the linear transformations I_r and $\mathcal{Y}$,

$$\mathbf{f}(\mathbf{c}) = \mathcal{Y}I_r\mathbf{R}(\mathbf{c}) \in \mathbb{K}[\mathbf{c}] \tag{3.1.0.8}$$

where $\mathbb{K} = \mathbb{Q}(\kappa)$. The equilibria of the set of $\mathbf{c}$ occurs when dynamical system $\dot{\mathbf{c}(t)} = \mathbf{f}(\mathbf{c}(t)) \equiv 0$, which is the variety of the ideal generated by $\mathbf{f}(\mathbf{c})$. To be more precise, the equilibria of the dynamical system are defined by the following variety

$$V(\mathcal{Y}I_rI_\kappa\Phi(\mathbf{c})) \tag{3.1.0.9}$$

Moreover, consider a reaction network $\mathcal{Y}I_rI_\kappa\Phi(\mathbf{c})$. If the *defect* $\theta = 0$ or a stronger condition, the *deficiency* $\delta = 0$, the equilibria set simplifies to

$$V(I_rI_\kappa\Phi(\mathbf{c})). \tag{3.1.0.10}$$

In order to locate the variety of a subset of polynomials, i.e. the equilibria of a chemical reaction network, one needs to study the structure the polynomials in the subset, for example, $\{\mathbf{f}\}$. However, by Lemma 3.1.2, instead of investigating the original generators, one may find useful to study another generators which generate the same vanishing ideal as $\{\mathbf{f}\}$. In particular, *Gröebner basis* of an ideal, as the basic computational tool needed through this chapter, is a good candidate to work with.

Definition 3.1.4 (Monomial Ordering)**.** [25] A monomial ordering $\prec$, on the set of monomials $\mathbf{c}^\alpha$ is a total order satisfying the following conditions:

1. if monomials $m_1 \prec m_2$, then for any monomial $m_3, m_1m_3 \prec m_2m_3$
2. every nonempty subset $\{m_i\}$ has a minimal monomial

The minimal monomial of $\mathbb{K}[\mathbf{c}]$ is $\mathbf{c^0} = 1$. The most commonly used monomial ordering is *lexicographic order*, which is defined as follows:

Definition 3.1.5 (Lexicographic Order)**.** [25] Given two monomials $\mathbf{c}^{\alpha_1}$ and $\mathbf{c}^{\alpha_2}$, we say $\mathbf{c}^{\alpha_1} \prec_{lex} \mathbf{c}^{\alpha_2}$, if the left-most nonzero entry of the difference vector $\alpha_1 - \alpha_2$ is negative.

Given a polynomial $f \in \mathbb{K}[\mathbf{c}]$ and a term order $\prec$, the initial term of f is defined as the leading term of f with respect to $\prec$, denoted by $\text{in}_{prec}(f)$. It is easy to show that the initial set of an ideal I forms an ideal.

$$\text{in}_{\prec}(I) := \{\text{in}_{\prec}(f) | f \in I\} \tag{3.1.0.11}$$

Definition 3.1.6 (Gröbner Basis)**.** For a finite collection of polynomials $G \subset I$, if

$$\text{in}_{\prec} G := \{\text{in}_{\prec}(g) | g \in G\} = \text{in}_{\prec}(I) \tag{3.1.0.12}$$

then, G is called a *Gröbner basis* of I with respect to the order $\prec$.

By *Buchberger's Algorithm* [25, Theorem 2.7.2] or more generally, by the *division algorithm* [25, Theorem 2.3.3], $< G >= I$.[2] The following theorem is a particular application of Gröbner basis in polynomial implicitization. First, the elimination ideal is defined as follows.

Definition 3.1.7 (Elimination Ideal)**.** [25] Let $I =< f_1, f_2, ..., f_s > \subset \mathbb{K}[\mathbf{c}]$ be an ideal, the $l-$th elimination ideal I_l is the ideal of $\mathbb{K}[c_{l+1}, c_{l+2}, ..., c_n]$ defined by

$$I_l = I \cap \mathbb{K}[c_{l+1}, c_{l+2}, ..., c_n] \tag{3.1.0.13}$$

[2]For the general property and analysis of Gröbner basis and the division algorithm see [23, 25]. Gröbner basis has application in computational algebraic geometry.

The basis of the elimination ideals can be directly calculated using Gröbner basis with respect to $\prec_{lex}$.

Theorem 3.1.8 (The Elimination Theorem). *[25] Let $I \subset \mathbb{K}[\mathbf{c}]$ be an ideal and let G be a Gröbner basis of I with respect to the lexicographic order $\prec_{lex}$. Then, for $0 \leq l \leq n$, the set*

$$G_l = G \cap \mathbb{K}[c_{l+1}, c_{l+2}, ..., c_n] \tag{3.1.0.14}$$

is a Gröbner basis of the l-th elimination ideal of I.

It would be helpful to get the information of the above set first. In fact, the image of the nonlinear mapping

$$\begin{aligned} \Phi : \mathbb{R}_+^m &\to \mathbb{R}_+^n \\ \mathbf{c} &\mapsto \Phi(\mathbf{c}) \end{aligned} \tag{3.1.0.15}$$

where

$$\begin{aligned} \Phi(\mathbf{c}) &= (\phi_1(\mathbf{c}), \phi_2(\mathbf{c}), ..., \phi_n(\mathbf{c})) \\ &= (\mathbf{c}^{\mathbf{y}_1}, \mathbf{c}^{\mathbf{y}_2}, ..., \mathbf{c}^{\mathbf{y}_n}) \\ &= (\prod_{i=1}^{m} c_i^{y_{i1}}, \prod_{i=1}^{m} c_i^{y_{i2}}, ..., \prod_{i=1}^{m} c_i^{y_{in}}) \end{aligned} \tag{3.1.0.16}$$

Since the *stoichiometric matrix* $\mathcal{Y} \in \mathbb{Z}^{n\times m}$ is a matrix with integer entries, then $\Phi(\mathbf{c})$ defines a monomial map $\mathbf{c}^{\mathcal{Y}}$. The closure of this image defines a *toric variety*.

Definition 3.1.9 (Toric Variety)**.** [6,23,92] The toric variety $X_{\mathcal{Y}}$ is the closure of the image of $\mathbf{c}^{\mathcal{Y}}$.

For a more extensive introduction to the computational aspects of toric varieties, see [6,23]. Notice that the definitions given in [6,23,92] are different from Fulton's definition [45]. The main difference is that normality is not required in the definition used here. For details on the role of normality, see [45]. Cox [24, chapter7] also give a geometric example to illustrate the difference.

The vanishing ideal $I_{\mathcal{Y}}$ of a toric variety $X_{\mathcal{Y}}$ is called a *toric ideal*. It can be defined as follows.

Definition 3.1.10 (Toric Ideal)**.**

$$I_{\mathcal{Y}} = \{f \in \mathbb{K}[z_1, z_2, ...z_n] | f(c^{\mathbf{y}_1}, c^{\mathbf{y}_2}, ..., c^{\mathbf{y}_n}) \equiv 0\} \tag{3.1.0.17}$$

By the elimination theorem, $I_{\mathcal{Y}}$ is the elimination ideal $\langle z_1 - c^{\mathbf{y}_1}, z_2 - c^{\mathbf{y}_2}, ..., z_n - c^{\mathbf{y}_n}\rangle \cap \mathbb{K}[z_1, ..., z_n]$. Theorem 3.1.8 also offers a constructive way to generate the Gröbner basis of $I_{\mathcal{Y}}$. Moreover, since $I_{\mathcal{Y}}$ is a toric ideal, it has the following constructive property.

Lemma 3.1.11. *[92, Lemma 4.1] The toric ideal $I_{\mathcal{Y}}$ is spanned by the set of binomials*

$$\{\mathbf{c}^{\mathbf{u}} - \mathbf{c}^{\mathbf{v}} | \mathcal{Y}\mathbf{u} = \mathcal{Y}\mathbf{v}, \ \textit{where } \mathbf{u}, \mathbf{v} \in \mathbb{N}^m\} \tag{3.1.0.18}$$

hence,

$$I_{\mathcal{Y}} = \langle \mathbf{c}^{\mathbf{u}} - \mathbf{c}^{\mathbf{v}} | \mathcal{Y}\mathbf{u} = \mathcal{Y}\mathbf{v}, \ \textit{where } \mathbf{u}, \mathbf{v} \in \mathbb{N}^m \rangle \tag{3.1.0.19}$$

Furthermore, each $\mathbf{u} \in \mathbb{Z}^m$, it can be rewritten as the difference of the non-negative vectors with disjoint support, i.e. $\mathbf{u} = \mathbf{u}^+ - \mathbf{u}^-$. Therefore,

Corollary 3.1.12. *[92]*

$$I_{\mathcal{Y}} = \langle \mathbf{c}^{\mathbf{u}^+} - \mathbf{c}^{\mathbf{u}^-} | \mathbf{u} \in \ker_{\mathbb{Z}} \mathcal{Y} \rangle \tag{3.1.0.20}$$

Let $\mathbb{Z}\mathcal{Y}$ be the lattice spanned by $\mathcal{Y}$ and $\dim \mathcal{Y}$ be the dimension of the lattice $\mathbb{Z}\mathcal{Y}$. The following fact is concerned with the dimension of the toric variety.

Lemma 3.1.13. *[92] The Krull dimension of the residue ring* $\mathbb{K}[\mathbf{c}]/I_{\mathcal{Y}}$ *is equal to* $\dim \mathcal{Y}$

Remark 3.1.14. It should be mentioned that even though Lemma 3.1.12 combined with elimination theorem 3.1.8 gives a constructive way to compute the the toric ideal, there are more efficient approaches to construct the Gröbner basis of the toric ideal, see [92, chapter12]. The combinatorial results on Gröbner basis of the saturation is introduced to restrict the working field of Gröbner basis to $\mathbb{K}[\mathbf{z}]$, instead of working on $\mathbb{K}[\mathbf{c}, \mathbf{z}]$.

3.2 A General Strategy to Solve the Equilibrium of Chemical Reaction Networks

In order to find the equilibra set of a particular chemical reaction network, as we mentioned before, one could investigate the solutions of the system of polynomials that arise from the system. However, to utilize the combinatorial properties of the network, one may first study the following intersection.

$$Q_f \cap \operatorname{Im}\Phi(\mathbf{c}),\ \text{or}\quad Q_c \cap \operatorname{Im}\Phi(\mathbf{c}),\ \text{or}\quad Q_v \cap (I_{\boldsymbol{\kappa}}\Phi(\mathbf{c})) \tag{3.2.0.21}$$

Therefore,

$$Q_f \cap \operatorname{Im}\Phi(\mathbf{c}) \subset Q_c \cap \operatorname{Im}\Phi(\mathbf{c}) \tag{3.2.0.22}$$

Mathematical characterization of the *complex cone* and the *current cone* can be found in the section 2.4. Due to the well-understanding of the structure of *Feinberg cone* (it is a direct sum of subspaces generated by single generators) 2.4.9 and close relation between the *Feinberg cone* and the *complex cone*, from now on, we focus on the study of $Q_c \cap \operatorname{Im}\Phi(\mathbf{c})$.

The image of each equilibrium $\mathbf{c}^*$ by the action Φ must exist in Q_c; hence, by studying their intersection, the equilibrium may be recovered from the intersection point. Moreover, remember that the feasible concentration vector $\mathbf{c}$ is in some *stoichiometric compatibility class* $\mathfrak{S}_{\mathbf{c}_0}$, an (unbounded) convex polytope, which is another restriction on the equilibrium $\mathbf{c}^*$. Therefore, in order to locate the equilibrium, the following convex sets should be closely

examined.

$$Q_c \cap \operatorname{Im} \Phi(\mathbf{c}), \ \textit{and} \quad \mathfrak{S}_{\mathbf{c}_0} \tag{3.2.0.23}$$

Any equilibrium has to satisfy these two conditions. In sum, to locate the equilibrium of an arbitrary chemical reaction network, we propose the following strategy.

Strategy 3.2.1. Given a chemical reaction network

$$\mathcal{Y} I_r I_\kappa \mathbf{c}^{\mathcal{Y}} = 0 \tag{3.2.0.24}$$

1. Solve the convex polyhedral $\ker \mathcal{Y} I_r I_\kappa \cap \mathbb{R}^n_+$, which is the *complex cone*.
2. Calculate the generalized deformed toric variety $V(I^\kappa_{\mathcal{Y}})$
3. Investigate the intersection of the projective toric variety and the solution $\mathbf{z}$
4. From step 3, it is possible to obtain a parametrization of the concentration variables $\mathbf{c}$ in terms of the intersection $\ker \mathcal{Y} I_r I_\kappa \cap \mathbb{R}^n_+$. The new parametrization of $\mathbf{c}$ gives a new toric variety
5. Examine the intersection between the new toric variety and the *stoichiometric polytope*

3.3 Generalized Deformed Toric Variety

The cone, Q_f as the kernel of the linear transformation $\mathcal{Y} I_r I_\kappa$ lies in the projective subspace $\mathbb{P}^n$. On the other hand, the image of the monomial map $\Phi(\mathbf{c})$ is generally hard to compute,

however, this nonlinear map defines a projective toric variety given by a homogeneous toric ideal. This toric variety is the Zariski closure of the image of the original map. It is relatively easy to study because the bionomial structure of the ideal. This is the underlying logic behind the Gatermann's definition of the *deformed toric variety*, see [48] for the description. Also note that the *deformed toric variety* originated from the idea of *toric deformation* [93].

However, the *deformed toric variety* has its own limitations when one studies the reaction network with the number of the linkage classes being greater than one. The definition can however be generalized to be useful in the investigation of more general reaction networks.

Each subspace exists in a projective subspace. Therefore the intersection points lie within the product of the projective subspaces. This idea leads to the following definition.

For an arbitrary chemical reaction network, as described in Chapter 2, the partition of the complexes set as linkage classes yields a partition of the integer sets

$$\{1, 2, ..., n\} = \bigcup_{1}^{l} \mathcal{L}_i \tag{3.3.0.25}$$

It is possible to relabel the complexes such that for any $p \in L_i$ and any $q \in L_j$, $p < q$ if $i < j$. Therefore, the following ideal is well-defined.

Definition 3.3.1 (Generalized Deformed Toric Ideal)**.**

$$I_{\mathcal{Y}^+} = \{f \in \mathbb{C}[z_1, z_2, ..., z_l] | f(\theta_1 \boldsymbol{\phi}_1(\mathbf{c}), \theta_2 \boldsymbol{\phi}_2(\mathbf{c}), ..., \theta_l \boldsymbol{\phi}_l(\mathbf{c})) \equiv 0\} \tag{3.3.0.26}$$

where $\boldsymbol{\phi}_i(\mathbf{c}) = (\phi_1(\mathbf{c}), ..., \phi_{l_i}(\mathbf{c}))$, and l_i is the number of the complexes in the linkage class i.

Correspondingly, the variety of the generalized deformed toric ideal is $V(I_{\mathcal{Y}}^+)$, which is the Zariski closure of the image of $\Phi(\mathbf{c})$ in $\mathbb{R}^n$. In other words, $V(I_{\mathcal{Y}}^+)$ is the smallest closed set containing $\mathrm{Im}(\Phi(\mathbf{c}))$, in Zariski topology. First, due to the relation between the Zariski closure and the original image,

$$Q_c \cap \mathrm{Im}(\Phi(\mathbf{c})) \subset Q_c \cap V(I_{\mathcal{Y}^+}) \tag{3.3.0.27}$$

Remark 3.3.2. In general, it is not easy to study $Q_c \cap \mathrm{Im}(\Phi(\mathbf{c}))$, since $\Phi(\mathbf{c})$ is a nonlinear mapping. However, the toric variety $V(I_{\mathcal{Y}^+})$ serves as an algebraic approximation of $\mathrm{Im}(\Phi(\mathbf{c}))$ when one considers the intersection of a convex cone and the image of non-linear mapping. Therefore, $Q_c \cap \mathrm{Im}(\Phi(\mathbf{c}))$ may be approximated by $Q_c \cap V(I_{\mathcal{Y}^+})$.

Lemma 3.3.3. *The generalized deformed toric ideal of a chemical reaction network* $\dot{\mathbf{c}} = \mathcal{Y} I_r I_\kappa \Phi(\mathbf{c})$ *is generated by the following binomials.*

$$\begin{aligned} I_{\mathcal{Y}^+} &= \langle \mathbf{z}_1 - \theta_1 \boldsymbol{\phi}_1(\mathbf{c}), ..., \mathbf{z}_l - \theta_l \boldsymbol{\phi}_l(\mathbf{c})) \rangle \cap \mathbb{C}[\mathbf{z}] \\ &= \langle \mathbf{z}^{\mathbf{u}^+} - \mathbf{z}^{\mathbf{u}^-} | \mathcal{Y}^+ \mathbf{u} = 0, \quad \mathbf{u} \in \mathbb{N}^n \rangle, \end{aligned} \tag{3.3.0.28}$$

where

$$\mathcal{Y}^+ = \begin{pmatrix} \mathbf{Y}_1 & \mathbf{Y}_2 & ... & \mathbf{Y}_l \\ \mathbf{1}_{n_1} & \mathbf{0}_{n_2} & ... & \mathbf{0}_{n_l} \\ \mathbf{0}_{n_1} & \mathbf{1}_{n_2} & ... & \mathbf{0}_{n_l} \\ \mathbf{0}_{n_1} & \mathbf{0}_{n_2} & ... & \mathbf{1}_{n_l} \end{pmatrix}$$

$$\mathbf{1}_i = (\underbrace{1, 1, .., 1}_{i \text{ components}}), \quad \mathbf{0}_i = (\underbrace{0, 0, .., 0}_{i \text{ components}}). \tag{3.3.0.29}$$

Furthermore, the following equality concerning the dimension of the variety is true for an arbitrary chemical reaction network:

$$\dim V(I_{\mathcal{Y}^+}) = \mathbf{rank}\, \mathcal{Y}^+ = s + l = n - \delta. \tag{3.3.0.30}$$

Proof. Equation 3.3.0.28 is a direct application of Corollary 3.1.12. Due to Lemma 3.1.13, the Krull dimension of the *generalized deformed toric variety* equals the rank of the $\mathcal{Y}^+$, $\dim V(I_{\mathcal{Y}^+}) = \mathbf{rank}\, \mathcal{Y}^+$. Moreover, by the following matrix transformation:

$$\mathcal{Y}^+ \xrightarrow{\mathcal{Y}^+ \cdot S} \widehat{\mathcal{Y}^+} \xrightarrow{\widehat{\mathcal{Y}^+} \cdot T} \widehat{\widehat{\mathcal{Y}^+}} \tag{3.3.0.31}$$

where $S = \text{diag}(S_1, S_2, ..., S_l)$ and

$$S_i = \begin{pmatrix} -1 & -1 & ... & -1 & 1 \\ 1 & 0 & ... & 0 & 0 \\ 0 & 1 & ... & 0 & 0 \\ \vdots & \vdots & ... & \vdots & \vdots \\ 0 & 0 & ... & 1 & 0 \end{pmatrix} \in GL(n_i, \mathbf{R}) \tag{3.3.0.32}$$

Carrying out the linear algebra steps, $\widehat{\mathcal{Y}^+}$ is,

$$\widehat{\mathcal{Y}^+} = \begin{pmatrix} \mathbf{Y}_1 - \mathbf{y}_{n_1(1)} & \mathbf{y}_{n_1(1)} & \mathbf{Y}_2 - \mathbf{y}_{n_2(1)} & \mathbf{y}_{n_2(1)} & ... & \mathbf{Y}_l - \mathbf{y}_{n_l(1)} & \mathbf{y}_{n_l(1)} \\ \mathbf{0}_{n_1-1} & 1 & \mathbf{0}_{n_2-1} & 0 & ... & \mathbf{0}_{n_l-1} & 0 \\ \mathbf{0}_{n_1-1} & 0 & \mathbf{0}_{n_2-1} & 1 & ... & \mathbf{0}_{n_l-1} & 0 \\ \vdots & \vdots & \vdots & \vdots & ... & \vdots & \vdots \\ \mathbf{0}_{n_1-1} & 0 & \mathbf{0}_{n_2-1} & 0 & ... & \mathbf{0}_{n_l-1} & 1 \end{pmatrix} \tag{3.3.0.33}$$

where $\mathbf{Y}_i$ denote the columns of $\mathcal{Y}$ corresponding to the i-th linkage class, $\mathbf{y}_{n_i(1)}$ denote the first column of $\mathbf{Y}_i$ after relabelling the indices of complexes[1], and $\mathbf{Y}_i - \mathbf{y}_{n_i(1)}$ denotes the matrix $\big(\mathbf{y}_{n_i(2)} - \mathbf{y}_{n_i(1)}, \mathbf{y}_{n_i(3)} - \mathbf{y}_{n_i(1)}, ..., \mathbf{y}_{n_i(n_i)} - \mathbf{y}_{n_i(1)}\big)$.

[1]The symbols $\mathbf{Y}_i$ and $\mathbf{y}_i$ will continue to serve as the columns of $\mathcal{Y}$ corresponding to the i-th linkage class, and i-th column of $\mathcal{Y}$, respectively, throughout this work.

Because T is a permutation matrix which exchanges the columns order of the matrix $\mathcal{Y}^+S$, $\widehat{\mathcal{Y}^+} \xrightarrow{\widehat{\mathcal{Y}^+}\cdot T} \widehat{\widehat{\mathcal{Y}^+}}$ yields

$$\widehat{\widehat{\mathcal{Y}^+}} = \begin{pmatrix} \mathcal{Y}_1 - \mathbf{y}_{n_1(1)} & \mathcal{Y}_2 - \mathbf{y}_{n_2(1)} & ... & \mathcal{Y}_l - \mathbf{y}_{n_l(1)} & \mathbf{y}_{n_1(1)} & \mathbf{y}_{n_2(1)} & ... & \mathbf{y}_{n_l(1)} \\ \mathbf{0}_{n_1-1} & \mathbf{0}_{n_2-1} & ... & \mathbf{0}_{n_l-1} & 1 & 0 & ... & 0 \\ \mathbf{0}_{n_1-1} & \mathbf{0}_{n_2-1} & ... & \mathbf{0}_{n_l-1} & 0 & 1 & ... & 0 \\ \vdots & \vdots & ... & \vdots & \vdots & \vdots & ... & \vdots \\ \mathbf{0}_{n_1-1} & \mathbf{0}_{n_2-1} & ... & \mathbf{0}_{n_l-1} & 0 & 0 & ... & 1 \end{pmatrix} \tag{3.3.0.34}$$

$$= \begin{pmatrix} (\mathcal{Y}_1 - \mathbf{y}_{n_1(1)}, \mathcal{Y}_2 - \mathbf{y}_{n_2(1)}, ..., \mathcal{Y}_l - \mathbf{y}_{n_l(1)}) & (\mathbf{y}_{n_1(1)}, \mathbf{y}_{n_2(1)}, ..., \mathbf{y}_{n_l(1)}) \\ \mathbf{0}_{l\times(n-l)} & Id_l \end{pmatrix} \tag{3.3.0.35}$$

In fact, the invertible matrix $T \in GL(n, \mathbf{R})$ can be constructed as follows:

$$T = \begin{pmatrix} Id_{n_1-1} & \mathbf{0}_{(n_1-1)\times(n_2-1)} & ... & \mathbf{0}_{(n_1-1)\times(n_l-1)} & \mathbf{0}_{(n_1-1)\times 1} & \mathbf{0}_{(n_1-1)\times 1} & ... & \mathbf{0}_{(n_1-1)\times 1} \\ \mathbf{0}_{n_1-1} & \mathbf{0}_{n_2-1} & ... & \mathbf{0}_{n_l-1} & 1 & 0 & ... & 0 \\ \mathbf{0}_{(n_2-1)\times(n_1-1)} & Id_{n_2-1} & ... & \mathbf{0}_{n_l-1} & \mathbf{0}_{(n_2-1)\times 1} & \mathbf{0}_{(n_2-1)\times 1} & ... & \mathbf{0}_{(n_2-1)\times 1} \\ \vdots & \vdots & ... & \vdots & \vdots & \vdots & ... & \vdots \\ \mathbf{0}_{n_1-1} & \mathbf{0}_{n_2-1} & ... & \mathbf{0}_{n_l-1} & 0 & 0 & ... & 1 \end{pmatrix} \tag{3.3.0.36}$$

Notice that the rank of the left upper corner of $\widehat{\widehat{\mathcal{Y}^+}}$ is equals to $\mathbf{rank}(\mathcal{Y}_1 - \mathbf{y}_{n_1(1)}, \mathcal{Y}_2 - \mathbf{y}_{n_2(1)}, ...\mathcal{Y}_l - \mathbf{y}_{n_l(1)})$. Because $S, T \in GL(n, \mathbf{R})$, by Lemma 2.3.13, we have the following equation:

$$\mathbf{rank}\, \mathcal{Y}^+ = \mathbf{rank}\, \widehat{\widehat{\mathcal{Y}^+}} = s + l = n - \delta \tag{3.3.0.37}$$

□

3.4 The Number of Equilibria

With the *generalized deformed toric variety*, we prove the following result.

Theorem 3.4.1. *Considering an arbitrary chemical reaction network* $\dot{\mathbf{c}} = \mathcal{Y} I_r I_\kappa \Phi(\mathbf{c})$*, for any point* $\boldsymbol{\xi} \in V(I_{\mathcal{Y}^+}) \cap Q_c$*, there exists an unique positive equilibrium* $\mathbf{c}^*(\boldsymbol{\xi}) \in \mathbb{R}^m_+$*, such that*

$$\mathcal{Y} I_r I_\kappa \Phi(\mathbf{c}^*(\boldsymbol{\xi})) = 0. \tag{3.4.0.38}$$

The immediate consequence of Theorem 3.4.1 is the following corollary concerning the number of equilibria of a chemical reaction network.

Corollary 3.4.2. *Considering an arbitrary chemical reaction network* $\dot{\mathbf{c}} = \mathcal{Y} I_r I_\kappa \Phi(\mathbf{c})$*, the number of positive equilibria is equal to the cardinality of the intersection between the complex cone and the generalized toric deformed variety. That is:*

$$|V(I_{\mathcal{Y}^+}) \cap Q_c^\circ|. \tag{3.4.0.39}$$

Before we give the proof of this theorem, the following lemma is proven regarding a general intersection of an arbitrary monomial toric variety and a convex cone. This is a generalization of *Birch's Theorem* [79, p. 14].

Lemma 3.4.3. *Assume a positive convex (unbounded) polytope is defined by:*

$$Q_{E,\mathbf{p}_0} := \{\mathbf{p}| \quad E\mathbf{p} = E\mathbf{p}_0, \quad \mathbf{p} \in \mathbb{R}^n_+\}, \tag{3.4.0.40}$$

where E is a $k \times n$ matrix. And a monomial non-linear mapping is defined as:

$$\boldsymbol{\phi} : \mathbb{R}^m_+ \to \mathbb{R}^n_+, \quad \mathbf{c} \mapsto \mathbf{c}^M, \tag{3.4.0.41}$$

where M is an $m \times n$ integer matrix. Suppose $\mathbf{rspan}\, E = \mathbf{rspan}\, M$*, then the intersection $Q_{E,\mathbf{p}_0} \cap \mathrm{Im}(\boldsymbol{\phi})$ is a singleton.*

Proof. The proof of Lemma relies on the construction of the following family of entropy function:

$$H_{\mathbf{p}^*} : \mathbb{R}^n_{\geq 0} \to \mathbb{R}, \quad \mathbf{p} \mapsto \sum_{i=1}^{n} p_i(\log(p_i) - 1 + p_i^*), \quad \mathbf{p}^* \in \mathbf{rspan}\, E. \tag{3.4.0.42}$$

This family of functions contains the following properties:

a) The family of functions is well-defined on $\mathbb{R}^n_{\geq 0} \to \mathbb{R}_{\geq 0}$, since $\lim_{x \to 0+} \log(x)x = 0$

b) Each $H_{\mathbf{p}^*}$ is strictly convex, since the Hessian matrix $(\frac{\partial^2 H_{\mathbf{p}^*}}{\partial p_i \partial p_j}) = \mathrm{diag}(\frac{1}{p_1^*}, ..., \frac{1}{p_n^*}) > 0$

Moreover, each coset $Q_{E,\mathbf{p}_0} \subset \mathbb{R}^n_+$ is also convex, therefore, any entropy function $H_{\mathbf{p}^*}$ assumes its minimum at an unique point $\hat{\mathbf{p}}$ on the polytope $Q_{E,\mathbf{p}_0}$. In fact, the following claim is true.

Claim: The family of the entropy functions $\{H_{\mathbf{p}^*}\}_{\mathbf{p}^* \in \mathbf{rspan}\, E}$ assumes their minimums at the same unique point $\hat{\mathbf{p}}_{E,\mathbf{p}_0} \in Q_{E,\mathbf{p}_0}$.

Proof of the claim: Assume that $H_{\mathbf{p}^*}$ and $H_{\mathbf{q}^*}$ attain their minimums at $\mathbf{p}_1$ and $\mathbf{p}_2$, respectively. First, because $\mathbf{p}^*, \mathbf{q}^* \in \mathbf{rspan}\, E$, there exists $\mathbf{b}_1, \mathbf{b}_2 \in \mathbb{R}^k$ such that

$$\mathbf{p}^* = E^T \mathbf{b}_1, \quad \mathbf{q}^* = E^T \mathbf{b}_2. \tag{3.4.0.43}$$

Therefore,

$$\begin{aligned}
H_{\mathbf{p}^*}(\mathbf{p}_1) \leq H_{\mathbf{p}^*}(\mathbf{p}_2) &= H_{\mathbf{q}^*}(\mathbf{p}_2) + \mathbf{p}^* \cdot \mathbf{p}_2 - \mathbf{q}^* \cdot \mathbf{p}_2 \\
&= H_{\mathbf{q}^*}(\mathbf{p}_2) + \mathbf{p}_2^T E^T \mathbf{b}_1 - \mathbf{p}_2^T E^T \mathbf{b}_2 \\
&= H_{\mathbf{q}^*}(\mathbf{p}_2) + \mathbf{p}_2^T E^T (\mathbf{b}_1 - \mathbf{b}_2) \\
&= H_{\mathbf{q}^*}(\mathbf{p}_2) + \mathbf{p}_0^T (\mathbf{b}_1 - \mathbf{b}_2) \\
&\leq H_{\mathbf{q}^*}(\mathbf{p}_1) + \mathbf{p}_0^T (\mathbf{b}_1 - \mathbf{b}_2) \\
&= H_{\mathbf{q}^*}(\mathbf{p}_1) + \mathbf{p}_1^T E^T (\mathbf{b}_1 - \mathbf{b}_2) \\
&= H_{\mathbf{q}^*}(\mathbf{p}_1) + \mathbf{p}_1^T E^T (\mathbf{b}_1 - \mathbf{b}_2) \\
&= H_{\mathbf{q}^*}(\mathbf{p}_1) + \mathbf{p}^* \cdot \mathbf{p}_1 - \mathbf{q}^* \cdot \mathbf{p}_1 \\
&= H_{\mathbf{p}^*}(\mathbf{p}_1)
\end{aligned} \tag{3.4.0.44}$$

Thus, all the "$\leq$" should be "=" in Equation 3.4.0.44. All the entropy functions $\{H_{\mathbf{p}^*}\}_{\mathbf{p}^* \in \mathbf{rspan}\, E}$ attain their minimums in a polytope $Q_{E,\mathbf{p}_0}$ at an unique point. The choice of the entropy function is irrelevant when one searches for the the minimum.

Furthermore, due to the special form of the entropy functions, this maximal $\hat{\mathbf{p}}_{E,\mathbf{p}_0}$ actually happens to exist in the image of the monomial mapping. To demonstrate this, consider the *first order necessary condition* of optimality,

$$\nabla H_{\mathbf{p}^*}(\hat{\mathbf{p}}_{E,\mathbf{p}_0}) \cdot \mathbf{u} = 0, \quad \forall \mathbf{u} \in \ker E. \tag{3.4.0.45}$$

Expanding equation 3.4.0.45, it can be simplified to the following equation.

$$\begin{aligned}\sum_i^n u_i(\log((\hat{\mathbf{p}}_{E,\mathbf{p}_0})_i) + p_i^*) &= \sum_i^n (u_i(\log((\hat{\mathbf{p}}_{E,\mathbf{p}_0})_i)) + \sum_i^n u_i p_i^* \\ &= \mathbf{u} \cdot (\log((\hat{\mathbf{p}}_{E,\mathbf{p}_0})_1), ..., \log((\hat{\mathbf{p}}_{E,\mathbf{p}_0})_n))^T + \mathbf{u} \cdot \mathbf{p}^* \\ &= 0 \end{aligned} \tag{3.4.0.46}$$

By assuming that $\mathbf{p}^* \in \mathbf{rspan}\, E$, and $\mathbf{u} \in \ker(E) = \mathbf{rspan}\, E^\perp$, therefore $\mathbf{u} \cdot \mathbf{p}^* = 0$ and

$$(\log((\hat{\mathbf{p}}_{E,\mathbf{p}_0})_1), ..., \log((\hat{\mathbf{p}}_{E,\mathbf{p}_0})_n))^T \in (\mathbf{rspan}\, E^\perp)^\perp = \mathbf{rspan}\, E. \tag{3.4.0.47}$$

Thus, there exists a vector $\mathbf{a} \in \mathbb{R}^k$, such that $(\log((\hat{\mathbf{p}}_{E,\mathbf{p}_0})_1), ..., \log((\hat{\mathbf{p}}_{E,\mathbf{p}_0})_n)) = \mathbf{a}^T E$, i.e.

,

$$\log((\hat{\mathbf{p}}_{E,\mathbf{p}_0})_i) = \sum_j^k a_j E_{ji} = \sum_j^k \log(e^{a_j}) E_{ji}. \tag{3.4.0.48}$$

Equivalently,

$$(\hat{\mathbf{p}}_{E,\mathbf{p}_0})_i = \exp(\sum_j^k a_j E_{ji}) = \prod_j^k (e^{\log(e^{a_j})})^{E_{ji}} = \exp(\mathbf{a})^{\mathbf{E_i}}, \tag{3.4.0.49}$$

where $\mathbf{E_i}$ is the i-th column of the matrix E, and $\exp(\mathbf{a}) = (e^{a_1}, e^{a_2}, ..., a^{a_k})$. Hence, the optimal of the entropy functions exists in the image of the map ϕ. With the help of the entropy function, we have shown that

$$Q_{E,\mathbf{p}_0} \cap \operatorname{Im} \phi \neq \emptyset. \tag{3.4.0.50}$$

It suffices to show the uniqueness of the intersection points. To see this, one may consider any point $\boldsymbol{\xi} \in Q_{E,\mathbf{p}_0} \cap \operatorname{Im} \phi$. Because $\xi_i = \mathbf{a}^{\mathbf{E}_i}$ for some $\mathbf{a} \in \mathbb{R}^k$, $(\log(\xi_1), ..., \log(\xi_k)) \in \mathbf{rspan}\, E$. Hence for any $\mathbf{u} \in \ker E$, equation 3.4.0.46 is valid under the assumption. Moreover, since the Hessian matrix is a constant positive matrix, by the *sufficient condition of optimality*, $\boldsymbol{\xi}$ is also an optimal in the convex polytope $Q_{E,\mathbf{p}_0}$. By the uniqueness of the optimality in a convex set, $\boldsymbol{\xi} = \hat{\mathbf{P}}_{E,\mathbf{p}_0}$. □

Remark 3.4.4. The lemma presented here relies upon the fundamental idea of *Birch's theorem* proved in [79], though the assumptions of *Birch's theorem* are much relaxed in this

lemma. For example, the matrices E and M are not required to be identical as long as their rows span the same subspaces. Moreover, the *zero row sum* condition which appears in *Birch's theorem* [79] is not required. However, the trade-off is that the form of the entropy functions becomes more complicated; in fact, we must construct a family of entropy functions, instead of one function. It is also interesting to see that all of these entropy functions assume their minimums at the same point, which is not obvious *a priori*.

In fact, the conditions of Lemma 3.4.3 can be relaxed further.

Lemma 3.4.5. *Assume a positive convex (unbounded) polytope is defined by:*

$$Q_{E,D,\mathbf{p}_0} := \{\mathbf{p}| \quad ED\mathbf{p} = ED\mathbf{p}_0, \quad \mathbf{p} \in \mathbb{R}^n_+\}, \tag{3.4.0.51}$$

where E is a $k \times n$ matrix and $D = \operatorname{diag}(d_1, d_2, ..., d_n) > 0$. And a monomial non-linear mapping is defined as:

$$\boldsymbol{\phi} : \mathbb{R}^m_+ \to \mathbb{R}^n_+, \quad \mathbf{c} \mapsto \mathbf{c}^M, \tag{3.4.0.52}$$

where M is an $m \times n$ integer matrix. Suppose $\mathbf{rspan}\, E = \mathbf{rspan}\, M$, then the intersection $Q_{E,D,\mathbf{p}_0} \cap \operatorname{Im}(\boldsymbol{\phi})$ is a singleton.

Sketch of Proof: The idea of the proof of this lemma is exactly the same as the proof of Lemma 3.4.3 except the entropy function family are defined as follows:

$$H_{\mathbf{p}^*} : \mathbb{R}^n_{\geq 0} \to \mathbb{R}, \quad \mathbf{p} \mapsto \sum_{i=1}^{n} p_i d_i (\log(p_i) - 1 + p^*_i), \quad \mathbf{p}^* \in \mathbf{rspan}\, E \tag{3.4.0.53}$$

Since this family of entropy also maintains the properties described in the proof of Lemma 3.4.3, the rest of the proof follows similarly. ∎

Corollary 3.4.6. *Consider a nonlinear map*

$$\mathbf{f} : \mathbb{R}^k_{\geq 0} \to \mathbb{R}^n_{\geq 0}, \quad \mathbf{w} \mapsto \mathbf{w}^M \tag{3.4.0.54}$$

where M is a $k \times n$ matrix. If $\mathbf{rspan}\, M = (\mathcal{Y} I_r)^\perp$, then the image of $\mathbf{f}$ intersects each stoichiometric compatibility class exactly once. In other words,

$$\operatorname{Im} \mathbf{f} \cap \mathfrak{S}_{\mathbf{c}_0} \text{ is a singleton}, \quad \forall \mathbf{c}_0 \in \mathbb{R}^n_+ \tag{3.4.0.55}$$

Proof. By Lemma 2.2.9, the *stoichiometric compatibility class* can be defined by the following subset:

$$\{\mathbf{c} |\ \ V\mathbf{c} = V\mathbf{c}_0, \quad \mathbf{rspan}(V) = \mathfrak{S}^\perp\}. \tag{3.4.0.56}$$

Since $\mathfrak{S} = \operatorname{Im}(\mathcal{Y} I_r)$, by Lemma 3.4.3, there exists an unique point in the intersection subset.

□

Now with Lemma 3.4.3 and Corollary 3.4.6, we now complete the proof of Theorem 3.4.1.

The proof of the Theorem 3.4.1

Proof. Assume that $\boldsymbol{\xi} \in Q_c \cap V(I_{\mathcal{Y}^+})$, by Lemma 3.3.3, for all $\mathbf{u} \in \ker_{\mathbb{Z}} \mathcal{Y}^+$

$$\boldsymbol{\xi}^{\mathbf{u}^+} - \boldsymbol{\xi}^{\mathbf{u}^-} = 0 \tag{3.4.0.57}$$

From here on, we denote $(\mathcal{Y}_1 - \mathbf{y}_{n_1(1)}, \mathcal{Y}_2 - \mathbf{y}_{n_2(1)}, ...\mathcal{Y}_l - \mathbf{y}_{n_l(1)})$ as $\mathcal{Y}_S$. The Smith normal form of the matrix $\mathcal{Y}_S$ is obtained by the following:

$$U \cdot \mathcal{Y}_S \cdot V = \begin{pmatrix} \alpha_1 & 0 & ... & 0 & 0 & ... & 0 \\ 0 & \alpha_2 & ... & 0 & 0 & ... & 0 \\ \vdots & \vdots & ... & \vdots & \vdots & ... & \vdots \\ 0 & 0 & ... & \alpha_s & 0 & ... & 0 \\ 0 & 0 & ... & 0 & 0 & ... & 0 \\ \vdots & \vdots & ... & \vdots & \vdots & ... & \vdots \\ 0 & 0 & ... & 0 & 0 & ... & 0 \end{pmatrix}. \tag{3.4.0.58}$$

where $U \in GL(m, \mathbb{Z}), V \in GL(n-l, \mathbb{Z})$, and $0 < \alpha_i | \alpha_{i+1} \in \mathbb{Z}$. The dimension of the stoichiometric subspace is s.

Define two, new, enlarged matrices $\bar{U} = \begin{pmatrix} U & 0 \\ 0 & Id_l \end{pmatrix}$ and $\bar{V} = \begin{pmatrix} V & 0 \\ 0 & Id_l \end{pmatrix}$. The Smith normal form ($\hat{U}$) leads to the following coordinate change,

$$\begin{aligned} \hat{\mathbf{c}} &= (\mathbf{c}, \theta_1, \theta_2, ..., \theta_l)^T \\ &= \hat{\mathbf{x}}^{\bar{U}} \\ &= (\mathbf{x}^U, \theta_1, \theta_2, ...\theta_l)^T \end{aligned} \tag{3.4.0.59}$$

where $\hat{x} = (x_1, ..., x_m, \theta_1, \theta_2, ..., \theta_l)^T$. Because U is invertible, the enlarged matrix $\hat{U}$ is also invertible, and the coordinate change is one-to-one correspondence. By the change of variables, for any $\boldsymbol{\xi} \in V(I_{\mathcal{Y}^+})$, $\boldsymbol{\xi} = \mathbf{c}^{\mathcal{Y}^+}$ is equivalent to the following equation.

$$\begin{aligned} &\boldsymbol{\xi}^{S \cdot T \cdot \bar{V}} \\ =&\hat{\mathbf{c}}^{\mathcal{Y}^+ \cdot S \cdot T \cdot \bar{V}} \\ =&\hat{\mathbf{x}} \begin{pmatrix} U & 0 \\ 0 & Id \end{pmatrix} \cdot \begin{pmatrix} \mathcal{Y}_S & (\mathbf{y}_{n_1(1)}, \mathbf{y}_{n_2(1)}, ..., \mathbf{y}_{n_l(1)}) \\ \mathbf{0}_{l \times (n-l)} & Id_l \end{pmatrix} \cdot \begin{pmatrix} V & 0 \\ 0 & Id \end{pmatrix} \\ =&\hat{\mathbf{x}} \begin{pmatrix} \mathrm{SNF}(\mathcal{Y}_S) & U(\mathbf{y}_{n_1(1)}, \mathbf{y}_{n_2(1)}, ..., \mathbf{y}_{n_l(1)}) \\ \mathbf{0} & Id \end{pmatrix} \end{aligned} \tag{3.4.0.60}$$

This is the following system of equations

$$\begin{cases} x_1^{\alpha_1} & = \left(\xi^{(S\cdot T)}\right)^{\bar{V}_1} \\ x_2^{\alpha_2} & = \left(\xi^{(S\cdot T)}\right)^{\bar{V}_2} \\ \ldots & \\ x_s^{\alpha_s} & = \left(\xi^{(S\cdot T)}\right)^{\bar{V}_s} \end{cases} \tag{3.4.0.61}$$

$$\begin{cases} 1 & = \left(\xi^{(S\cdot T)}\right)^{\bar{V}_{s+1}} \\ 1 & = \left(\xi^{(S\cdot T)}\right)^{\bar{V}_{s+2}} \\ \ldots & \\ 1 & = \left(\xi^{(S\cdot T)}\right)^{\bar{V}_{n-l}} \end{cases} \tag{3.4.0.62}$$

$$\text{and} \begin{cases} \hat{\mathbf{x}}^{(U\cdot(\mathbf{y}_{n_1(1)},\mathbf{y}_{n_2(1)},\ldots,\mathbf{y}_{n_l(1)}))_1}\theta_1 & = \left(\xi^{(S\cdot T)}\right)^{\bar{V}_{n-l+1}} \\ \hat{\mathbf{x}}^{(U\cdot(\mathbf{y}_{n_1(1)},\mathbf{y}_{n_2(1)},\ldots,\mathbf{y}_{n_l(1)}))_1}\theta_2 & = \left(\xi^{(S\cdot T)}\right)^{\bar{V}_{n-l+2}} \\ \ldots & \\ \hat{\mathbf{x}}^{(U\cdot(\mathbf{y}_{n_1(1)},\mathbf{y}_{n_2(1)},\ldots,\mathbf{y}_{n_l(1)}))_l}\theta_l & = \left(\xi^{(S\cdot T)}\right)^{\bar{V}_n} \end{cases} \tag{3.4.0.63}$$

In order to solve $\boldsymbol{\xi} = \mathbf{c}^{\mathcal{Y}^+}$, we need solve all three system of equations 3.4.0.61, 3.4.0.62, and 3.4.0.63 simultaneously. Among these equations, equation 3.4.0.63 is not of interest, since we can always choose the proper θ to balance the equations, i.e., θ are free variables.

Equation 3.4.0.62 is satisfied when $\boldsymbol{\xi} \in V(I_{\mathcal{Y}^+})$. To see this, consider the map:

$$\psi : \mathbb{R}_+^n \to \mathbb{R}_+^n, \boldsymbol{\xi} \mapsto \boldsymbol{\xi}^{(S \cdot T)}. \tag{3.4.0.64}$$

Because S and T are both invertible, ψ is a one-to-one correspondence. Moreover, since

$$\mathcal{Y}^+(ST\hat{V}_i) = \mathbf{0}, \quad \forall s+1 \leq i \leq n-1, \tag{3.4.0.65}$$

$(ST\hat{V}_i)$ is in the kernel of the matrix $\mathcal{Y}^+$, and by Lemma 3.3.3,

$$\boldsymbol{\xi}^{(ST\hat{V}_i)} = 1, \quad \forall s+1 \leq i \leq n-1. \tag{3.4.0.66}$$

Therefore, the question is reduced to solving equation 3.4.0.61. In fact, we may now prove the following similar claim:

Claim:

$$\Phi^{-1}(\boldsymbol{\xi}) = \bigcup_{p=1}^{\prod_1^s \alpha_i} \mathrm{Im}(\Psi_i) \tag{3.4.0.67}$$

where $\mathrm{Im}(\Psi_i) : (\mathbb{C}^*)^{m-s+1} \to (\mathbb{C}^*)^{m-s+1}$ and $\alpha_1, \alpha_2, ..., \alpha_s$ are the elementary divisors of the matrix $\mathcal{Y}^+$.

Proof of the claim: By solving Equation 3.4.0.61, there are exactly $\prod_1^s \alpha_i$ solution vectors $\check{\mathbf{x}} := (x_1, ..., x_s)^T \in (\mathbb{C}^*)^s$. In addition, $\hat{\mathbf{x}} = (x_{s+1}, x_{s+2}, ..., x_m)^T \in (\mathbb{C}^*)^s$ is the free variable vector. For a fixed truncated solution $\check{\mathbf{x}} \in (\mathbb{C}^*)^s$ of Equation 3.4.0.60, consider the

following map:

$$\Psi_{\check{\mathbf{x}}} : (\mathbb{C}^*)^{m-s+1} \to (\mathbb{C}^*)^m$$
$$\hat{\mathbf{x}} \mapsto \left(\begin{pmatrix} \check{\mathbf{x}} \\ \\ \hat{\mathbf{x}} \end{pmatrix}^{\mathbf{u}_1}, ..., \begin{pmatrix} \check{\mathbf{x}} \\ \\ \hat{\mathbf{x}} \end{pmatrix}^{\mathbf{u}_m} \right)^T \tag{3.4.0.68}$$

Evaluating at $\check{\mathbf{x}}$,

$$\begin{aligned} \Psi_{\check{\mathbf{x}}}(\hat{\mathbf{x}}) &= (\check{\mathbf{x}}^{\check{\mathbf{u}}_1}\hat{\mathbf{x}}^{\hat{\mathbf{u}}_1}, ..., \check{\mathbf{x}}^{\check{\mathbf{u}}_m}\hat{\mathbf{x}}^{\hat{\mathbf{u}}_m})^T \\ &= \operatorname{diag}(\check{\mathbf{x}}^{\check{\mathbf{u}}_1}, ..., \check{\mathbf{x}}^{\check{\mathbf{u}}_m}) \cdot (\hat{\mathbf{x}}^{\hat{\mathbf{u}}_1}, ..., \hat{\mathbf{x}}^{\hat{\mathbf{u}}_m})^T \\ &= D(\check{\mathbf{x}}) \cdot (\hat{\mathbf{x}}^{\hat{\mathbf{u}}_1}, ..., \hat{\mathbf{x}}^{\hat{\mathbf{u}}_m})^T \qquad (3.4.0.69) \\ &= D(\check{\mathbf{x}}) \cdot \hat{\mathbf{x}}^{\hat{U}} \qquad (3.4.0.70) \end{aligned}$$

where $\hat{\mathbf{u}}_i = (u_{s+1}, u_{s+2}, .., u_m)$ and $\check{\mathbf{u}}_i = (u_1, u_2, .., u_s)$. There are exactly $\prod_1^s \alpha_i$ diagonal matrices $D(\check{\mathbf{x}})$ corresponding to each $\boldsymbol{\xi}$, thus, there are $\prod_1^s \alpha_i$ solution branches in $(\mathbb{C}^*)^{m-s+1}$. Among the solution branches, there exist $2s$ real solution branches. An exactly unique, positive, real solution branch exists when $D(\check{\mathbf{x}}) > 0$. The proof of the claim is complete.

Because all the complex vectors exits in some *stoichiometric compatibility class*, one needs to investigate the following intersection:

$$\mathfrak{S}_{\mathbf{c}_0} \cap \operatorname{Im} \Psi_{\check{\mathbf{x}}}(\hat{\mathbf{x}}) \tag{3.4.0.71}$$

In fact, due to equation 3.4.0.58 and the invertibility of the matrix U,

$$\mathbf{rspan}\,\hat{U} = \mathfrak{S}^{\perp} \tag{3.4.0.72}$$

By the definition of the stoichiometric polytope, the positive branch of the intersection class $\mathfrak{S}^{+}_{\mathbf{c}_0}$ is defined as

$$\mathfrak{S}^{+}_{\mathbf{c}_0} = \{\mathbf{c} \in \mathbb{R}^n_+ | P\mathbf{c} = P\mathbf{c}_0, \text{ where } \mathbf{rspan}(P) = \mathfrak{S}^{\perp}\} \tag{3.4.0.73}$$

We denote

$$\begin{aligned}\mathfrak{S}^{+}_{\mathbf{c}_0,\check{\mathbf{x}}} &= \{\mathbf{x} \in \mathbb{R}^m_+ | P(D(\check{\mathbf{x}})\hat{\mathbf{x}}^{\hat{U}}) = P\mathbf{c}_0, \text{ where } \mathbf{rspan}(P) = \mathfrak{S}^{\perp}\} \\ &= \{\mathbf{x} \in \mathbb{R}^m_+ | (PD(\check{\mathbf{x}}))\hat{\mathbf{x}}^{\hat{U}} = P\mathbf{c}_0, \text{ where } \mathbf{rspan}(P) = \mathfrak{S}^{\perp}\}\end{aligned} \tag{3.4.0.74}$$

Notice that $\mathbf{rspan}\,\hat{U} = \mathfrak{S}^{\perp}$, by Lemma 3.4.5. The proof is completed. □

Remark 3.4.7. In this section, we show that if there exists a point at the intersection of the *generalized toric variety* and the *complex cone*, there is exactly one unique equilibrium corresponding to this intersection point. Hence, the number of equilibria depends only upon the the cardinality of $V(I_{\mathcal{Y}^+}) \cap Q_c$. This is an important fact because it reduces the problems of counting and locating equilibria to study the structure of $V(I_{\mathcal{Y}^+}) \cap Q_c$.

3.5 A Constructive Proof on the Deficiency Zero Theorem

The *Deficiency Zero Theorem* is one of the most important results in CRNT. Within this section, we give a constructive approach to this theorem, by using the *toric variety*.

3.5.1 Single linkage

The theorem here is an stronger version of Feinberg's *Deficiency Zero Theorem*, except in the Feinberg's context [36,39], the ranks condition is even stronger concerning the deficiency of the subnetworks and the total reaction network itself. And the proof presented here is more constructive, leading to the algorithmic results to determine the equilibrium.

Theorem 3.5.1. *For a arbitrary chemical reaction network* $\dot{\mathbf{c}} = \mathcal{Y} I_r I_\kappa \Phi(\mathbf{c})$*, suppose the following conditions hold:*

a*) the value the deficiency* $\delta = 0$

b*) it is weakly reversible.*

c*) the value of the number of the linkage classes,* $l = 1$

Then for any $\mathbf{k} \in \bar{\mathbb{R}}^r_+$*, there exists an equilibrium* $\mathbf{c}^* \in \mathbb{R}^m_+$*, which is unique.*

Proof. Following the *general strategy* 3.2.1, the first step is to characterize the polyhedral cone

$$\ker \mathcal{Y} I_r I_\kappa \cap \mathbb{R}^n_+ \tag{3.5.1.1}$$

Because of the assumed condition $\delta = 0$,$\theta = 0$. Thus the task is reduced to solve *Feinberg's cone* $Q_f \in \mathbb{R}^n_+$. Under the condition that the chemical reaction network is weakly reversible and the single linkage condition, Theorem 2.4.9 implies that *Feinberg's cone* Q_f is generated by a single vector $\boldsymbol{\xi}$ which lies in the positive orthant. Next, in order to solve the system of equations, $\boldsymbol{\xi}$, as a point in the projective space $\mathbb{P}^n$, should also be a point in the generalized deformed toric variety in this system.

Due to Lemma 3.1.13, the Krull dimension of the generalized deformed toric variety is given by the dimension of $\mathcal{Y}^+$, which is equivalent to

$$\begin{aligned} \mathbf{rank}\, \mathcal{Y}^+ &= \mathbf{rank} \begin{pmatrix} \mathcal{Y} \\ \\ \mathbf{1}_n \end{pmatrix} \\ &\overset{\mathcal{Y}^+ \cdot S}{=} \mathbf{rank} \begin{pmatrix} \mathbf{y}_2 - \mathbf{y}_1 & \cdots & \mathbf{y}_n - \mathbf{y}_1 & \mathbf{y}_1 \\ \\ 0 & \cdots & 0 & 1 \end{pmatrix} \end{aligned} \tag{3.5.1.2}$$

where S is defined in the previous section. Because $l = 1$ and the reaction network is weakly reversible, the rank of the $\mathcal{Y}^+$ is equal to

$$s + 1 = n - l - \delta + 1 = n - \delta = n \tag{3.5.1.3}$$

Hence, the dimension of the generalized toric variety is n, which means that the toric variety is isomorphic to the entire projective space $\mathbb{P}^n$. Thus, the single point $\boldsymbol{\xi}$ is also in the *generalized toric variety*. Therefore, by Theorem 3.4.1, there exists exactly one equilibrium. □

Let us compute a simple example using the proposed strategy.

Example 2.1.2 (continued)

In Example 2.1.2, the defect $\theta = 0$, the *Feinberg cone* and complex cone are calculated as follows:

$$Q_f = Q_c = \mathbf{span}\{(\frac{\kappa_2 + \kappa_3}{\kappa_4}, \frac{\kappa_2}{\kappa_1}, 1)\} \cap \mathbb{R}^3_+ \tag{3.5.1.4}$$

Denote the solution $\boldsymbol{\xi} = (\frac{\kappa_2+\kappa_3}{\kappa_4}, \frac{\kappa_2}{\kappa_1}, 1)^T$. Since the network is zero defect, and weakly reversible, the *generalized toric variety* is equal to

$$\mathcal{Y}^+ = \begin{pmatrix} 2 & 0 & 0 \\ 0 & 1 & 0 \\ 0 & 0 & 1 \\ 1 & 1 & 1 \end{pmatrix} \tag{3.5.1.5}$$

Because the toric variety is isomorphic to the whole projective space, then it is not necessary to check the *generalized toric variety*. One can solve the equation $\boldsymbol{\xi} = \mathbf{c}^{\mathcal{Y}^+}$ directly. Then

we have

$$c_1 = \sqrt{\frac{\kappa_2 + \kappa_3}{\kappa_4 c_0}} \tag{3.5.1.6}$$

$$c_2 = \frac{\kappa_2}{\kappa_1 c_0} \tag{3.5.1.7}$$

$$c_3 = \frac{1}{c_0} \tag{3.5.1.8}$$

Substituting $\sqrt{\frac{1}{c_0}} = u$, we have the monomial mapping as follows:

$$c_1 = \sqrt{\frac{\kappa_2 + \kappa_3}{\kappa_4}} u \tag{3.5.1.9}$$

$$c_2 = \frac{\kappa_2}{\kappa_1} u^2 \tag{3.5.1.10}$$

$$c_3 = u^2 \tag{3.5.1.11}$$

This is a one dimensional curve in the space, which intersects each *stoichiometric compatibility class* exactly once. See the following figures. This is illustrated in Figures 3.1 and 3.2.

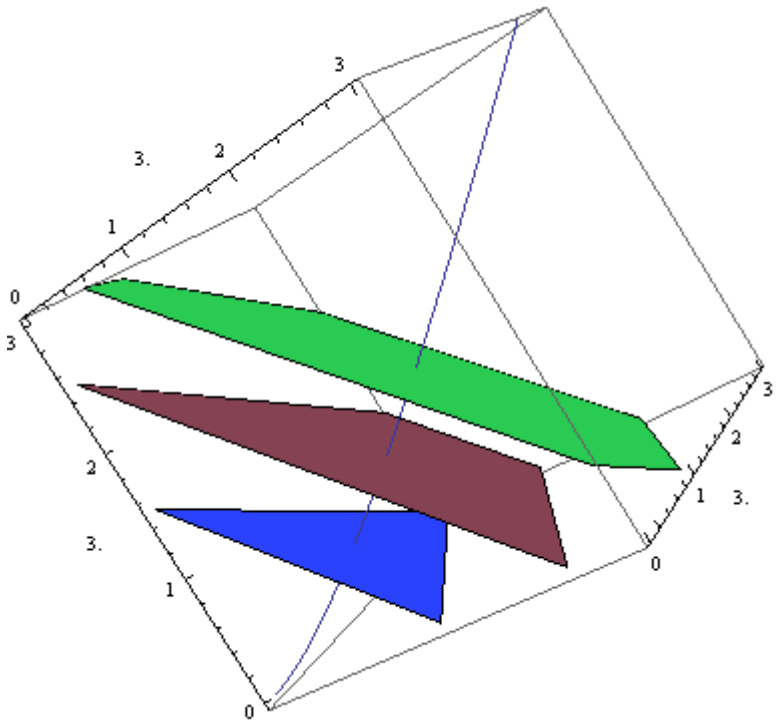

Figure 3.1: The parametric curve $(\sqrt{\frac{\kappa_2+\kappa_3}{\kappa_4}}u, \frac{\kappa_2}{\kappa_1}u^2, u^2)$ intersects different stoichiometric compatibility classes. This numeric rate constants are $\kappa_1 = \kappa_2 = \kappa_3 = \kappa_4 = 1$.

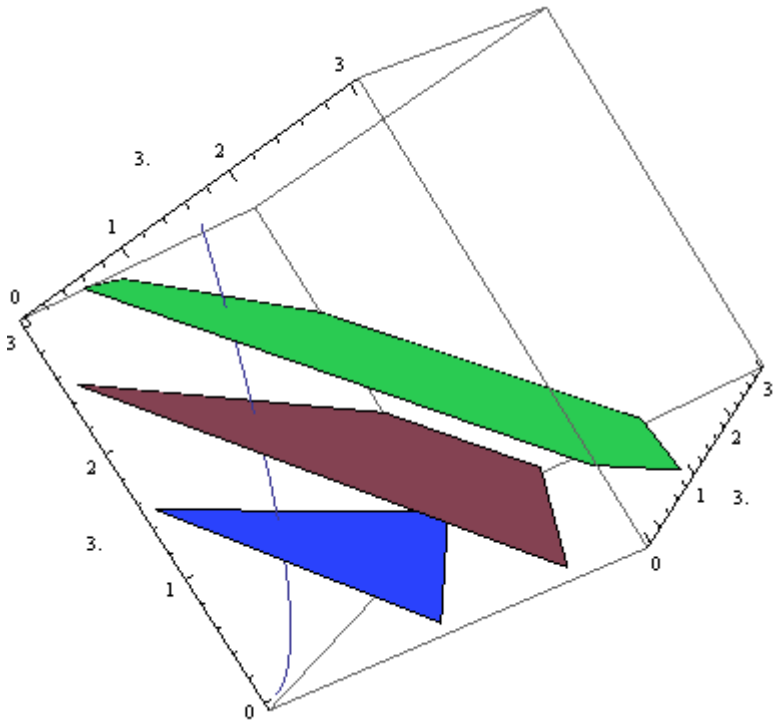

Figure 3.2: The parametric curve $(\sqrt{\frac{\kappa_2+\kappa_3}{\kappa_4}}u, \frac{\kappa_2}{\kappa_1}u^2, u^2)$ intersects different stoichiometric compatibility classes. This numeric rate constants are $\kappa_1 = 3, \quad \kappa_2 = 20, \quad \kappa_3 = 1,$ and $\kappa_4 = 1$.

In fact, one can solve for the intersection between any *stoichiometric compatibility class* $\mathfrak{S}_{\mathbf{c}_0}$ and the image of the curve.

$$\sqrt{\frac{\kappa_2+\kappa_3}{\kappa_4}}u + 2\frac{\kappa_2}{\kappa_1}u^2 + u^2 = 0 \tag{3.5.1.12}$$

Equation 3.5.1.12 is a quadratic equation, which has one positive solution,

$$u^* = \frac{-\kappa_1\sqrt{\frac{\kappa_2+\kappa_3}{\kappa_4}} + \frac{\sqrt{\kappa_1}\sqrt{\kappa_1\kappa_2+\kappa_3\kappa_1+8d\kappa_1\kappa_4+8d\kappa_4\kappa_2}}{\sqrt{\kappa_4}}}{4(\kappa_1+\kappa_2)}, \tag{3.5.1.13}$$

where $d = (1, 2, 2)\mathbf{c}_0$.

3.5.2 Generalized cases

Theorem 3.5.2. *For a arbitrary chemical reaction network* $\dot{\mathbf{c}} = \mathcal{Y} I_r I_\kappa \Phi(\mathbf{c})$*, suppose the following conditions hold:*

a*) the value the deficiency* $\delta = 0$

b*) it is weakly reversible.*

Then for any $\mathbf{k} \in \bar{\mathbb{R}}^r_+$*, there exists an equilibrium* $\mathbf{c}^* \in \mathbb{R}^m_+$*, which is unique.*

Proof. Again, following the *general strategy* 3.2.1, our first step is to characterize the polyhedral cone

$$\ker \mathcal{Y} I_r I_\kappa \cap \mathbb{R}^n_+ \tag{3.5.2.1}$$

Because of the condition $\delta = 0$, $\theta = 0$. Thus the task is reduced to solve the *Feinberg's cone* $Q_f \in \mathbb{R}^n_+$. Moreover, under the weakly reversibility and the single linkage conditions, Theorem 2.4.9 mandates that *Feinberg's cone* Q_f is the direct sum of l orthogonal subspaces. Each one of the subspace is generated by a single vector. We will denote these vectors as

$\hat{\boldsymbol{\xi}}_1, \hat{\boldsymbol{\xi}}_2, ..., \hat{\boldsymbol{\xi}}_l \in \bar{\mathbb{R}}^n_+$. In fact, the structure of $\hat{\boldsymbol{\xi}}_i$ is simple as follows,

$$\begin{cases} \hat{\boldsymbol{\xi}}_1 & = (\underbrace{\boldsymbol{\xi}_1}_{n_1}, \underbrace{0, ..., 0}_{n-n_1}) \\ \hat{\boldsymbol{\xi}}_2 & = (\underbrace{0, ..., 0}_{n_1}, \underbrace{\boldsymbol{\xi}_2}_{n_2}, \underbrace{0, ..., 0}_{n-n_1-n_2}) \\ ... & \\ \hat{\boldsymbol{\xi}}_l & = (\underbrace{0, ..., 0}_{n-n_l}, \underbrace{\boldsymbol{\xi}_l}_{n_l}) \end{cases} \tag{3.5.2.2}$$

where $\boldsymbol{\xi}_i \in \mathbb{R}^{n_i}_+$.

Clearly, Q_f is isomorphic to a single point

$$\boldsymbol{\xi} = (\boldsymbol{\xi}_1, \boldsymbol{\xi}_2, ..., \boldsymbol{\xi}_l) \in \bigoplus_1^l \mathbb{P}^{n_i} \tag{3.5.2.3}$$

Next, in order to solve the system of equations, $\boldsymbol{\xi}$ as a point in the direct product of projective spaces $\bigoplus_1^l \mathbb{P}^{n_i}$, should also be a point in the generalized deformed toric variety in this system. Moreover, due to Lemma 3.1.13, the Krull dimension of the generalized deformed toric variety is given by the dimension of $\mathcal{Y}^+$. By lemma 2.3.5, the rank of $\mathcal{Y}^+$ is equal to

$$s + l = \sum_1^l (n_i - 1) - \delta + l = n - l - \delta + l = n \tag{3.5.2.4}$$

Then by an argument similar to the argument made for the single linkage class, the proof is completed. □

CHAPTER 4
BELOUSOV-ZHABOTINSKY REACTION

In this chapter, the Belousov-Zhabotinsky (BZ) reaction is investigated for its own interesting and complex dynamic behavior, especially the bifurcation phenomenon that the reaction exhibits. The mathematical analysis of the Belousov-Zhanbotinsky reaction has been mainly focused on the numerical simulation, which has been proved a great success in modelling the chemical reaction mechanisms. However, it is also interesting to know the parameter values where the bifurcations occur by a robust algorithm. The BZ reaction system is given by a weighted directed graph and a weighted bipartite graph. Mass action kinetics is used to model the system. We examine the bifurcation surface of the BZ reaction system by applying the chemical reaction network theory (CRNT) and the Hopf Bifurcation computing method developed by Guckenheimer [57, 58]. With the help of the singularity theory, the norm form of the BZ reaction is investigated and properties of bifurcations are also discussed.

While most of the research that has been done so far has been focusing on the computer simulation of the reaction, we try to understand and examine this reaction by augmenting the equilibrium conditions such that instead of looking for a singular point of a system, we now look for an isolated, regular point. The theoretical background is reviewed in the section 4.3, and the result of the application will be presented in section 4.5.

4.1 Chemistry

The BZ reaction, is a family of interesting, and also complicated reactions which involve a non-equilibrium thermodynamic behavior, resulting in the establishment of a nonlinear chemical oscillator. One specific example of the BZ reaction involves the oxidation of an organic species such as malonic acid by an acidified bromated solution in the presence of a metal ion catalyst. The importance of the reaction lies in the fact that the reaction is not dominated by equilibrium thermodynamic behavior. For the historical survey, see an article by Winfree [98]. One of the most important steps made by previous chemists and mathematicians is the Oregnator model set up by Field, Koros and Noyes (1972) [44], which has significant influence on the following research.

Noticing that Clarke also investigated on the Hopf and saddle-node bifurcation surfaces [15], we put emphasis on the Hopf Algorithms,and the singularity theory rather than Hurwitz determinant.

4.2 Oregonator

As the simplest realistic model describing the oscillatory behaviour of the BZ reaction, the Oregonator has an enormous influence on the researches on the oscillatory dynamics.

The model is frequently written in the form as follows: The FKN mechanism is shown as following [43]:

Table 4.1: The rate constants of FKN mechanism

$(R1)$ $Br^- + HOBr + H^+ \leftrightharpoons Br_2 + H_2O$	$k_+ = 8 \times 10^9 M^{-2}s^{-1}$	$k_- = 110 s^{-1}$
$(R2)$ $Br^- + HOBr + H^+ \leftrightharpoons HOBr + HOBr$	$k_+ = 3 \times 10^6 M^{-2}s^{-1}$	$k_- = 2 \times 10^{-5} M^{-1}s^{-1}$
$(R3)$ $Br^- + BrO_3^{-1} + 2H^+ \leftrightharpoons HOBr + HBrO_2$	$k_+ = 2 M^{-3}s^{-1}$	$k_- = 3.2 M^{-1}s^{-1}$
$(R4)$ $HBrO_2 + HBrO_2 \leftrightharpoons HOBr + BrO_3^- + H^+$	$k_+ = 3 \times 10^3 M^{-1}s^{-1}$	$k_- = 1 \times 10^{-8} M^{-2}s^{-1}$
$(R5)$ $HBrO_2 + BrO_3^{-1} + H^+ \leftrightharpoons Br_2O_4 + H_2O$	$k_+ = 42 M^{-2}s^{-1}$	$k_- = 2.2 \times 10^3 s^{-1}$
$(R5a)$ $Br_2O_4 \leftrightharpoons 2BrO_2$	$k_+ = 7.4 \times 10^4 s^{-1}$	$k_- = 1.4 \times 10^9 M^{-1}s^{-1}$
$(R6)$ $Ce(III) + BrO_2 + H^+ \leftrightharpoons Ce(IV) + HBrO_2$	$k_+ = 8 \times 10^4 M^{-2}s^{-1}$	$k_- = 8.9 \times 10^3 M^{-1}s^{-1}$

By denoting all the chemical species with mathematical symbols,

Table 4.2: Identifiction of symbols for Oregonator model

c_1	$HBrO_2$
c_2	Br^-
c_3	M_{ox}
A	BrO_3^-
B	$CH_2(COOH)_2$
P	HOBr

The original FKN mechanism is represented as follow:

$$
\begin{aligned}
A + X_2 &\overset{k_{1\varrho}}{\to} X_1 + P \\
X_1 + X_2 &\overset{k_{2\varrho}}{\to} 2P \\
A + X_1 &\overset{k_{3\varrho}}{\to} 2X_1 + 2X_3 \\
2X_1 &\overset{k_{4\varrho}}{\to} A + P \\
B + X_3 &\overset{k_{c\varrho}}{\to} \frac{1}{2} f X_2
\end{aligned}
\tag{4.2.0.1}
$$

Moreover, since the species A, B and P are normally present in much higher concentrations than the dynamic intermediate species X, Y and Z and are assumed to be constant on the time scale of a few oscillations, ie. we can suppose $A = [\mathrm{BrO_3^-}]$, $B = [\mathrm{CH_2(COOH)_2}]$ and $P = [\mathrm{HOBr}]$ are time independent.

Moreover, since $A = [\mathrm{BrO_3^-}]$, $B = [\mathrm{CH_2(COOH)_2}]$ and $P = [\mathrm{HOBr}]$ are considered to be constant during the reaction, the information of the concentration of A and B can be encoded in the kinetic constants, by this way, the chemical reaction network can be simplified as follows:

$$X_2 \overset{k_1}{\to} X_1$$

$$X_1 + X_2 \overset{k_2}{\to} \square$$

$$X_1 \overset{k_3}{\to} 2X_1 + 2Z$$

$$2X_1 \overset{k_4}{\to} A$$

$$X_3 \overset{k_c}{\to} \frac{1}{2} f X_2 \tag{4.2.0.2}$$

where

$$k_1 = k_{1o}A. \;\; k_2 = k_{2o}, \;\; k_3 = k_{3o}A, \;\; k_4 = k_{4o} \;\; k_{co} = k_c B \tag{4.2.0.3}$$

The complex graph and the complex-species graph defined in Chapter 2 are shown in Figure 4.1

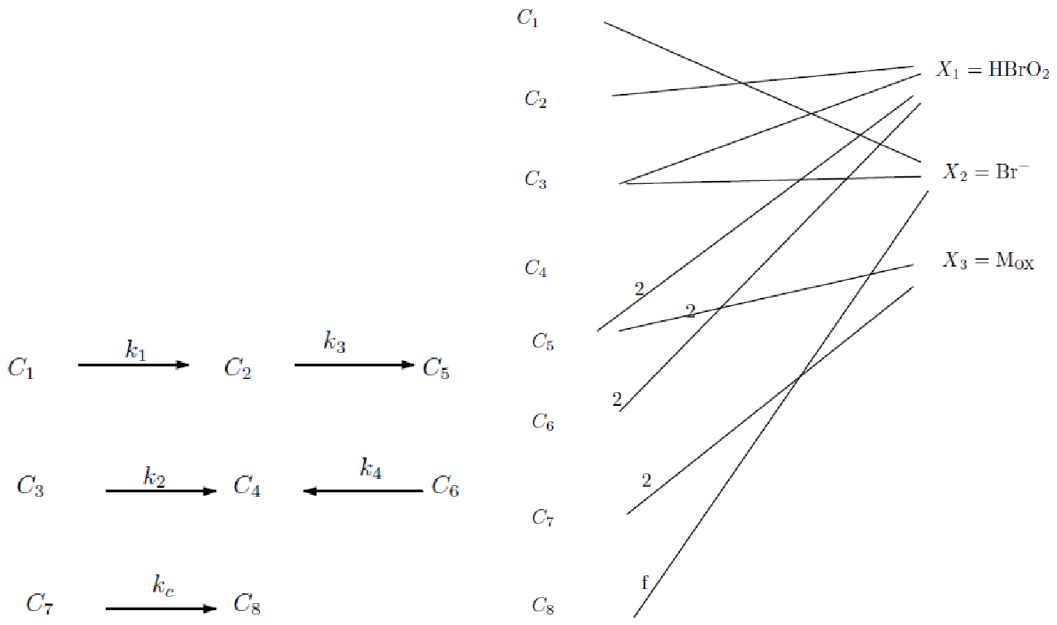

(a) Complexes Graph (b) Complex-Species Graph

Figure 4.1: Complexes Graph and Complex-Species Graph

$$K = \begin{pmatrix} 0 & 0 & 0 & 0 & 0 & 0 & 0 & 0 \\ k_1 & 0 & 0 & 0 & 0 & 0 & 0 & 0 \\ 0 & 0 & 0 & 0 & 0 & 0 & 0 & 0 \\ 0 & 0 & k_2 & 0 & 0 & k_4 & 0 & 0 \\ 0 & k_3 & 0 & 0 & 0 & 0 & 0 & 0 \\ 0 & 0 & 0 & 0 & 0 & 0 & 0 & 0 \\ 0 & 0 & 0 & 0 & 0 & 0 & 0 & 0 \\ 0 & 0 & 0 & 0 & 0 & 0 & k_c & 0 \end{pmatrix}, \quad L = \begin{pmatrix} -k_1 & 0 & 0 & 0 & 0 & 0 & 0 & 0 \\ k_1 & -k_3 & 0 & 0 & 0 & 0 & 0 & 0 \\ 0 & 0 & -k_2 & 0 & 0 & 0 & 0 & 0 \\ 0 & 0 & k_2 & 0 & 0 & k_4 & 0 & 0 \\ 0 & k_3 & 0 & 0 & 0 & -k_4 & 0 & 0 \\ 0 & 0 & 0 & 0 & 0 & 0 & 0 & 0 \\ 0 & 0 & 0 & 0 & 0 & 0 & -k_c & 0 \\ 0 & 0 & 0 & 0 & 0 & 0 & k_c & 0 \end{pmatrix} \tag{4.2.0.4}$$

To sum up, the system defines the following equation.

$$\dot{\mathbf{c}} = Y I_a I_\kappa \Phi(\mathbf{c}), \text{ with } \Phi(\mathbf{c}) = (\mathbf{c}^{\mathcal{Y}_1}, \mathbf{c}^{\mathcal{Y}_2}, \cdots, \mathbf{c}^{\mathcal{Y}_n})^T \tag{4.2.0.5}$$

where

$$\mathcal{Y} = \begin{pmatrix} 0 & 1 & 1 & 0 & 2 & 2 & 0 & 0 \\ 1 & 0 & 1 & 0 & 0 & 0 & 0 & \frac{1}{2}f \\ 0 & 0 & 0 & 0 & 2 & 0 & 1 & 0 \end{pmatrix}, \qquad I_a = \begin{pmatrix} -1 & 0 & 0 & 0 & 0 \\ 1 & 0 & -1 & 0 & 0 \\ 0 & -1 & 0 & 0 & 0 \\ 0 & 1 & 0 & 1 & 0 \\ 0 & 0 & 1 & 0 & 0 \\ 0 & 0 & 0 & -1 & 0 \\ 0 & 0 & 0 & 0 & -1 \\ 0 & 0 & 0 & 0 & 1 \end{pmatrix} \tag{4.2.0.6}$$

$$I_\kappa = \begin{pmatrix} \kappa_1 & 0 & 0 & 0 & 0 & 0 & 0 & 0 \\ 0 & 0 & \kappa_2 & 0 & 0 & 0 & 0 & 0 \\ 0 & \kappa_3 & 0 & 0 & 0 & 0 & 0 & 0 \\ 0 & 0 & 0 & \kappa_4 & 0 & 0 & 0 & 0 \\ 0 & 0 & 0 & 0 & 0 & 0 & \kappa_c & 0 \end{pmatrix}, \quad \Phi(\mathbf{c}) = (c_2, c_1, c_1c_2, 0, c_1^2c_2^2, c_1^2, 2c_3, c_2^{\frac{f}{2}})^T \tag{4.2.0.7}$$

hence

$$\mathcal{Y}I_aI_k = \begin{pmatrix} k_1 & k_3 & -k_2 & 0 & 0 & -2k_4 & 0 & 0 \\ -k_1 & 0 & -k_2 & 0 & 0 & 0 & \frac{1}{2}fk_5 & 0 \\ 0 & 2k_3 & 0 & 0 & 0 & 0 & -k_5 & 0 \end{pmatrix} \tag{4.2.0.8}$$

The mathematical model of this reaction would be described by the equation system

$$\dot{\mathbf{c}} = Y I_a I_k \Phi(c) \tag{4.2.0.9}$$

which is

$$\dot{c}_1 = k_3 a c_1 - 2k_4 c_1^2 + k_1 a c_2 - k_2 c_1 c_2 \tag{4.2.0.10}$$

$$\dot{c}_2 = -k_1 a c_2 - 2k_2 c_1 c_2 + f k_5 b c_3 \tag{4.2.0.11}$$

$$\dot{c}_3 = 2k_3 a c_1 - k_5 b c_3 \tag{4.2.0.12}$$

Table 4.3: Rate constants for Oregonator model: "Lo" and "Hi" Values

	Lo Value	Hi Value
k_1	$2\text{M}^{-3}\text{s}^{-1}$	$2\text{M}^{-3}\text{s}^{-1}$
k_2	$10^6\text{M}^{-2}\text{s}^{-1}$	$2 \times 10^6\text{M}^{-2}\text{s}^{-1}$
k_3	$10\text{M}^{-2}\text{s}^{-1}$	$2000\text{M}^{-2}\text{s}^{-1}$
k_4	$2000\text{M}^{-1}\text{s}^{-1}$	$4 \times 10^8\text{M}^{-1}\text{s}^{-1}$
kc	$1\text{M}^{-1}\text{s}^{-1}$	$1\text{M}^{-1}\text{s}^{-1}$

Most of the mathematical analysis of Belousov-Zhabatinsky reaction are based on the simplified dimensionless version of the Oregonator. Mazzotti and Morbidelli and Serravalle proposed a modified model of the Oregonator [75], which examined the effect of reactant concentrations (a = $[BrO_3^-]$, b = $[CH_2(COOH)_2]$)has been investigated. In this section, we will incorporate a similar nondimensionless approach as in Tyson [96] in order to perform a numerical simulation and also verify analytical results.

First, let

$$c_1 = \frac{c_1}{c_{10}}, c_2 = \frac{c_2}{c_{20}}, c_3 = \frac{c_3}{c_{30}}, \tau = \frac{t}{t_0}, a = \frac{A}{A_0}, b = \frac{B}{B_0} \tag{4.2.0.13}$$

Where

$$c_{01} = \frac{k_3 A_0}{2k_4}, c_{20} = \frac{k_3 A_0}{k_2}, c_{30} = \frac{(k_3 A_0)^2}{k_4 B_0}, t_0 = \frac{1}{B_0} \tag{4.2.0.14}$$

Some simple algebraic calculation leads to the following dimensionless equations

$$\begin{aligned} \epsilon_1 \frac{dx_1}{d\tau} &= aqx_2 - x_1x_2 + x_1(a - x_1) \\ \epsilon_2 \frac{dx_2}{d\tau} &= -qax_2 - x_1x_2 + fk_cbx_3 \\ \frac{dx_3}{d\tau} &= ax_1 - k_cbx_3 \end{aligned} \tag{4.2.0.15}$$

where

$$\epsilon_1 = \frac{k_c}{k_3}, \epsilon_2 = \frac{2k_c k_4}{k_2 k_3}, q = \frac{2k_1 k_4}{k_2 k_3} \tag{4.2.0.16}$$

The numerical simulation is performed in MATLAB, with ode solver "ode15s", which has been successfully applied to stiff differential equation systems.

Moreover, the orbit generated by $c_2(t), c_3(t)$ has also been plotted.

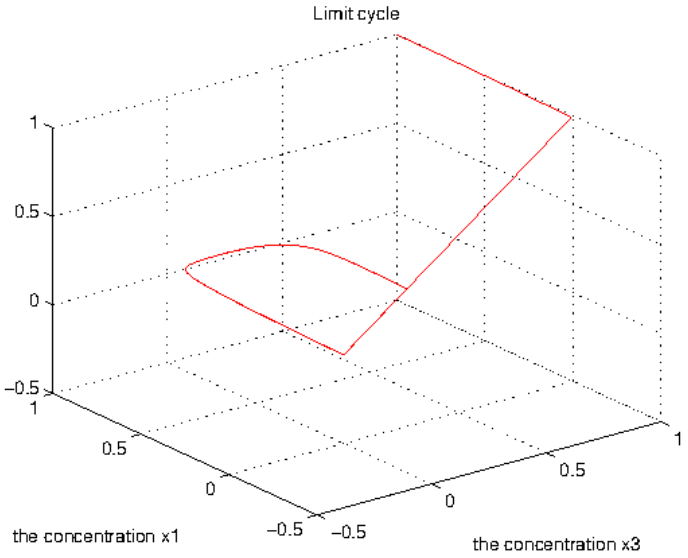

Figure 4.2: The trajectory of the Oregonator

Notice the trajectory of the concentration vectors start from $(1, 1)$, then enters an orbit.

Theorem 4.2.1 (Hopf [56]). *Suppose that the system* $\dot{x} = f_\mu(x), (x, \mu) \in \mathbb{R}^n \times \mathbb{R}$ *has an quilibrium* (x_0, μ_0) *at which the following properties are satisfied:*

(H1) $D_x f_{\mu_0}(x_0)$ *has a simple pair of pure imaginary eigenvalues and no other eigenvalues with zero real parts.*

Then (H1) implies that there is a smooth curve of equilibria $(x(\mu), \mu)$ *with* $x(\mu_0) = x_0$. *The*

eigenvalues $\lambda(\mu), \bar{\lambda}(\mu)$ *of* $D_x f_{\mu_0}(x(\mu))$ *which are imaginary at* $\mu = \mu_0$ *vary smoothly with* μ. *If, moreover,*

(H2)

$$\frac{d}{d\mu}(Re\lambda(\mu))|_{\mu=\mu_0} = d \neq 0 \tag{4.2.0.17}$$

then there is a unique three-dimensional center manifold passing through $(x_0, \mu_0) \in \mathbb{R}^n \times \mathbb{R}$ *and a smooth system of coordintes (preserving the planes* $\mu =$ *const.) for which the Talyor expansion of degree 3 on the center manifold is given by (3.4.8). If* $a \neq 0$, *there is a surface of periodic solutions in the center manifold which has quadratic tangency with the eigenspace of* $\lambda(\mu_0), \bar{\lambda}(\mu_0)$ *agreeing to second order with the paraboloid* $\mu = -(a/d)(x^2 + y^2)$. *If* $a < 0$, *then these periodic solutions are stable limit cycles, while if* $a > 0$, *the periodic solutions are repelling.*

4.3 Review of Hopf Bifurcation Algorithms

In this section, we will overview the mathematical preliminary. Consider a n-dimensional system of ordinary differential equations

$$\dot{x} = f(x, \alpha; \beta) \tag{4.3.0.18}$$

where $x \in \mathbb{R}^n$ and $f : U \subset \mathbb{R}^n \times \mathbb{R} \times \mathbb{R} \to \mathbb{R}^n$. The equilibrium of the system are defined as x where $f(x, \lambda; \beta) = 0$. The bifurcation may occur when the parameter $\beta \in \mathbb{R}$ changes,which

is called bifurcation parameters. The Jacobian matrix of the vector field is defined as follows:

$$J(x, \alpha; \beta) := \frac{\partial f}{\partial x}(x, \alpha; \beta) \tag{4.3.0.19}$$

One is interested in the bifurcation locus when $J(x, \alpha; \beta)$ has pure imaginary eigenvalues at the equilibrium. Instead of solving for the eigenvalues along the bifurcation parameter space, one could study this by augmenting our system by another c^2-smooth function $g : \mathbb{R}^n \times \mathbb{R} \times \mathbb{R} \to \mathbb{R}^{n+1}$. The new system

$$F(x, \alpha; \beta) = \begin{pmatrix} f(x, \alpha; \beta) \\ g(x, \alpha; \beta) \end{pmatrix} \tag{4.3.0.20}$$

vanishes at the Hopf locus, moreover, the function g can be obtained in the way that the Hopf points are regular solution of the augmented system. Consider the characteristic polynomial

$$p(\lambda) = a_0 + a_1\lambda + a_2\lambda^2 + ... + \lambda^n \tag{4.3.0.21}$$

p has the nonzero root pair $\lambda, -\lambda$ if only if

$$p(\lambda) + p(-\lambda) = p(\lambda) - p(-\lambda) = 0 \tag{4.3.0.22}$$

Substituting $z = \lambda^2$ to the above two equations leads to new system of equations

$$\begin{pmatrix} r_e(z) \\ r_0(z) \end{pmatrix} = 0 \tag{4.3.0.23}$$

where

$$r_e(z) = p(\lambda) + p(-\lambda)|_{\lambda^2=z}, r_e(z) = p(\lambda) - p(-\lambda)|_{\lambda^2=z} \tag{4.3.0.24}$$

The above functions share a common root if and only if they share a common factor. Let $\mathcal{S}_0$ denote the matrix obtained from an arbitrary matrix, $\mathcal{S}$ by deleting the rows 1 and 2, $\mathcal{S}_1$ denote the matrix obtained from $\mathcal{S}$ by deleting the rows 1 and 3. Then, we have the following result

Theorem 4.3.1. *[57] Let $\mathcal{S}$ be the Sylvester matrix for the polynomial r_e and r_o. Then the Jacobian has precisely on pair of pure imaginary eigenvalues if*

$$\det \mathcal{S} = 0 \ \textit{and} \ \det \mathcal{S}_1 \det \mathcal{S}_0 > 0 \tag{4.3.0.25}$$

Proof. From the elementary properties of resultants, $\det \mathcal{S} = 0$ if only if r_e and r_o share a common factor, and also,

$$\det \mathcal{S}_0 + \det \mathcal{S}_1 z = h_1(z) r_e(z) + h_2(z) r_o(z) \tag{4.3.0.26}$$

for two polynomials $h_1, h_2 \in \mathbb{R}[z]$. The existence of solution of $\det \mathcal{S}_0 + \det \mathcal{S}_1 z = 0$ implies that there is an unique, negative real common root of r_e, r_o. □

Corollary 4.3.2. *Assume the characteristic polynomial of the system $\dot{x} = f(x, \alpha, \beta)$ with degree 3 is*

$$p(\lambda) = a_0 + a_1\lambda + a_2\lambda^2 + \lambda^3 \tag{4.3.0.27}$$

if $a_0 - a_1 a_2 = 0$ and $a_1 > 0$, then the system undergoes a Hopf bifurcation.

Proof.

$$\det \mathcal{S} = a_0 - a_1 a_2, \quad \det \mathcal{S}_1 \det \mathcal{S}_2 = a_1 \tag{4.3.0.28}$$

□

4.4 Hopf Algorithms and Oregonator

The Oregonator model of Belousov-Zhanbotinsky reaction exhibits an unstable steady state. It also has the capacity to exhibit a limit cycle. There have been tremendous experimental and analytic results on Belousov-Zhabatinsky Reaction, particularly on the Oregonator. However, in general, the explicit close form of the bifurcation surface is not expected. The special structure of the Hopf Bifurcation points allows us to do so. To better understand the mechanism of Belousov-Zhabatinsky reaction, it is reasonable to investigate the original Oregonator rather than the dimensionless version.

$$\dot{c}_1 = k_3 a c_1 - 2k_4 c_1^2 + k_1 a c_2 - k_2 c_1 c_2$$

$$\dot{c}_2 = -k_1 a c_2 - 2k_2 c_1 c_2 + f k_5 b c_3$$

$$\dot{c}_3 = 2k_3 a c_1 - k_5 b c_3 \tag{4.4.0.29}$$

The characteristic polynomial of the Jacobian matrix is as follows

$$p(\lambda) = \lambda^3 + \sum_{i=0}^{2} a_i(c_1, c_2, c_3, k_1, k_2, k_3, k_4; a, b, k_5, f)\lambda^i \tag{4.4.0.30}$$

where

$$a_2 = -ak_1 - c_1 k_2 - c_2 k_2 + ak_3 - 4c_1 k_4 - bk_5 \tag{4.4.0.31}$$

$$a_1 = -2ac_2 k_1 k_2 + a^2 k_1 k_3 + ac_1 k_2 k_3 - 4ac_1 k_1 k_4 - 4c_1^2 k_2 k_4 - abk_1 k_5 -$$

$$bc_1 k_2 k_5 - bc_2 k_2 k_5 + abk_3 k_5 - 4bc_1 k_4 k_5 \tag{4.4.0.32}$$

$$a_0 = -2abc_2 k_1 k_2 k_5 + a^2 bk_1 k_3 k_5 + abfk_1 k_3 k_5 + abc_1 k_2 k_3 k_5 - bc_1 fk_2 k_3 k_5 -$$

$$4abc_1 k_1 k_4 k_5 - 4bc_1^2 k_2 k_4 k_5 \tag{4.4.0.33}$$

By Corollary 4.3.2, the locus of the Hopf bifurcation can be examined by inspecting the vanishing locus of

$$a_0 - a_1 a_2 \tag{4.4.0.34}$$

.

The Hopf bifurcation locus in the (f, k_5) plane will be first investigated, followed by the study of the Hopf bifurcation surface in the $(f, a/b)$ plane. The reason why we study $(f, a/b)$ instead of (f, a, b) is explained in the last section. The locus of Hopf Bifurcation points are computed as a curve parametrized by c_1^*. For a given c_1^*,

$$c_3^* = \frac{2k_3 a c_1^*}{k_5 b}, \quad c_2^* = \frac{2k_3 a f c_1^*}{k_1 a + 2k_1 c_1} \tag{4.4.0.35}$$

Notice that the equilibrium c_2^* is independent of k_5, hence the first equation of the system is independent of k_5, which can be used to solve for the bifurcation data $f(c_1^*)$, and the determining function $\det \mathcal{S}$ depends quadratically on k_5. Therefore, we could can solve equation 4.4.0.34 for the values k_5^+ where the Hopf bifurcation occurs. The main ideal is similar to the one presented in [57] except for the dependence of the bifurcation parameters.

1. Choose c_1^*
2. Evaluate c_2^*, c_3^* symbolically
3. Reduce f symbolically by substituting c_1^*, c_2^*, c_3^* into the first equation of the system

4. Substitute $c_2^*, c_3^*, f(c_1^*)$ expressions into the the Hopf determining conditions $a_0 - a_1 a_2$ and reduce to k_5

5. Check the sign of a_1

And the parametrized bifurcation surface are drawn as follows for different parameters.

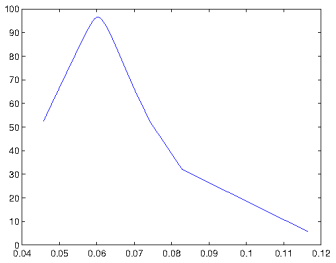

(a) The bifurcation surface1

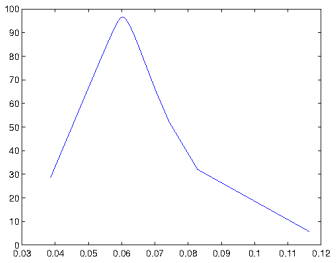

(b) The bifurcation surface2

Where the first is drawn based on the parameter $c_{10} \in (1e-7, 1e-4)$, and the second is based on $c_{10} \in (1e-7, 1.5e-4)$

4.5 Lyapunov-Schmidt Reduction and Oregonator

Singularity theory has been proved a successful tool to study Bifurcation and other nonlinear behaviours [53, 54]. The Lyapunov-Schmidt reduction, as a powerful tool to reduce the dimension of the problem, plays an important role in the singularity analysis. In this section, the simplified Oregonator is investigated by using singularity theory techniques to study the behaviour of the periodic solutions bifurcating from the equilibrium solution of the Oregonator model. Golubitsky' classification invariants of the degenerate Hopf bifurcation are

also been computed, such that we are able to establish the contact equivalence relationship between the Oregonator and generalized Hopf Bifurcation germs of codimension 1.

The Oregonator model has been described in the first section, see 4.2.0.15. Corresponding to a parameter set (q, f), there is a steady state of the system, namely,

$$\begin{aligned} x_0 &= \frac{1}{2}\left(\sqrt{f^2+6fq-2f+q^2+2q+1}-f-q+1\right), \\ y_0 &= \frac{-q\sqrt{f^2+6fq-2f+q^2+2q+1}+3fq+q^2+q}{4q}, \\ z_0 &= \frac{1}{2}\left(\sqrt{f^2+6fq-2f+q^2+2q+1}-f-q+1\right) \end{aligned} \tag{4.5.0.36}$$

As the numerical analysis done in the last section, the bifurcation locus has been detected. First, it is convenient to convert our coordinates in 4.5.0.36 so that the origin of $\mathbb{R}^4$ becomes the steady state.

$$x = x_0 + u, y = y_0 + v, z_3 = z_0 + w \tag{4.5.0.37}$$

After introducing these incremental variables, the systems becomes

$$\dot{u} = e_1(qv + qy_0 - u^2 - uv - 2ux_0 - uy_0 + u - vx_0 - x_0^2 - x_0y_0 + x_0) \tag{4.5.0.38}$$

$$\dot{v} = e_2(fw + fz_0 - qv - qy_0 - uv - uy_0 - vx_0 - x_0y_0) \tag{4.5.0.39}$$

$$\dot{w} = u - w + x_0 - z_0 \tag{4.5.0.40}$$

The change of the coordinate reduces the original problem to the form in 4.5.0.40 for the convenience of the calculation of the invariants.

4.6 Generalized Hopf bifurcation

First of all, the notion of the germs is introduced.

Definition 4.6.1. [53] Two functions $f, g \in \mathbb{C}^\infty$ are equal as germs if there is some neighbourhood of the origin on which they coincide.

The introduction of germs enables one to focus on the local behaviour of some fixed point, i.e. the primary concern would be constrained in a sufficiently small neighbourhood of some fixed point.

Example 4.6.2. [53]

$$f(x,\lambda) = x, g(x,\lambda) = \begin{cases} x, & \text{if } \lambda \leq 1, \\ x + e^{-\frac{1}{\lambda - 1}}, & \text{if } \lambda > 1 \end{cases} \tag{4.6.0.41}$$

By our definition of the germs, the two functions f and g are equivalent since they coincide in the small disk $\{x^2 + \lambda^2 \leq 1\}$.

Definition 4.6.3. Two germs $g(\mathbf{c}, \lambda), h(\mathbf{c}, \lambda)$ at $(0, \lambda_1)$ are contact equivalent if there exists a smooth function of changes of coordinates $\mathbf{c}(x, \lambda)$, a deforming of parameter $\Lambda(\lambda)$, and a invertible function $S(x, \lambda)$ such that the relation

$$g(x,\lambda) = S(x,\lambda)h(\mathbf{c}(x,\lambda), \Lambda(\lambda)) \tag{4.6.0.42}$$

The change of the coordinates $\mathbf{c}$ and Λ must also satisfy:

$$c(0,\lambda)=0, \quad \Lambda(\lambda_1)=\lambda_2, \quad \det D_x(0,\lambda_1)\neq 0, \frac{d\Lambda}{\lambda}(\lambda_1)>0 \tag{4.6.0.43}$$

Geometrically, if two germs are contact equivalent, they have the same qualitative behaviour locally. In our example, as investigating the local bifurcation behaviour, the germs of the contact equivalence form an equivalent class, which all have the same number of periodic orbits for corresponding values of parameter value λ. Moreover, they also have the same qualitative feature of their amplitude graphs. This kind of the problem are extensively discussed in [53] as 'recognition problem' in the study of the singularity theory.

Theorem 4.6.4 (Hopf)**.** *[53] Assume the system*

$$\dot{x}=F(x,\lambda)=0 \tag{4.6.0.44}$$

satisfies the following assumptions:

1. *$D_xF(0,\lambda^*)$ has a pair of pure imaginary eigenvalues $\pm\theta i$*

2. *$D_xF(0,\lambda^*)$ has no other eigenvalues lying on the imaginary axis.*

Then there exists a smooth germ $g(x,\lambda) = xr(x^2,\lambda)$ *where* $r(0,\lambda) = 0$*, such that the local solutions to* $g(x,\lambda) = 0$ *are correspondence with the orbits of small amplitude periodic solutions of the original system 4.6.0.44*

By this theorem, the study of the periodic solutions of the nonlinear system can be surprisingly reduced to the study of the steady states. It also possesses the potential to study the degenerate Hopf bifurcations where the traditional analysis technique fails.

Corollary 4.6.5. *If the system 4.6.0.44 satisfies the conditions in the above theorem and*

$$r_z(0,\lambda) \neq 0 \text{ and } r_\lambda r(0,\lambda^*) \tag{4.6.0.45}$$

then g belongs to one of the two contact equivalent classes(Pitchfork)

$$\epsilon x^3 + \delta x \tag{4.6.0.46}$$

where $\epsilon = \operatorname{sgn} r_z(0,0)$ *and* $\delta = \operatorname{sgn} r_\lambda$

Thus, the coefficient μ determines the direction of the bifurcation.

$$\mu = -\frac{r_z}{r_\lambda} \tag{4.6.0.47}$$

We have computed $r_z(0, \lambda^*, q)$ at the two bifurcation points of the Oregonator. First, the operator is defined as follows.

$$\Phi(u, v, f) = \frac{\partial}{\partial t} \begin{pmatrix} u \\ \\ v \end{pmatrix} + L \begin{pmatrix} u \\ \\ v \end{pmatrix} + N(u, v, f) \tag{4.6.0.48}$$

where the linear part given by the Jacobian,

$$A_0 = \begin{pmatrix} -2x_0\mathrm{e}1 - y_0\mathrm{e}1 + \mathrm{e}1 & \mathrm{e}1q - \mathrm{e}1x_0 & 0 \\ \\ -\mathrm{e}2y_0 & -\mathrm{e}2q - \mathrm{e}2x_0 & \mathrm{e}2f \\ \\ 1 & 0 & -1 \end{pmatrix} \tag{4.6.0.49}$$

and the nonlinear part is given by

$$N(u, v) = \begin{pmatrix} e_1(-u^2 - uv) \\ \\ e_2(-uv) \\ \\ 0 \end{pmatrix} \tag{4.6.0.50}$$

The characteristic polynomial corresponding to the system is

$$p(\lambda) = \alpha_0 + \alpha_1\lambda + \alpha_2\lambda^2 + \lambda^3 \tag{4.6.0.51}$$

where

$$\alpha_0 = -e_1e_2fq + e_1e_2fx_0 + 2e_1e_2qx_0 + 2e_1e_2qy_0 - e_1e_2q + 2e_1e_2x_0^2 - e_1e_2x_0$$

$$\alpha_1 = 2e_1e_2qx_0 + 2e_1e_2qy_0 - e_1e_2q + 2e_1e_2x_0^2 + 2e_1x_0 + e_1y_0 - e_1 + e_2q + e_2x_0$$

$$\alpha_2 = 2e_1x_0 + e_1y_0 - e_1 + e_2q + e_2x_0 + 1 \tag{4.6.0.52}$$

From the analysis in the last section, the bifurcation happens when

$$\alpha_0 - \alpha_1\alpha_2 \tag{4.6.0.53}$$

Moreover, from simple algebra, we know that, when the bifurcation occurs, the system admits two simple eigenvalues

$$\lambda_{1,2} = \pm ai = \pm\sqrt{\alpha_1}i \tag{4.6.0.54}$$

In order to determine the stability of the local bifurcation, it is necessary to compute the following

$$r_z(0, f*), \text{ and } r_f \tag{4.6.0.55}$$

where $g(x, f) = xr(x^2, f)$ is the reduced determining germ after the Lyapunov-Schmidt Reduction. For our calculation,the whole procedure of the Lyapunov-Schmidt Reduction is not included in this chapter, however, the formulae introduced in [58] are used, and performed

in the MATHEMATICA program [99].

$$r_f(0, f^*) = \frac{1}{2}\frac{\partial \operatorname{trace} A_0(f^*)}{\partial f} \tag{4.6.0.56}$$

$$r_z(0, f^*) = \frac{1}{4}\operatorname{Re}\{\bar{\mathbf{d}}^t \cdot [\mathbf{d}^2 F(\mathbf{c}, \mathbf{b}_0) + \mathbf{d}^2 F(\bar{\mathbf{c}}, \mathbf{b}_2) + \frac{1}{4} d^3 F(\mathbf{c}, \mathbf{c}, \bar{\mathbf{c}})]\} \tag{4.6.0.57}$$

where $c, d, b_0, b_2 \in \mathbb{C}^n$ are defined as follows

$$\begin{aligned} A_0 \cdot \mathbf{c} &= -ai \cdot \mathbf{c} \\ A_0^t \cdot \mathbf{d} &= ai \cdot \mathbf{d} \\ A_0 \cdot \mathbf{b}_0 &= -\frac{1}{2}\mathbf{d}^2 F(\mathbf{c}, \bar{\mathbf{c}}) \\ (A_0 + 2iI) \cdot \mathbf{b}_2 &= -\frac{1}{4}\mathbf{d}^2 F(\mathbf{c}, \bar{\mathbf{c}}) \end{aligned} \tag{4.6.0.58}$$

$$r_f(0, f^*) = \frac{1}{2}\frac{\partial \operatorname{trace} A_0(f^*)}{\partial f} \tag{4.6.0.59}$$

$$= \frac{1}{2}\frac{\partial \operatorname{trace}(-2e_1 x_0 - e_1 y_0 + e_1 - e_2 q - e_2 x_0 - 1)}{\partial f} \tag{4.6.0.60}$$

$$\tag{4.6.0.61}$$

our parameter set is given from the reference

$$e_1 = 9.9 \times 10^3, e_2 = 1.98 \times 10^5, q = 4 \times 10^{-3} \tag{4.6.0.62}$$

then on the left hopf bifurcation point, we have

$$r_f(0, f_l^*) \approx 201114 > 0 \tag{4.6.0.63}$$

while on the right Hopf bifurcation point, we have

$$r_f(0, f_r^*) \approx -4077.6 < 0 \tag{4.6.0.64}$$

On the other hand,

$$\operatorname{sgn} r_z(0, f_l^*) = -1 \tag{4.6.0.65}$$

$$\operatorname{sgn} r_z(0, f_r^*) = -1 \tag{4.6.0.66}$$

Thus, the Oregonator system is contact equivalent to a supcritical pitchfork bifurcation on the low-f bifurcation, while it is equivalent to a subcritical pitchfork bifurcation on the high-f bifurcation.

CHAPTER 5
A MODEL OF THE (BIO)NANO PARTICLE CONFIGURATIONS

One of the fundamental problems in biochemical research is the development of suitable analytical techniques for the determination of the presence and concentration of bio-markers. This need has led to the development of techniques that have used the formation of "nanoparticle clustering" using the biomarkers as the mechanism for formation of the cluster. Here the nanoparticle is covered with a layer of antibody. The presence of an antigen with multiple binding sites permits the formation of a nanoparticle-antibody-antigen-antibody-nanoparticle complex which we henceforth call a nanoparticle cluster. Detection of these nanoparticle clusters is then connected to the concentration of the antigen in solution.

We note that two methods for detection of nanoparticles clusters have been presented in the recent literature. One technique that has been studied is to use the change in the magnetic moment to detect the configuration [18, 62, 69–71]. Another technique that has been developed for this is the use of dynamic light scattering to detect the presence of the configuration [1, 59, 74]. The presence of the resulting "nanoparticle cluster" can then be detected by the increase in the mean hydrodynamic radius of the nanoparticles in solution.

This chapter provides a theoretical modeling of the process of formation of nanoparticle clusters using the method of mass-action kinetics. Mass-action kinetics and stoichiometric modeling are common tools for the modeling of chemical reactions. However, the use of this model in modeling nanoparticle configurations has been extremely limited. We propose to

demonstrate that for deciding the kinetics of nanoparticle cluster agglomeration, the method of mass-action kinetics is in good agreement with experimental results.

Previous results have used statistical modeling [87,88,101,102], as well as graph-theoretical techniques [55, 60, 61], to analyze the relation between the detection of the clusters and the underlying concentration of the antibodies. See also [55] for a summary of the history of this problem to 1988.

This chapter considers the following model. Nanoparticles with a layer of antibody are placed in solution with antigens having two binding points for the antibodies. The nanoparticles with the attached ligand and antibody bind with the antigen to form 'dimer' nanoparticle clusters where the 'bond' is formed by the antibody-antigen-antibody complex. It is assumed in this model that only dimer nanoparticle configurations are formed as more complicated configurations having the structure of a larger graphical network represent higher entropy states that will occur only in extremely low concentrations.

We use a modified form of the model described in [55]. We assume: first, after transition to the steady-state that our system is at equilibrium. Second, the bond-forming processes at the sites are independent. Third, the bonding constants are dependent only on the site and not dependent on the configuration. Fourth, the system is well-mixed and in solution. Fifth, due to our interest in very low antigen concentrations that in addition to not forming ring complexes, the rarity of bond formation provides that the formation of complexes beyond dimer configurations is not main concern in this chapter, though we will give a generalization in section 6.

We also study the transition towards the steady-state for these solutions under two regimes. First is the case in which the binding sites on the antigen are symmetric and the second is the cases in which the binding sites are asymmetric with one site having a reaction rate 100 times the rate of the other. The reaction rates in this study are taken from the case where the antigen-antibody paring is associated with α-TSH [90] (TSH is Thyroid Stimulating Hormone, also known as thyrotopin.)

To simulate the case where there are 20 antibodies attached, rather than one ligand and one antibody is attached. We also study the situation where there the rates are 20 times higher.

The application of chemical reaction network theory (CRNT) to the nanoparticle-clustering model offers very limited information because this model lies in a special category where the parent chemical reaction network has deficiency one, and the subnetworks have their own deficiency zero. The advanced deficiency one algorithm implies that multistationarity is impossible in our model. However, the existence of a positive equilibrium is still unknown. Because all antibody molecules present at least two antigen binding sites per molecule, it is natural to look at a model which permits two ligands to bind each antigen. For simplicity, we assume that the antigen only allows two distinct epitopic sites (the linear complexes are the main subject of interest). Moreover, as the formation of the nanoparticle clustering is stepwise, it becomes more and more thermodynamically difficult to form bigger complexes. The probability(affinity) to form different complexes is encoded in the rate constants.

The content of this chapter is previously presented in [8].

5.1 The Experimental Data and Quantitative analysis

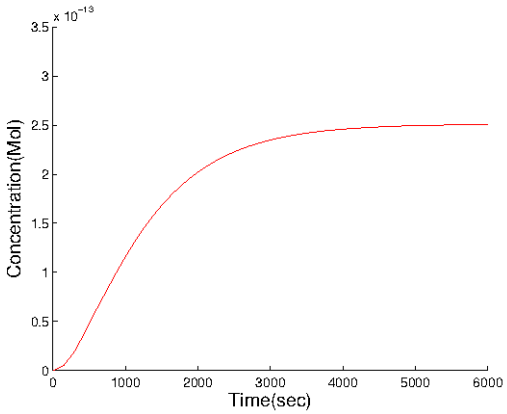

(a) r=1

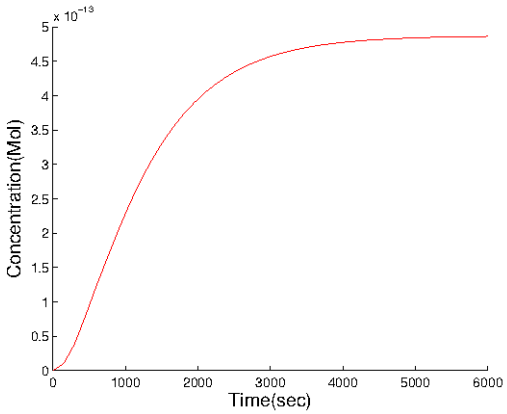

(b) r=2

Figure 5.1: Comparison 1 of the concentrations c_5 by changing the ratio r

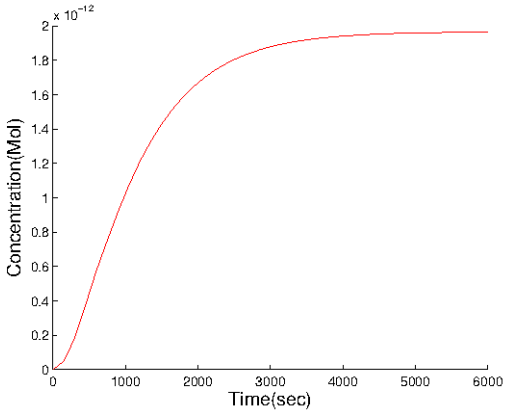

(a) r=10

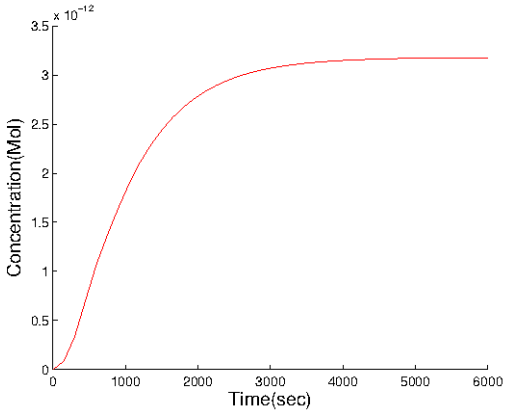

(b) r=20

Figure 5.2: Comparison 2 of the concentrations c_5 by changing the ratio r

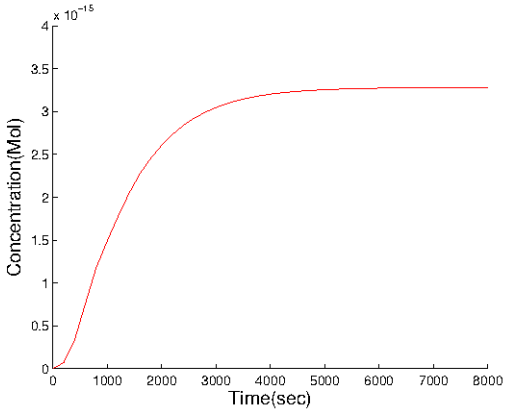

(a) k1=1000

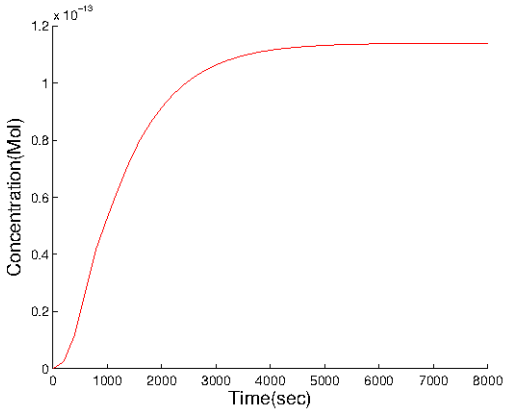

(b) k1=6000

Figure 5.3: Comparison 3 of the concentrations c_5 by changing the the rate constant k_1

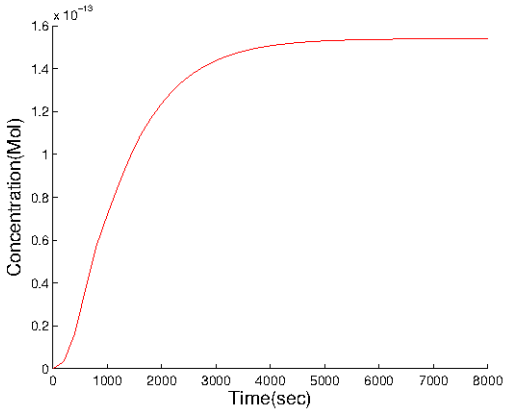

(a) k1=7000

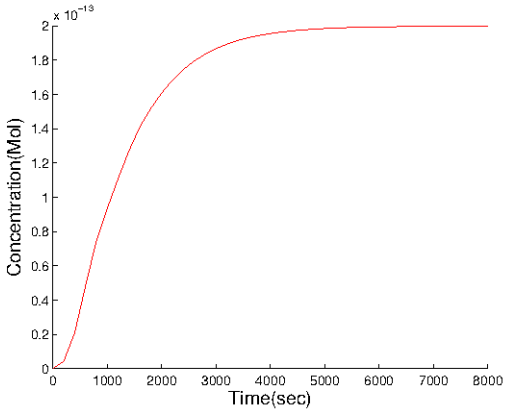

(b) k1=8000

Figure 5.4: Comparison 4 of the concentrations c_5 by changing the rate constant $k1$

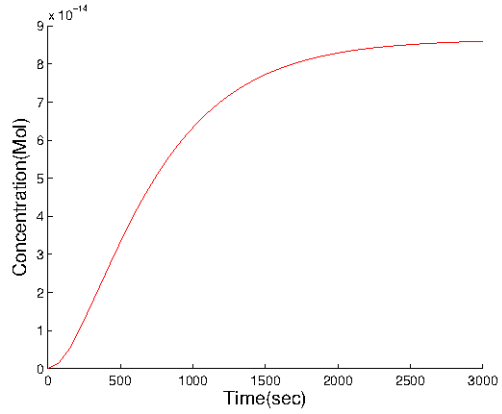

(a) k2=.0019

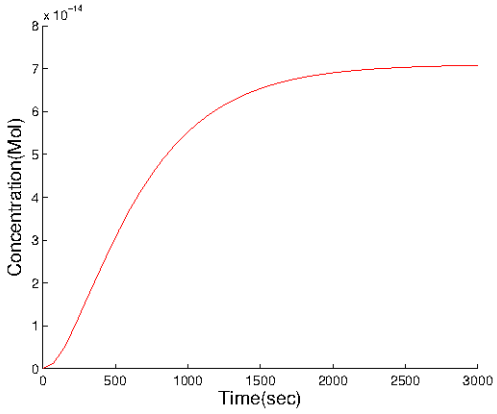

(b) k2=.0021

Figure 5.5: Comparison 1 of the concentrations c_5 by changing the the rate constant k_2

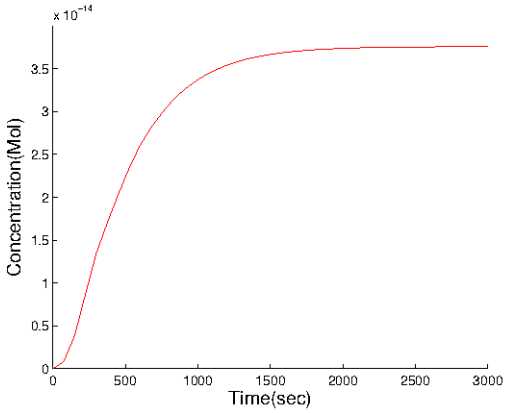

(a) k2=.0029

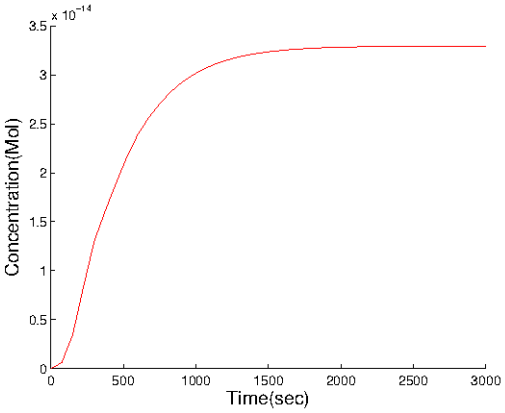

(b) k2=.0031

Figure 5.6: Comparison 2 of the concentrations c_5 by changing the rate constant $k2$

By changing the input parameters of the model, the numerical results matches the experiment data well. From the experiment data, we may exclude that the multistationarity or other unusual dynamical behaviors, such as oscillations, and chaos. It would be interesting to know whether the dynamical behavior exhibited in the experiment is coincidence with special

amounts of the reactants or it is more general situation. In the next sections, we give a rigorous mathematical proof of the existence and uniqueness of the positive equilibrium for any reaction rates κ or reactants amounts.

5.2 The uniqueness and the existence of the positive steady state

We assume a solution of nanoparticles, each with a layer of antibody and antigens with two distinct binding sites, such that the antibody will attach to either site, but potentially with different affinities.

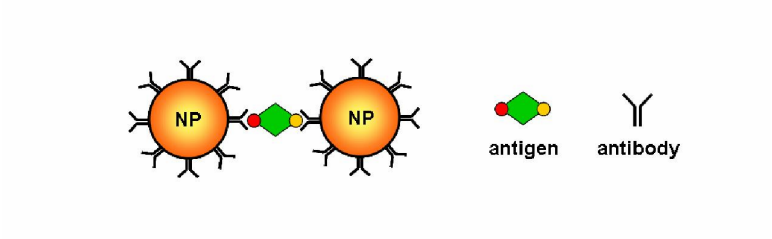

Figure 5.7: The reaction elements

This results in five species:

The proposed model therefore examines five species, S_1, S_2, S_3, S_4, and S_5, and eight reactions which are symbolically displayed in figure 5.8 and are listed below. The constants $k_1, \ldots, k_8$ are the rate constants for the reactions.

Table 5.1: The representation of the reactant species

S_1	the nanoparticle with a layer of antibodies
S_2	the antigen
S_3	the nanoparticle with a layer of antibodies conjugated to the antigen at the first binding site
S_4	the nanoparticle with a layer of antibodies conjugated to the antigen at second binding site
S_5	a pair of nanoparticle-antigen-nanoparticle conjugate

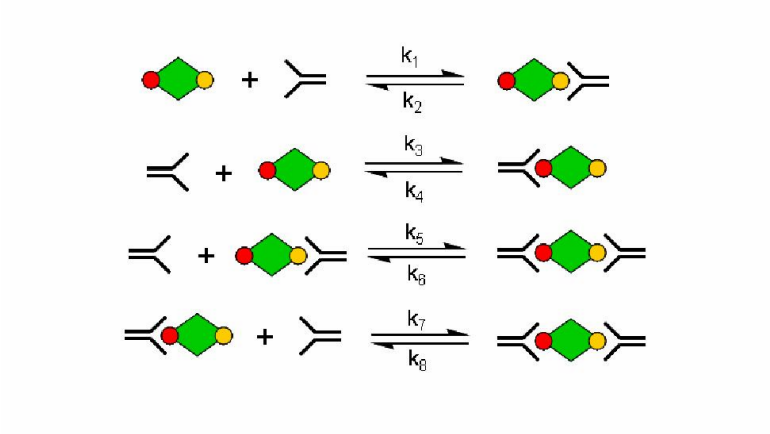

Figure 5.8: The reaction scheme

$$
\begin{aligned}
S_1 + S_2 &\xrightarrow{k_1} S_3 \\
S_3 &\xrightarrow{k_2} S_1 + S_2 \\
S_1 + S_2 &\xrightarrow{k_3} S_4 \\
S_4 &\xrightarrow{k_4} S_1 + S_2 \\
S_3 + S_2 &\xrightarrow{k_5} S_5 \\
S_5 &\xrightarrow{k_6} S_3 + S_2 \\
S_4 + S_2 &\xrightarrow{k_7} S_5 \\
S_5 &\xrightarrow{k_8} S_4 + S_2
\end{aligned}
\tag{5.2.0.1}
$$

Writing the concentration of the ℓ-th species by the variable x_ℓ the associated dynamical system that governs the concentrations of all of the species is given by the system of differential equations

$$
\begin{aligned}
\frac{dc_1}{dt} &= (-k_1 - k_3)c_1c_2 + k_2c_3 + k_4c_4 \\
\frac{dc_2}{dt} &= (-k_1 - k_3)c_1c_2 + k_2c_3 - k_5c_2c_3 + k_4c_4 - k_7c_2c_4 + (k_6 + k_8)c_5 \\
\frac{dc_3}{dt} &= k_1c_1c_2 - k_2c_3 - k_5c_2c_3 + k_6c_5 \\
\frac{dc_4}{dt} &= k_3c_1c_2 - k_4c_4 - k_7c_2c_4 + k_8c_5 \\
\frac{dc_5}{dt} &= k_5c_2c_3 + k_7c_2c_4 + (-k_6 - k_8)c_5. \qquad (5.2.0.2)
\end{aligned}
$$

Assuming that the distinctiveness of the binding sites and the supposition that the binding affinity of the antibody to theantigen is largely dependent on the local geometry of the binding site, we will assume that $k_1 = k_7, k_2 = k_8$ and that $k_3 = k_5, k_4 = k_6$. We will also assume that the disassociation rate constants k_2, k_4, k_6, k_8 are all equal to a constant μ.

Let r be the ratio of k_3 to k_1 and set $\lambda = k_1$. With this notation we can re-express the previous system as the following.

$$
\begin{aligned}
\frac{dc_1}{dt} &= (-(1 + r)\lambda)c_1c_2 + \mu(c_3 + c_4) \\
\frac{dc_2}{dt} &= (-(1 + r)\lambda)c_1c_2 - r\lambda c_2c_3 - \lambda c_2c_4 + \mu(c_3 + c_4 + 2c_5) \\
\frac{dc_3}{dt} &= \lambda c_1c_2 - r\lambda c_2c_3 + \mu(c_5 - c_3) \\
\frac{dc_4}{dt} &= r\lambda c_1c_2 - \lambda c_2c_4 + \mu(c_5 - c_4) \\
\frac{dc_5}{dt} &= r\lambda c_2c_3 + \lambda c_2c_4 - 2\mu c_5. \qquad (5.2.0.3)
\end{aligned}
$$

In the special case that $r = 1$ the dynamical system becomes

$$\begin{aligned}
\frac{dc_1}{dt} &= -2\lambda c_1 c_2 + \mu(c_3 + c_4) \\
\frac{dc_2}{dt} &= -\lambda c_2(2c_1 + c_3 + c_4) + \mu(c_3 + c_4 + 2c_5) \\
\frac{dc_3}{dt} &= \lambda c_2(c_1 - c_3) + \mu(c_5 - c_3) \\
\frac{dc_4}{dt} &= \lambda c_2(c_1 - c_4) + \mu(c_5 - c_4) \\
\frac{dc_5}{dt} &= \lambda c_2(c_3 + c_4) - 2\mu c_5. \qquad (5.2.0.4)
\end{aligned}$$

The space of steady state solutions is the intersection of the positive polyhedral cone by the affine toric variety [49] defined by the vanishing of the right hand sides of the differential equations defining the system. The toric variety that is defined by the system 5.2.0.3 is a 2-dimensional surface that is birational to $\mathbb{P}^2$. In particular the coordinates of the toric variety can be expressed as rational functions of the coordinates c_1 and c_2 of the point on the variety by the following formulae

$$\begin{aligned}
c_3 &= \frac{c_1 c_2(k_1k_4k_6 + k_1k_4k_8 + (k_1k_6k_7 + k_3k_6k_7)c_2)}{(k_2k_4k_6 + k_2k_4k_8) + (k_2k_6k_7 + k_4k_5k_8)c_2)} \\
c_4 &= \frac{c_1 c_2(k_2k_3k_6 + k_2k_3k_8 + (k_1k_5k_8 + k_3k_5k_8)c_2)}{(k_2k_4k_6 + k_2k_4k_8) + (k_2k_6k_7c_2 + k_4k_5k_8)c_2} \\
c_5 &= \frac{c_1 c_2^2((k_1k_4k_5 + k_2k_3k_7) + (k_1k_5k_7 + k_3k_5k_7)c_2)}{(k_2k_4k_6 + k_2k_4k_8) + (k_2k_6k_7 + k_4k_5k_8)c_2}.
\end{aligned}$$

Under the assumption that $\lambda = k_1 = k_7, \mu = k_2 = k_4 = k_6 = k_8$ and $r\lambda = k_3 = k_5$ this becomes

$$\begin{aligned} c_3 &= \frac{\lambda}{\mu} c_1 c_2 \\ c_4 &= r\frac{\lambda}{\mu} c_1 c_2 \\ c_5 &= r\frac{\lambda^2}{\mu^2} c_1 c_2^2. \end{aligned}$$

The problem now is to relate the steady state solution to the initial state of the system. We will assume that the initial state of the system ($t = 0$) is of the form

$$c_1(0) = a, \quad c_2(0) = b, \quad c_3(0) = c_4(0) = c_5(0) = 0 \tag{5.2.0.5}$$

There are two conservation laws that now come into consideration. Invariance of the concentration of the antibody leads to the equation

$$a = c_1 + c_3 + c_4 + c_5, \tag{5.2.0.6}$$

and invariance of the concentration of the antigen leads to the equation

$$b = c_2 + c_3 + c_4 + 2c_5 \tag{5.2.0.7}$$

In particular, we note that the equation

$$c_5 = (b - a) - (c_2 - c_1) \tag{5.2.0.8}$$

holds.

The invariance of the concentration of the antibody specifies the c_1 coordinate of the steady-state solution in terms of the c_2 coordinate of the steady state solution as

$$c_1 = \frac{a\mu^2}{(\lambda c_2 + \mu)(r\lambda c_2 + \mu)} \tag{5.2.0.9}$$

This allows the expression of all the coordinates of the steady-state solution in terms of the coordinate c_2 and the constants a, r, λ and μ.

Evaluating the formula for the invariance of the antigen at the steady-state solution and clearing denominators we obtain the following cubic equation which is satisfied by the steady-state coordinate c_2

$$0 = A_0 + A_1 c_2 + A_2 c_2^2 + A_3 c_2^3 \tag{5.2.0.10}$$

where $A_3 = r\lambda^2\mu^2, A_2 = \lambda\mu^2((2a-b)r\lambda+(1+r)\mu), A_1 = \mu^2((1+r)\lambda\mu(a-b)+\mu^2),$ and $A_0 = -b\mu^4$. The constant coefficient is $A_0 < 0$ and the leading coefficient of the cubic is $A_3 > 0$. So the cubic has at least one real positive root.

Consider now the difference between the coefficients of c_2^2 and c_2 of the cubic equations 5.2.0.10. The difference is

$$b\lambda + r\mu + (r-1)a\lambda \tag{5.2.0.11}$$

This expression is positive if $r \geq 1$. Therefore in this case the coefficients of the cubic equation for c_2 have at most one sign change and by *Descartes' rule of signs* [68] the cubic equation has exactly one positive root. Hence for $r > 1$ the value of c_2 and therefore the value of all of the coordinates of the steady-state are completely determined by the initial conditions.

The case that $r < 1$ follows by symmetry.

To summarize we have shown the following result.

Theorem 5.2.1. *The model admits a unique positive steady-state solution determined by the initial conditions.*

The solutions of the cubic for c_2 are given by the implementation of Cardano's formula in MATHEMATICA [99]. For the complete proof of this theorem, see [8]. The reader is cautioned that these solutions are numerically unstable over the range of values that we employ.

5.3 Application

We examine a specific initial value problem associated with an antigen-antibody pairing of α-TSH.

The specific initial value problem examined for the dynamical system is the one evolving from $c_1(0) = 1 \times 10^{-8}M, c_2(0) = 1 \times 10^{-9}M, c_3(0) = c_4(0) = c_5(0) = 0$. This is a typical concentration ratio to be considered for the detection of small amounts of proteins in solution.

Consider first the symmetric case (5.2.0.4) where the parameter λ has the value 90000$\mathrm{M}^{-1}\mathrm{sec}^{-1}$ and the parameter μ has the value 0.0011sec^{-1} [90].

Implementing the Runga-Kutta-Fehlberg method of numerical integration we obtain a solution for the system (5.2.0.4) as indicated in Figure 5.9.

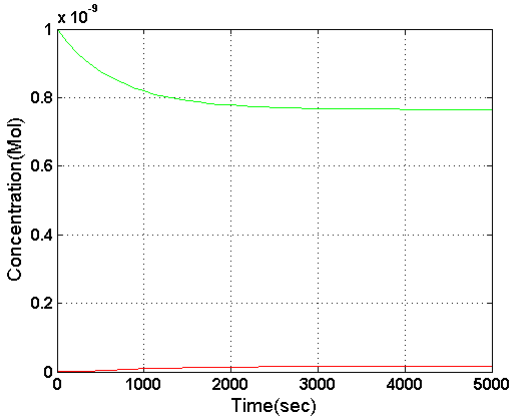

Figure 5.9: The molar concentration of antigen S_2 (in green) and the molar concentration of S_5 (in red) as a function of time in the symmetric case.

The model indicates that the solution reaches equilibrium in approximately 50-80 minutes as can be seen in Figure5.12.

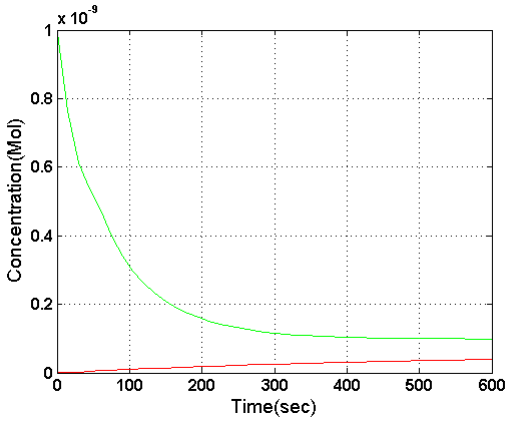

Figure 5.10: The molar concentration of S_5 (in red) as a function of time in the symmetric case.

For the solution of the steady state of the system we consider the cubic polynomial associated with this set of parameters. The plot of the the polynomial for this set of parameters is given in Figure5.11.

For the asymmetric case, we will consider the typical asymmetric case where the parameters $k_1 = k_7 = 9000\text{M}^{-1}\text{sec}^{-1}$ and the parameters $k_3 = k_5 = 9000000M^{-1}\text{sec}^{-1} = 100k_1$, The remaining parameters taking on the value $\mu = k_2 = k_4 = k_6 = k_7 = 0.0011\text{sec}^{-1}$. The initial conditions considered is

$$c_1(0) = 1 \times 10^{-8}\text{M}, \quad c_2(0) = 1 \times 10^{-9}\text{M} \quad c_3(0) = c_4(0) = c_5(0) = 0 \tag{5.3.0.12}$$

Implementing the Runga-Kutta-Fehlberg method of numerical integration we obtain a solution for the system (5.2.0.4) as indicated in Figure5.10.

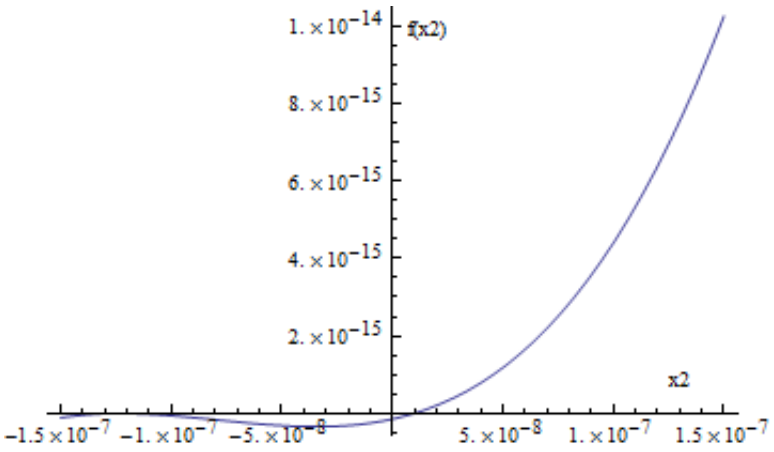

Figure 5.11: The plot of the cubic polynomial associates with the symmetric $r = 1$ case $\lambda = 9000\text{M}^{-1}\text{sec}^{-1}$

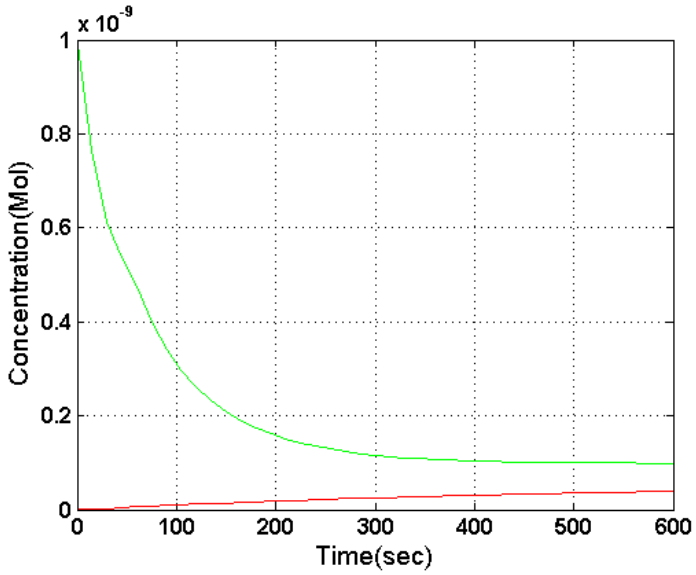

Figure 5.12: The molar concentration of antigen S_2 (in green) and the molar concentration of S_5 (in red) as a function of time for the asymmetric case with $r = 100$.

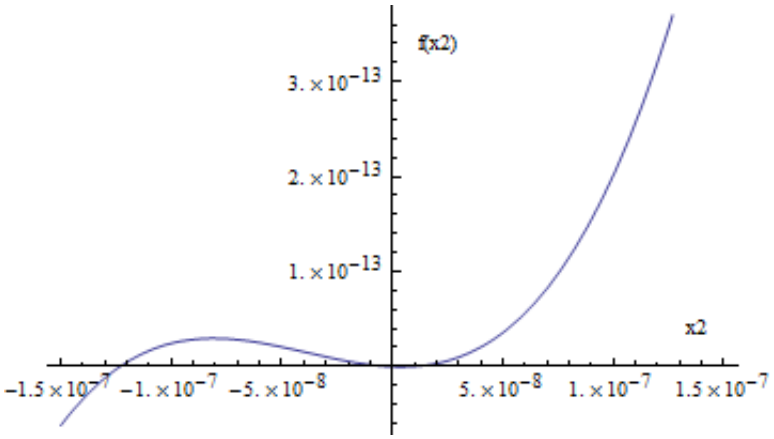

Figure 5.13: The plot of the cubic polynomial associated with the asymmetric $r = 100$ case $\lambda = 9000\mathrm{M}^{-1}\mathrm{sec}^{-1}$.

Regarding the steady-state solution of the system, we again consider the roots of the cubic polynomial associated with the system. The plot of the the polynomial for this set of parameters is given in Figure 5.13.

To more clearly indicate the properties of the positive solution, the positive root of the polynomial is indicated in Figure 5.14

To indicate the behavior of the associated cubic polynomial and the presence of a unique positive root, we provide a graph showing the behavior of the polynomial for values of r between 1 and 100 for the previously specified values of λ and μ.

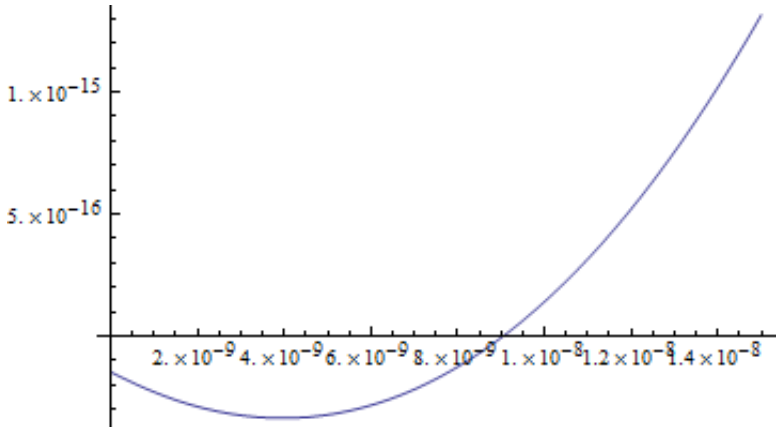

Figure 5.14: Root of the associated cubic polynomial in the aysymmetric $r = 100$ case $\lambda = 9000\mathrm{M}^{-1}\mathrm{sec}^{-1}$.

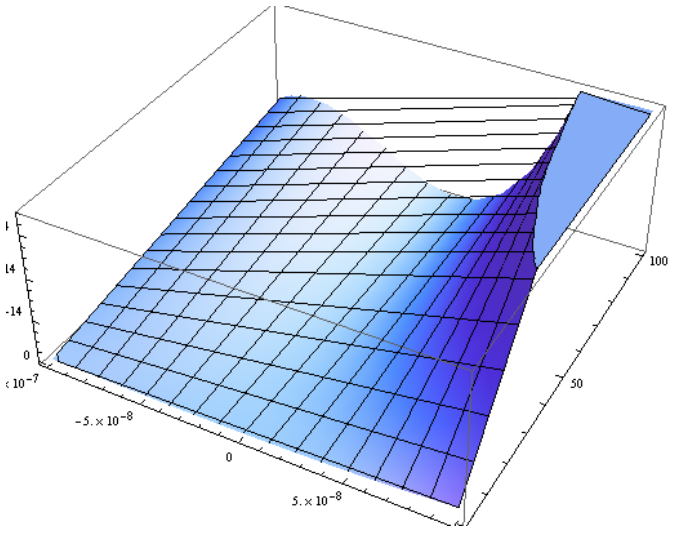

Figure 5.15: The behavior of the associated cubic polynomial as a function of r and c_2.

5.4 Revisiting Nanoparticle Model with CRNT

Although we have already proved the uniqueness and the existence of the positive steady state of the nanoparticle model, there are several interesting questions that remain to be answered. If we consider our model in the context of the CRNT [3, 4, 21, 36, 39, 40] it may be possible to derive new information from the nanoparticle clustering model, such as the dynamic property of the equilibrium, and the possibility of the multistationarity behavior.

Secondly, even though the existence and uniqueness of the positive steady states of the system is verified, in practice, it is interesting to know if there is a way we could calculate that unique steady state, or reduce the dimension of the equilibria as an orbit. Inspired by Karin Gatermann's early work [47–49], following the procedures we described in Chapter 2, we will investigate the intersection of a toric variety and a convex cone, in order to look for the positive steady state under some mass conservation constraints. the presence of mass conservation constraints is to be expected, since the whole reaction system is a closed, homogeneous system.

First, the chemical reaction network is as following:

Example 5.4.1.

$$S_3 \underset{k_1}{\overset{k_2}{\rightleftharpoons}} S_1 + S_2 \underset{k_4}{\overset{k_3}{\rightleftharpoons}} S_4 \tag{5.4.0.13}$$

$$S_2 + S_3 \underset{k_6}{\overset{k_5}{\rightleftharpoons}} S_5 \underset{k_7}{\overset{k_8}{\rightleftharpoons}} S_2 + S_4 \tag{5.4.0.14}$$

The network involves 5 species $\{S_1, S_2, S_3, S_4, S_5\}$ and 6 complexes $\{S_1 + S_2, S_3, S_4, S_3 + S_2, S_5, S_4 + S_2\}$. Each species is associated with the concentration as a continuous function of time t. Let c_1, c_2, c_3, c_4, c_5 denote the concentrations of S_1, S_2, S_3, S_4, S_5, respectively.

The adjacency matrix and incidence matrix are defined as follows.

$$I_r := \begin{bmatrix} 1 & -1 & 0 & 0 & 0 & 0 & 0 & 0 \\ -1 & 1 & -1 & 1 & 0 & 0 & 0 & 0 \\ 0 & 0 & 1 & -1 & 0 & 0 & 0 & 0 \\ 0 & 0 & 0 & 0 & -1 & 1 & 0 & 0 \\ 0 & 0 & 0 & 0 & 1 & -1 & 1 & -1 \\ 0 & 0 & 0 & 0 & 0 & 0 & -1 & 1 \end{bmatrix}, I_\kappa := \begin{bmatrix} 0 & k_1 & 0 & 0 & 0 & 0 \\ k_2 & 0 & 0 & 0 & 0 & 0 \\ 0 & k_3 & 0 & 0 & 0 & 0 \\ 0 & 0 & k_4 & 0 & 0 & 0 \\ 0 & 0 & 0 & k_5 & 0 & 0 \\ 0 & 0 & 0 & 0 & k_6 & 0 \\ 0 & 0 & 0 & 0 & 0 & k_7 \\ 0 & 0 & 0 & 0 & k_8 & 0 \end{bmatrix} \tag{5.4.0.15}$$

$$-L = I_r \cdot I_\kappa = \begin{bmatrix} -k_2 & k_1 & 0 & 0 & 0 & 0 \\ k_2 & -k_1 - k_3 & k_4 & 0 & 0 & 0 \\ 0 & k_3 & -k_4 & 0 & 0 & 0 \\ 0 & 0 & 0 & -k_5 & k_6 & 0 \\ 0 & 0 & 0 & k_5 & -k_6 - k_8 & k_7 \\ 0 & 0 & 0 & 0 & k_8 & -k_7 \end{bmatrix} \tag{5.4.0.16}$$

$$\frac{d\mathbf{c}}{dt} = \mathcal{Y} \cdot I_r \cdot I_\kappa \cdot \mathbf{c}^Y = \begin{pmatrix} k_2 & -k_1 - k_3 & k_4 & 0 & 0 & 0 \\ k_2 & -k_1 - k_3 & k_4 & -k_5 & k_6 + k_8 & -k_7 \\ -k_2 & k_1 & 0 & -k_5 & k_6 & 0 \\ 0 & k_3 & -k_4 & 0 & k_8 & -k_7 \\ 0 & 0 & 0 & k_5 & -k_6 - k_8 & k_7 \end{pmatrix} \cdot \begin{pmatrix} c_3 \\ c_1 c_2 \\ c_4 \\ c_2 c_3 \\ c_5 \\ c_2 c_4 \end{pmatrix} \tag{5.4.0.17}$$

This again generates the equation 5.2.0.2. Moreover, the decoupling of this system gives us more information, with the help of the CRNT. More specifically, the deficiency of the parent network $\delta = n - s - l = \dim YI_r = 1$, hence it is not covered by the Deficiency-Zero-Theorem. By the decomposition of the matrix I_r, the deficiencies of the corresponding

subnetworks $\delta_1 = \delta_2 = 0$. Since the parent network is not a direct sum of the subnetworks, the Deficiency-One-Theorem does not apply either.

Since the experiment is performed in a closed homogeneous system, hence, the total concentration of species S_1, S_2 are constant by the mass conservation law. The conservation law leads to the following relation.

In terms of the concentration of the antibody,

$$\mathbf{v}_1^T \cdot \mathbf{c}(t) = (1, 0, 1, 0, 1) \cdot \mathbf{c} = c_1 + c_3 + c_4 + c_5 = \alpha_1 \tag{5.4.0.18}$$

In terms of the concentration of the gold nanoparticle.

$$\mathbf{v}_2^T \cdot \mathbf{c}(t) = (0, 1, 1, 1, 2) \cdot \mathbf{c} = c_2 + c_3 + c_4 + 2c_5 = \alpha_2 \tag{5.4.0.19}$$

More generally, we have the following equations

$$\dot{\mathbf{c}} = Y I_r I_\kappa \Phi(\mathbf{c}) = N \cdot v(\mathbf{c}) \tag{5.4.0.20}$$

$$\mathbf{v}^T \mathbf{c} = \alpha. \tag{5.4.0.21}$$

where the stoichiometric matrix [16] is given by

$$N = \begin{bmatrix} -1 & 1 & -1 & 1 & 0 & 0 & 0 & 0 \\ -1 & 1 & -1 & 1 & -1 & 1 & -1 & 1 \\ 1 & -1 & 0 & 0 & -1 & 1 & 0 & 0 \\ 0 & 0 & 1 & -1 & 0 & 0 & -1 & 1 \\ 0 & 0 & 0 & 0 & 1 & -1 & 1 & -1 \end{bmatrix} \tag{5.4.0.22}$$

By investigating the intersection of the polyhedral cone $\ker N$ and the $\operatorname{Im}\Phi(\mathbf{c})$, following the procedure of the Deficiency-One-Algorithm, we conclude that for the nanoparticle clustering model, there is no multistationary behavior.

5.5 Conclusion and Discussion

In this chapter a model for the growth of nanoparticle configurations arising from antibody-antigen "bonds" was developed using mass-action kinetics. This model has an associated dynamical system which can be solved analytically for the passage to the steady-state. In the model the steady-state locus is a toric variety. Given an initial condition for the dynamical system with only species of pure antigen and pure nanoparticle-antibody content, this model is used to estimate the time necessary to reach the steady-state and the distribution of

various species. The species distribution in the steady-state is shown to depend only on the parameters of the problem and the initial conditions.

Both the time to steady state, and the distribution of product that is indicated by the model is in good accord with that found through experiment [1].

CHAPTER 6
BIFUCTATIONS AND CHAOS IN A MODIFIED DRIVEN CHEN'S SYSTEM

6.1 Introduction

Hyperchaotic systems, exhibiting more than one positive Lyapunov exponent, have been extensively studied in recent years in systems such as Chua's circuit and the Rossler system [72, 73, 80, 81, 83, 103]. Among such systems, often generated by addition of controllers or drivers to known chaotic systems, the hyperchaos in a modified driven Chen's system has recently been numerically studied [7, 46, 100].

In order to understand the onset of such hyperchaos better, we study bifurcations in this modified Chen system leading from simpler dynamics into the hyperchaotic regime. In particular, we demonstrate that the existence of only one fixed point of the system implies that this simple point attractor may only be destabilized via a Hopf or double Hopf bifuraction as system parameters are varied – saddle-node, transcritical and pitchfork bifuractions are precluded.

In the post Hopf or post-double Hopf parameter regime, one may have one of three possible scenarios:

a. a new stable periodic orbit or attractor created by a supercritical bifurcation, further bifurcations of which [52, 78] may lead into chaotic regimes via the usual period doubling and other routes, or

b. a post-subcritical-bifurcation scenario with no stable local attractors and the system blowing up in finite time (an attractor at infinity), or

c. a different post-subcritical-bifurcation scenario where there are no stable local attractors, but the existence of strong dissipation precludes the system flying off to infinity. In this case, the only remaining possibility is the formation of a nonlocal attractor (via the usual stretching and folding mechanism) on which the system exhibits long-term bounded aperiodic dynamics. In the modified Chen's system, earlier numerical results [7, 46, 100] suggest that such an attractor would indeed be chaotic or hyperchaotic, exhibiting at least one, and most likely more than one, positive Lyapunov exponent.

In Section 2, we demonstrate that only Hopf or double-Hopf bifurcations are possible, and that other local bifurcations of fixed points are impossible. The conditions for Hopf bifurcation are analyzed and used to derive parameter values at which the former bifurcation occurs. Section 3 briefly considers the local dissipative/dilatory behavior of the system in various parameter regimes. In Section 4, we derive analytical expressions for the periodic orbits resulting from the Hopf bifurcation, and thus analyze their stability via the resulting normal form. Supercritical cases correspond to scenario a above, while subcritical cases satisfying strong dissipativity (using the results of Section 3) lead to scenario c, and the possible onset of chaos. In Section 5, these predictions from the normal form are verified using numerical simulations, and the various types of post-bifurcation dynamics are further investigated and characterized via the use of numerical diagnostics.

The content of this chapter is previously included in [11].

6.2 Linear stability and Hopf bifurcation analysis

The modified Chen system [7, 46, 100] is obtained by adding a simple linear controller to the second equation of the famous three-dimensional autonomous Chen's chaotic system. It is described by the equations:

$$\begin{aligned} \dot{x} &= a(y - x) \\ \dot{y} &= -dx - xz + cy - w \\ \dot{z} &= xy - bz \\ \dot{w} &= x + k \end{aligned} \tag{6.2.0.1}$$

The only fixed (alternatively, equilibrium or critical) points of (6.2.0.1) are

$$(x_0, y_0, z_0, w_0) = (-k, -k, \frac{k^2}{b}, \frac{k(-bc + bd + k^2)}{b}) \tag{6.2.0.2}$$

We shall analyze the stability of this fixed point, and the subsequent, more complex, dynamics which is possible in this system. However, note that the presence of a single fixed point in all parameter ranges precludes the possibility of the fixed point undergoing saddle-node, pitchfork or transcritical bifurcations, all of which involve creation/annihilation or exchange of stability of a pair of fixed points. Hence, the only local bifurcation possible in

this system is a Hopf bifurcation. Following standard methods of phase-plane analysis, the Jacobian matrix of (1) at (x_0, y_0, z_0, w_0) is:

$$\begin{pmatrix} -a & a & 0 & 0 \\ -d - z_0 & c & -x_0 & -1 \\ y_0 & x_0 & -b & 0 \\ 1 & 0 & 0 & 0 \end{pmatrix} \tag{6.2.0.3}$$

which equals

$$\begin{pmatrix} -a & a & 0 & 0 \\ -d - \frac{k^2}{b} & c & k & -1 \\ -k & -k & -b & 0 \\ 1 & 0 & 0 & 0 \end{pmatrix} \tag{6.2.0.4}$$

The eigenvalues of this matrix satisfy the characteristic equation

$$\lambda^4 + b_1\lambda^3 + b2\lambda^2 + b_3\lambda + b_4 = 0 \tag{6.2.0.5}$$

where

$$
\begin{aligned}
b_1 &= a + b - c \\
b_2 &= ab - ac - bc + ad + k^2 + \frac{ak^2}{b} \\
b_3 &= a - abc + abd + 3ak^2 \\
b_4 &= ab
\end{aligned}
\tag{6.2.0.6}
$$

For (x_0, y_0, z_0, w_0) to be a stable fixed point within the linearized analysis, all the eigenvalues must have negative real parts. From the Routh-Hurwitz criterion, the necessary and sufficient conditions for (6.2.0.5) to have $\mathrm{Re}(\lambda_{1,2,3,4} < 0)$ are:

$$b_1 > 0 \tag{6.2.0.7}$$

$$b_4 > 0 \tag{6.2.0.8}$$

$$b_1 b_2 - b_3 > 0 \tag{6.2.0.9}$$

$$b_1(b_2 b_3 - b_1 b_4) - b_3^2 > 0 \tag{6.2.0.10}$$

By (6.2.0.5), $b_1 > 0$ and $b_4 > 0$ would be satisfied if we choose a, b, c to be positive. The third condition would also be satisfied if we picked k^2 to satisfy

$$\begin{aligned} &-a + a^2b + ab^2 - a^2c - 2abc - b^2c + ac^2 \\ &+bc^2 + a^2d - acd - ak^2 + (a^2k^2)/b + bk^2 - ck^2 - (ack^2)/b > 0 \end{aligned} \tag{6.2.0.11}$$

The final condition is satisfied when

$$f(k) \equiv c_1k^4 + c_2k^2 + c_3 > 0 \tag{6.2.0.12}$$

where

$$c_1 = -3a^2 + (3a^3)/b + 3ab - 3ac - (3a^2c)/b \tag{6.2.0.13}$$

$$\begin{aligned} c_2 = (&-4a^2 + a^3/b + ab + 3a^3b + 3a^2b^2 - ac \\ &- 4a^3c - (a^2c)/b - 5a^2bc - 4ab^2c \\ &+ 4a^2c^2 + 4abc^2 + 4a^3d - a^2bd + \\ &ab^2d - 4a^2cd - abcd) \end{aligned} \tag{6.2.0.14}$$

$$
\begin{aligned}
c_3 = (&-a^2 - a^2b^2 - ab^3 - a^3c + a^2bc + ab^2c \\
&- a^3b^2c - a^2b^3c + a^2c^2 + a^3bc^2 \\
&+ 2a^2b^2c^2 + ab^3c^2 - a^2bc^3 - ab^2c^3 \\
&+ a^3d - a^2bd + a^3b^2d + a^2b^3d - a^2cd \\
&- 2a^3bcd - 2a^2b^2cd - ab^3cd + \\
&2a^2bc^2d + ab^2c^2d + a^3bd^2 - a^2bcd^2)
\end{aligned}
\tag{6.2.0.15}
$$

The existence of at least one real positive root of $f(k) = 0$ at

$$
\begin{aligned}
l_0 &= k_0^2 \\
&= (-(a^2/(2(3a^2 - 3ab + 3b^2 - 3ac - 3bc))) + (2ab)/(3a^2 - 3ab + 3b^2 - 3ac - 3bc) \\
&\quad - b^2/(2(3a^2 - 3ab + 3b^2 - 3ac - 3bc)) - (3a^2b^2)/(2(3a^2 - 3ab + 3b^2 - 3ac - 3bc)) \\
&\quad - (3ab^3)/(2(3a^2 - 3ab + 3b^2 - 3ac - 3bc)) + (ac)/(2(3a^2 - 3ab + 3b^2 - 3ac - 3bc)) \\
&\quad + (bc)/(2(3a^2 - 3ab + 3b^2 - 3ac - 3bc)) + (2a^2bc)/(3a^2 - 3ab + 3b^2 - 3ac - 3bc) \\
&\quad + (5ab^2c)/(2(3a^2 - 3ab + 3b^2 - 3ac - 3bc)) + (2b^3c)/(3a^2 - 3ab + 3b^2 - 3ac - 3bc) \\
&\quad - (2abc^2)/(3a^2 - 3ab + 3b^2 - 3ac - 3bc) - (2b^2c^2)/(3a^2 - 3ab + 3b^2 - 3ac - 3bc) \\
&\quad - (2a^2bd)/(3a^2 - 3ab + 3b^2 - 3ac - 3bc) + (ab^2d)/(2(3a^2 - 3ab + 3b^2 - 3ac - 3bc)) \\
&\quad - (b^3d)/(2(3a^2 - 3ab + 3b^2 - 3ac - 3bc)) + (2abcd)/(3a^2 - 3ab + 3b^2 - 3ac - 3bc) \\
&\quad + (b^2cd)/(2(3a^2 - 3ab + 3b^2 - 3ac - 3bc)) \\
&\quad + ((a - b + c)\Gamma)/(2(3a^2 - 3ab + 3b^2 - 3ac - 3bc))
\end{aligned}
\tag{6.2.0.16}
$$

where

$$\begin{aligned}\Gamma^2 = a^2 + 2ab + b^2 + 6a^2b^2 - 18ab^3 + 12b^4 + 9a^2b^4 \\ + 4a^2bc - 4ab^2c - 8b^3c - 12a^2b^3c - 12ab^4c \\ + 4a^2b^2c^2 + 8ab^3c^2 + 4b^4c^2 - 4a^2bd - \\ 2ab^2d + 2b^3d + 12a^2b^3d - 6ab^4d - 8a^2b^2cd \\ - 4ab^3cd + 4b^4cd + 4a^2b^2d^2 - 4ab^3d^2 + b^4d^2\end{aligned} \tag{6.2.0.17}$$

The inequality, corresponding to (6.2.0.12), governing the change in stability is only linear in l. If the discriminant is negative , then l_0 is complex and the fixed point (x_0, y_0, z_0, w_0) is stable for all relevant values of l. If the discriminant is positive and the four real solutions for k_0 are $k_{01-}, k_{02-}, k_{01+}, k_{02+}$, and the two real solutions for l_0 are l_{01} and l_{02}(without loss of generality, we can even assume $k_{01-} < k_{02-} < 0 < k_{02+} < k_{01+}$) or equivalently, $l_{01} > l_{02}$. Then, the fixed point is unstable if $0 < k_{01+} < k < k_{02+}$ or $k_{01-} < k < k_{02-} < 0$, or equivalently, $l_{02} < l < l_{01}$. On the other hand, suppose that $k_{02-} < k < k_{02+}$ or $k > k_{01+}$ or $k < 01-$, or equivalently, $l > l_{01}$ or $0 < l < l_{02}$, (x_0, y_0, z_0, w_0) is stable.

We will perform a Hopf bifurcation analysis to show that as the value of l passes through the critical values l_0, periodic solutions occur. To determine the behavior of the eigenvalues λ as l varies, we employ the Hopf bifurcation theorem:

Theorem 6.2.1. *Let*

$$\frac{d\vec{x}}{dt} = \vec{F}(\vec{x}, \mu) \tag{6.2.0.18}$$

be an autonomous system of differential equations for each value of the parameter $\mu \in (-\mu_0, \mu)$*, where* μ_0 *is a positive number and the vector function*

$$\vec{F} \in \mathbb{C}^2(DX(-\mu_0, \mu_0)) \tag{6.2.0.19}$$

where D *is a domain in* $\mathbb{R}^n$*. Suppose that the system* (6.2.0.18) *has a critical point* $\vec{x}_0(\mu)$*,that is,*

$$\vec{F}(\vec{x}_0(\mu), \mu) = 0 \tag{6.2.0.20}$$

Let $\vec{J}(\mu)$ *be a Jacobian matrix of system* (6.2.0.18) *at* $\vec{x}_0(\mu)$*. Suppose that* $\det|\vec{J}(\mu) - \lambda I| = 0$ *has a complex conjugate pair of solution* $\lambda(\mu)$*,* $\bar{\lambda(\mu)}$ *such that for* $\mu > 0$ *the* $Re(\lambda(\mu)) > 0$*; for* $\mu < 0, Re(\lambda(\mu)) < 0, \frac{dRe(\lambda(\mu))}{d\mu}|_{\mu=0} > 0$*. Assume that all other* λ*'s are distinct,* (6.2.0.18) *has a periodic solution in some neighborhood of* $\mu = 0$ *and* $\vec{x}$ *in some neighborhood of* $\vec{x}_0(\mu)$

In order to apply this theorem to (6.2.0.13), define the bifurcation parameter

$$\mu = \frac{1}{l} - \frac{1}{l_0}, \quad l(\mu) = \frac{l_0}{1 + l_0\mu} \tag{6.2.0.21}$$

) with $\mu = 0$ at $l = l_{01}$. For $\mu > 0, l < l_{01}$ and $\mathrm{Re}(\lambda_1(\mu)) > 0$. For $\mu < 0, l > l_{01}$ and $\mathrm{Re}(\lambda_1(\mu)) < 0$. Thus, the first set of conditions in the theorem is valid and it remains only to show that

$$\frac{\mathrm{Re}(\lambda_1(l(\mu)))}{d\mu}|_{\mu=0} = \frac{\mathrm{Re}(\lambda_1(l(\mu)))}{da}\frac{da}{d\mu}|_{\mu=0} > 0 \tag{6.2.0.22}$$

The analysis is standard and follows the details in [12] for instance. Hence, we omit the details. Note that physical parameters where Hopf bifurcation may occur must satisfy both $l_0 > 0$ as well as the angular frequency of the resulting oscillation ω be real, i.e. $\omega^2 = b_3/b_1 > 0$

Although the full analysis of the double-Hopf bifurcations in this system and the resulting dynamics will be deferred to a subsequent paper, the conditions for its occurrence may be directly derived by matching the characteristic polynomial to that from two pairs of conjugate pure imaginary eigenvalues, thus yielding

$$b_1 = b_3 = 0 \quad \text{and} \quad \omega^2 = (b_2 \pm (b_2^2 - 4b_4)^{\frac{1}{2}} \tag{6.2.0.23}$$

6.3 Dissipative/Dilatory Regimes

In the vicinity of the fixed point 6.2.0.2, the local rate of change of volume (the Lie Derivative of the vector field) in the four-dimensional (x, y, z, w) phase-space is given by the trace of the Jacobian, i.e.

$$\mathrm{Tr}\, J(x, y, z, w) = -a - b - k^2/b \tag{6.3.0.24}$$

This is clearly negative for physical parameters with a, b and k positive. As we shall subsequently see in the following sections, the degree of negativity will be important in the post-Hopf bifurcation regime. In particular, $\mathrm{Tr}\, J$ large negative, or a strongly dissipative

system following a subcritical Hopf bifurcation is often a reliable indicator of chaos provided no other local (periodic or quaisperiodic) attractors are present

6.4 Analytical construction of periodic orbits

6.4.1 Hyper-chaos model

In this section, we will use the method of multiple scales to construct analytical approximations for the periodic orbits arising through the Hopf bifurcation of the fixed point of the hyper-chaos model 6.2.0.1 discussed above. The parameter k will be used as the control parameter. The limit cycle is determined by expanding about the fixed point using progressively slower time scales. The expansions take the form

$$x = x_0 + \sum_{n=1}^{3} \epsilon^n x_n(T_0, T_1, T_2) + ..., \tag{6.4.1.1}$$

$$y = y_0 + \sum_{n=1}^{3} \epsilon^n y_n(T_0, T_1, T_2) + ..., \tag{6.4.1.2}$$

$$z = z_0 + \sum_{n=1}^{3} \epsilon^n z_n(T_0, T_1, T_2) + ..., \tag{6.4.1.3}$$

$$w = w_0 + \sum_{n=1}^{3} \epsilon^n w_n(T_0, T_1, T_2) + ...,, \tag{6.4.1.4}$$

where $T_n = \epsilon^n t$ and ϵ is a small positive non-dimensional parameter that is introduced as a bookkeeping device and will be set to unity in the final analysis. Utilizing the chain rule, the time derivative becomes

$$\frac{d}{dt} = D_0 + \epsilon D_1 + \epsilon^2 D_2 + \epsilon^3 D_3..., \tag{6.4.1.5}$$

where $D_n = \partial/\partial T_n$. Using the standard expansion for Hopf bifurcations [12, 52], the delay parameter k is ordered as

$$k = k_0 + \epsilon^2 k_2 \tag{6.4.1.6}$$

where k_0 is given by (6.2.0.16). This allows the influence from the nonlinear terms and the control parameter to occur at the same order.

Using (6.4.1.1)-(6.4.1.6) in (6.2.0.1) and equating like powers of ϵ yields equations at $\mathrm{O}(\epsilon^i), i = 1, 2, 3$ of the form :

$$L_1(x_i, y_i, z_i, w_i) = S_{i,1} \tag{6.4.1.7}$$

$$L_2(x_i, y_i, z_i, w_i) = S_{i,2} \tag{6.4.1.8}$$

$$L_3(x_i, y_i, z_i, w_i) = S_{i,3} \tag{6.4.1.9}$$

$$L_4(x_i, y_i, z_i, w_i) = S_{i,4} \tag{6.4.1.10}$$

where the $L_i, i = 1, 2, 3, 4$ are the differential operators

$$L_1(x_i, y_i, z_i, w_i) = D_0 x_i + a x_i - a y_i \tag{6.4.1.11}$$

$$L_2(x_i, y_i, z_i, w_i) = D_0 y_i + w_i + d x_i + z_0 x_i - c y_i + x_0 z_i \tag{6.4.1.12}$$

$$L_3(x_i, y_i, z_i, w_i) = D_0 z_i - y_0 x_i - x_0 y_i + b z_i \tag{6.4.1.13}$$

$$L_4(x_i, y_i, z_i, w_i) = D_0 w_i - x_i \tag{6.4.1.14}$$

The source terms $S_{i,j}$ for $i = 1, 2, 3$ and $j = 1, 2, 3, 4$ i.e. at $\mathrm{O}(\epsilon), \mathrm{O}(\epsilon^2)$, and $\mathrm{O}(\epsilon^3)$ are given as follows,

$$
\begin{aligned}
S_{1,1} &= 0 \\
S_{1,2} &= 0 \\
S_{1,3} &= 0 \\
S_{1,4} &= 0 \\
S_{2,1} &= -D_1 x_1 \\
S_{2,2} &= -D_1 y_1 - x_1 z_1 \\
S_{2,3} &= -D_1 z_1 + x_1 y_1 \\
S_{2,4} &= -D_1 w_1 + k_2 \\
S_{3,1} &= -D_2 x_1 - D_1 x_2 \\
S_{3,2} &= -D_2 y_1 - D_1 y_2 - x_2 z_1 - x_1 z_2 \\
S_{3,3} &= -D_2 z_1 - D_1 z_2 + x_2 y_1 + x_1 y_2 \\
S_{3,4} &= -D_2 w_1 - D_1 w_2
\end{aligned}
\tag{6.4.1.15}
$$

Also, (6.4.1.10) may be solved for x_i in terms of w_i . Using this in (6.4.1.7), we can get y_i in terms of w_i. Next, using these two relations in (6.4.1.8), we have z_i in terms of w_i. And finally, using all of the these relations in (6.4.1.9) yields the composite equation

$$
L_c w_i = \Gamma_i \tag{6.4.1.16}
$$

where

$$L_c = \beta_4 D_0^4 + \beta_3 D_0^3 + \beta_2 D_0^2 + \beta_1 D_0 + \beta_0 \tag{6.4.1.17}$$

and

$$\begin{aligned}
\beta_4 &= -\frac{1}{ax_0} \\
\beta_3 &= -\frac{1}{x_0} - \frac{b}{ax_0} + \frac{c}{ax_0} \\
\beta_2 &= -\frac{b}{x_0} + \frac{c}{x_0} + \frac{bc}{ax_0} - \frac{d}{x_0} - \frac{x_0}{a} - \frac{z_0}{x_0} \\
\beta_1 &= -\frac{1}{x_0} + \frac{bc}{x_0} - \frac{bd}{x_0} - x_0 - y_0 - \frac{bz_0}{x_0} \\
\beta_0 &= -\frac{b}{x_0}
\end{aligned} \tag{6.4.1.18, 6.4.1.19}$$

The composite source Γ_i is equal to

$$\begin{aligned}
r_{43} D_0^3 S_{i4} + r_{42} D_0^2 S_{i4} + r_{41} D_0 S_{i4} + r_{40} S_{i4} + S_{i3} + r_{21} D_0 S_{i2} + r_{20} S_{i2} \\
+ r_{12} D_0^2 S_{i1} + r_{11} D_0 S_{i1} + r_{10} S_{i1}
\end{aligned} \tag{6.4.1.20}$$

Where

$$
\begin{aligned}
r_{43} &= -\frac{1}{ax_0} \\
r_{42} &= -\frac{1}{x_0} - \frac{b}{ax_0} + \frac{c}{ax_0} \\
r_{41} &= -\frac{b}{x_0} + \frac{c}{x_0} + \frac{bc}{ax_0} - \frac{d}{x_0} - \frac{x_0}{a} - \frac{z_0}{x_0} \\
r_{40} &= \frac{bc}{x_0} - \frac{bd}{x_0} - x_0 - y_0 - \frac{bz_0}{x_0} \\
r_{21} &= -\frac{1}{x_0} \\
r_{20} &= -\frac{b}{x_0} \\
r_{12} &= -\frac{1}{ax_0} \\
r_{11} &= -\frac{b}{ax_0} + \frac{c_0}{ax_0} \\
r_{10} &= \frac{bc}{ax_0} - \frac{x_0}{a}
\end{aligned}
\tag{6.4.1.21}
$$

We shall use (6.4.1.16) later to identify and suppress secular terms in the solutions of (6.4.1.7)-(6.4.1.10)

Let us now turn to finding the solutions of (6.4.1.7)-(6.4.1.10). We will solve order by order in the usual way.

For $i = 1$ or $\mathrm{O}(\epsilon)$ we know $S_{1,1} = S_{1,2} = S_{1,3} = S_{1,4} = 0$. Hence we pick up a solution for the first order population using the known eigenvalues (from the previous section) at Hopf bifurcation, i.e.

$$w_1 = e^{i\omega t}\alpha[T1, T2] + e^{-i\omega t}\beta[T1, T2] + \gamma e^{\lambda_3 t} + \zeta e^{\lambda_4 t} \tag{6.4.1.22}$$

where $\lambda_1 = i\omega$, and $\beta = \bar{\alpha}$ is the complex conjugate of α since $\lambda_2 = \bar{\lambda}_1$ and w_1 is real. As is evident , the α and β modes correspond to the center manifold where $\lambda_{1,2}$ are purely imaginary and where the Hopf bifurcation occurs, while γ, ζ correspond to the attractive direction or the stable manifold. Since we wish to construct and analyze the stability of the periodic orbits which lie in the center manifold, we suppress the two eigenvalues with non-zero real parts, i.e.,

$$\gamma = \zeta = 0 \tag{6.4.1.23}$$

Using (6.4.1.22) and (6.4.1.23) in (23) − (26) for $i = 1$

$$x_1 = i\omega e^{i\omega t}\alpha[T1, T2] - i\omega e^{-i\omega t}\beta[T1, T2] \tag{6.4.1.24}$$

$$y_1 = \frac{-\omega^2 e^{i\omega t}\alpha[T1, T2] - \omega^2 e^{-i\omega t}\beta[T1, T2] + a(i\omega e^{i\omega}\alpha[T1, T2] - i\omega e^{-i\omega t}\beta[T1, T2])}{a} \tag{6.4.1.25}$$

$$
\begin{aligned}
z_1 = \frac{1}{ax_0}(&i\omega^3 e^{i\omega t}\alpha[T1,T2] - i\omega^3 e^{-i\omega t}\beta[T1,T2] \\
&- a(e^{i\omega t}\alpha[T1,T2] + e^{-i\omega t}\beta[T1,T2]) + ac(i\omega e^{i\omega t}\alpha[T1,T2] \\
&- i\omega e^{-i\omega t}\beta[T1,T2]) - ad(i\omega e^{i\omega t}\alpha[T1,T2] - i\omega e^{-i\omega t}\beta[T1,T2]) \\
&- az_0(i\omega e^{i\omega t}\alpha[T1,T2] - i\omega e^{-i\omega t}\beta[T1,T2]) - a(-\omega^2 e^{i\omega t}\alpha[T1,T2] \\
&- \omega^2 e^{-i\omega t}\beta[T1,T2]) + c(-\omega^2 e^{i\omega t}\alpha[T1,T2] - \omega^2 e^{-i\omega t}\beta[T1,T2]))
\end{aligned}
\tag{6.4.1.26}
$$

Now that the first order solutions (6.4.1.22),(6.4.1.24),(6.4.1.25),(6.4.1.26) are known, the second-order sources $S_{2,1}, S_{2,2}, S_{2,3}, S_{2,4}$ may be evaluated, using 6.4.1.15. Setting the coefficients of the secular $e^{\lambda_{1,2}t}$ terms in these sources to zero yields

$$
D_1\alpha = \frac{\partial\alpha}{\partial T_1} = 0, \quad D_1\beta = \frac{\partial\beta}{\partial T_1} = 0 \tag{6.4.1.27}
$$

Next, using the second-order sources, and (6.4.1.27) , the second-order particular solution is taken in the usual form to balance the zeroth and second harmonic terms at this order, i.e.,

$$
w_2 = w_{20} + w_{22}e^{2i\omega t} \tag{6.4.1.28}
$$

Using this in (6.4.1.16) for $i = 2$, and balancing the DC, or time-independent, and second-harmonic terms, the coefficients in the second-order particular solution (6.4.1.28) are

$$
\begin{aligned}
w_{22} = (&-ab\omega\alpha[T1,T2]^2 - 2ia\omega^2\alpha[T1,T2]^2 + iabc\omega^2\alpha[T1,T2]^2 \\
&- iabd\omega^2\alpha[T1,T2]^2 + ab\omega^3\alpha[T1,T2]^2 - 2ac\omega^3\alpha[T1,T2]^2 \\
&- bc\omega^3\alpha[T1,T2]^2 + 2ad\omega^3\alpha[T1,T2]^2 + 2ia\omega^4\alpha[T1,T2]^2 + \\
&ib\omega^4\alpha[T1,T2]^2 - 2ic\omega^4\alpha[T1,T2]^2 - 2\omega^5\alpha[T1,T2]^2 + ia\omega^2x_0^2\alpha[T1,T2]^2 \\
&- \omega^3x_0^2alp[T1,T2]^2 - iab\omega^2z_0\alpha[T1,T2]^2 + 2a\omega^3z_0\alpha[T1,T2]^2) \\
&/(x_0(iab - 2a\omega + 2abc\omega - 2abd\omega - 4iab\omega^2 + 4iac\omega^2 + 4ibc\omega^2 - 4iad\omega^2 + 8a\omega^3 \\
&+ 8b\omega^3 - 8c\omega^3 + 16i\omega^4 - 2a\omega x_0^2 - 4i\omega^2x_0^2 - 2a\omega x_0y_0 - 2ab\omega z_0 - 4ia\omega^2z_0))
\end{aligned}
\tag{6.4.1.29}
$$

$$
\begin{aligned}
w_{20} = \frac{1}{abx_0}(&-abck_2x_0 + abdk_2x_0 + ak_2x_0^3 + ak_2x_0^2y_0 + abk_2x_0z_0 \\
&- 2abc\omega^2\alpha[T1,T2]\beta[T1,T2] + 2abd\omega^2\alpha[T1,T2]\beta[T1,T2] \\
&- 2b\omega^4\alpha[T1,T2]\beta[T1,T2] - 2a\omega^2x_0^2\alpha[T1,T2]\beta[T1,T2] \\
&+ 2ab\omega^2z_0\alpha[T1,T2]\beta[T1,T2])
\end{aligned}
\tag{6.4.1.30}
$$

Using w_2 in (6.4.1.7)-(6.4.1.10) for $i = 2$, together with the second-order sources, yields the other second-order fields $x_2, y_2,$ and z_2. Using these, together with the first-order results, we may evaluate the coefficients of the secular terms in the composite source Γ_3, from 6.4.1.15 and 6.4.1.16. Suppressing these secular, first-harmonic, terms to obtain uniform expansions

yields the final equation for the evolution of the coefficients in the linear solutions on the slow second-order time scales

$$\frac{\partial \alpha}{\partial T_2} = C_1\alpha + C_2\beta\alpha^2 \tag{6.4.1.31}$$

where the very large expressions for the coefficients C_i are omitted for the sake of brevity.

This equation (6.4.1.31) is the normal form, or simplified system in the center-manifold, in the vicinity of the Hopf bifurcation point(s). We shall now proceed to compare the predictions for the post-bifurcation dynamics from this normal form with actual numerical simulations. In addition, complex solutions in the post-bifurcation regime will be characterized via the use of numerical diagnostics.

6.5 Numerical Results and Discussion

6.5.1 Predictions from the Normal Form

To proceed, we need sets of parameter values at the Hopf bifurcation point. For the purpose of this analysis, we chose the values $a = 1, b = 4, c = 2.2, d = 40$ recalling that the bifurcation or control parameter k_0 is given by (6.2.0.16). We note that the chosen values yield two positive values for k_0, each of which leads to a Hopf bifurcation and a corresponding periodic orbit.

Using Eqs. 6.2.0.2 and 6.2.0.16, the fixed point is given by

$$\begin{aligned} x_0 &= 10.9418 \\ y_0 &= 10.9418 \\ z_0 &= 29.9307 \\ w_0 &= -741.094 \end{aligned} \tag{6.5.1.1}$$

and from 6.2.0.16, the bifurcation occurs at

$$l_{01} = 119.723, \quad l_{02} = -50.856 \tag{6.5.1.2}$$

since $k = \sqrt{l}$ has to be real, so equivalently, we have

$$\begin{aligned} k_{01-} &= -10.9418 \\ k_{01+} &= 10.9418 \end{aligned} \tag{6.5.1.3}$$

The characteristic polynomial Eq. 6.2.0.3 corresponding to l_{01} yields the eigenvalues

$$\lambda_1 = -2.79216$$

$$\lambda_2 = -0.00784413$$

$$\lambda_3 = -13.5141i$$

$$\lambda_4 = 13.5141i \tag{6.5.1.4}$$

With parameters corresponding to l_{01}, the normal form (6.4.1.31) becomes

$$\frac{\partial \alpha}{\partial T_2} = (0.0287502 - 1.00623i)k_2\alpha + (0.222009 + 13.3218I)\beta\alpha^2 \tag{6.5.1.5}$$

Writing $\alpha = \frac{1}{2}Ae^{i\zeta}$ and separating this equation into real and imaginary parts yields

$$\frac{\partial A}{\partial T_2} = 0.05550225A^3 + 0.0287502Ak_2 \tag{6.5.1.6}$$

$$\frac{\partial \zeta}{\partial T_2} = 3.33045A^2 - 1.00623k_2 \tag{6.5.1.7}$$

In the usual way, the fixed points of (6.5.1.6)

$$A_1 = 0, A_{2,3} = \pm\sqrt{-0.5180006215964218k_2} \tag{6.5.1.8}$$

give the amplitude of the solution $\alpha = \frac{1}{2}Ae^{i\theta}$ with $A_{2,3}$ corresponding to the bifurcating periodic orbits in the post-Hopf regime (as seen by putting $\alpha = \frac{1}{2}Ae^{i\zeta}$ in the first-order

fields in Equations (6.4.1.24), (6.4.1.25), (6.4.1.26), and (6.4.1.22)). Clearly, $A_{2,3}$ are real fixed points (corresponding to bifurcating periodic orbits) for $k_2 < 0$. The Jacobian of the (6.5.1.6) evaluated at $A_{2,3}$ is $-0.1110045k_2 > 0$, thus indicating that these fixed points (the periodic orbits) are unstable. Thus, the Hopf bifurcation at l_{01} is subcritical. Hence there is no stable periodic orbit in the post-Hopf regime with $k_2 < 0$. Also, for the parameter set chosen here $a = 1, b = 4, c = 2.2, d = 40, k = -10.9418$, the trace of the Jacobian of the original nonlinear system of equations at the fixed point (from Equation 6.2.0.4) is - 2.8, or quite strongly negative (this is really a logarithmic derivative, and so exponentiated in the actual rate of phase-space volume change). Thus the system is fairly dissipative and, given the absence of a local periodic attractor, as well as the fixed point being unstable after the Hopf bifurcation, we may anticipate either complex bounded dynamics or blow-up in the post-bifurcation regime. We shall verify this prediction numerically and characterize the resulting dynamical behavior.

Analogous treatments may now be carried out for some other cases. For the case $a = 1, b = 4.5, c = 3, d = 10$, recalling that k_0 is given by (6.2.0.16) , we note that the chosen values given two positive values for k_0, each of which leads to a Hopf bifurcation and a corresponding periodic orbit.

The fixed point is given by

$$x_0 = 17.7635$$

$$y_0 = 17.7635$$

$$z_0 = 70.1204$$

$$w_0 = -1192.29 \tag{6.5.1.9}$$

and the bifurcation occurs at

$$l_{01} = 315.542, \text{ or } l_{02} = 3.62472 \tag{6.5.1.10}$$

Or equivalently, the values of k at bifurcation are

$$k_{01-} = -17.7635$$

$$k_{01+} = 17.7635$$

$$k_{02-} = 1.90387$$

$$k_{02+} = -1.90387 \tag{6.5.1.11}$$

$$\tag{6.5.1.12}$$

The eigenvalues of the characteristic polynomial corresponding to l_{01} are

$$\begin{aligned}\lambda_1 &= -2.49517\\ \lambda_2 &= -0.00482666\\ \lambda_3 &= -19.33i\\ \lambda_4 &= 19.33i\end{aligned} \tag{6.5.1.13}$$

and those corresponding to l_{02} are

$$\begin{aligned}\lambda_1 &= -4.16238\\ \lambda_2 &= -0.806437\\ \lambda_3 &= 0.806437\\ \lambda_4 &= 1.66238\end{aligned} \tag{6.5.1.14}$$

For l_{01}, the final normal form becomes

$$\frac{\partial \alpha}{\partial T_2} = (0.00260237 - 1.12287i)k_2\alpha + (0.911164 + 21.3008i)\beta\alpha^2 \tag{6.5.1.15}$$

As before, writing $\alpha = \frac{1}{2}Ae^{i\zeta}$ and separating this equation into real and imaginary parts yields

$$\frac{\partial A}{\partial T_2} = 0.227791A^3 + 0.00260237Ak_2 \tag{6.5.1.16}$$

$$\frac{\partial \zeta}{\partial T_2} = 5.3252A^2 - 1.12287k_2 \tag{6.5.1.17}$$

Once again, the fixed points of (6.5.1.16)

$$A_1 = 0, A_{2,3} = \pm\sqrt{-0.01142437585k_2} \tag{6.5.1.18}$$

give the amplitude of the solution $\alpha = \frac{1}{2}Ae^{i\theta}$ with $A_{2,3}$ corresponding to the bifurcating periodic orbits. Clearly , $A_{2,3}$ are real fixed points for $k_2 < 0$ and the Jacobian of the (6.5.1.16) evaluated at $A_{2,3}$ is $-0.00520474k_2 > 0$ for $k_2 < 0$ indicating that these fixed points are unstable. Thus, the Hopf bifurcation at l_{01} is once again subcritical. In this case too, the trace of the Jacobian matrix of the original nonlinear system at the fixed point has the value -2.5, indicating, once again the possibility of bounded complex dynamics or blow-up in the post-subcritical-Hopf-bifurcation domain, where there is neither a stable fixed point, nor a stable periodic orbit. A blow-up would be precluded by a very large negative value of the Jacobian, but cannot be ruled out in this case.

For the third case with $a = 2, b = 15, c = 2, d = 1$, the fixed point is given by

$$x_0 = 3.57531$$

$$y_0 = 3.57531$$

$$z_0 = 0.852191$$

$$w_0 = 0.528462 \tag{6.5.1.19}$$

and the bifurcation occurs at

$$l_{01} = 12.7829, \text{ or } l_{02} = -7.93439 \tag{6.5.1.20}$$

For k real, we pick up l_{01}, or equivalently,

$$k_{01-} = -3.57531$$

$$k_{01+} = 3.57531 \tag{6.5.1.21}$$

The characteristic polynomial corresponding to l_{01} yields the eigenvalues

$$\lambda_1 = -14.3563$$

$$\lambda_2 = -0.643672$$

$$\lambda_3 = -1.8018i$$

$$\lambda_4 = 1.8018i \tag{6.5.1.22}$$

The normal form, separated as before into real and imaginary parts, yields

$$\frac{\partial A}{\partial T_2} = -0.15450425A^3 + 0.425255Ak_2 \tag{6.5.1.23}$$

$$\frac{\partial \zeta}{\partial T_2} = 0.13955375A^2 - 0.699404k_2 \tag{6.5.1.24}$$

The non-zero fixed points of (6.5.1.23)

$$A_{2,3} = \pm\sqrt{2.7523838k_2} \tag{6.5.1.25}$$

giving the amplitude of the bifurcating periodic orbits are real for $k_2 > 0$, and the Jacobian of the (6.5.1.23) evaluated at $A_{2,3}$ is $-0.85051k_2 < 0$ for $k_2 > 0$ indicating that these fixed points are stable. Thus, the Hopf bifurcation at l_{01} is supercritical, and we should observe periodic behavior on the resulting stable periodic orbit in the post-bifurcation regime.

As a final case, we take $a = 1, b = 10, c = 1, d = 1$ recalling that k_0 is given by (6.2.0.16). The fixed point is given by

$$\begin{aligned} x_0 &= 2.52089 \\ y_0 &= 2.52089 \\ z_0 &= 0.635487 \\ w_0 &= -1.60199 \end{aligned} \tag{6.5.1.26}$$

and the bifurcation occurs at

$$l_{01} = 6.35487, \quad l_{02} = -6.56321 \tag{6.5.1.27}$$

For l_{01},

$$\begin{aligned} k_{01-} &= -2.52089 \\ k_{01+} &= 2.52089 \end{aligned} \tag{6.5.1.28}$$

The eigenvalues corresponding to l_{01} are

$$\lambda_1 = -9.47394$$

$$\lambda_2 = -0.526064$$

$$\lambda_3 = -1.4165i$$

$$\lambda_4 = 1.4165i \tag{6.5.1.29}$$

The resulting normal form, separated as before, becomes

$$\frac{\partial A}{\partial T_2} = -0.091977A^3 + 0.37304Ak_2 \tag{6.5.1.30}$$

$$\frac{\partial \zeta}{\partial T_2} = 0.05915825A^2 - 0.455487k_2 \tag{6.5.1.31}$$

The non-zero fixed points of (6.5.1.30)

$$A_{2,3} = \pm\sqrt{4.055796557835111k_2} \tag{6.5.1.32}$$

giving the amplitude of the solution corresponding to the bifurcating periodic orbits are real for $k_2 > 0$, and the Jacobian of the (6.5.1.30) evaluated at $A_{2,3}$ is $-0.74608k_2 < 0$ for $k_2 > 0$ indicating that these fixed points are stable. Thus, the Hopf bifurcation at l_{01} is clearly supercritical, and we anticipate periodic behavior in the post-bifurcation regime.

Next we shall proceed to verify these predictions by actual numerical simulations, and also characterize the solutions by the use of numerical diagnostics.

6.5.2 Numerical Results

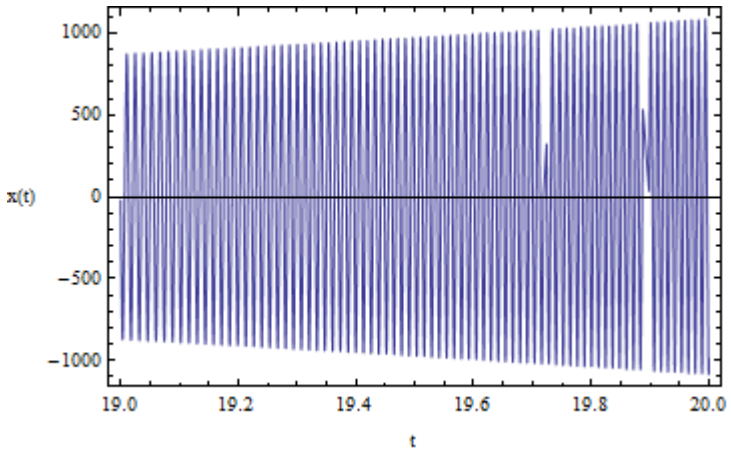

Figure 6.1: The function $x(t)$ versus time for equation 6.2.0.1 for $a = 1, b = 4, c = 2.2, d = 40, k = -11$. Note the aperiodic, intermittent, behavior.

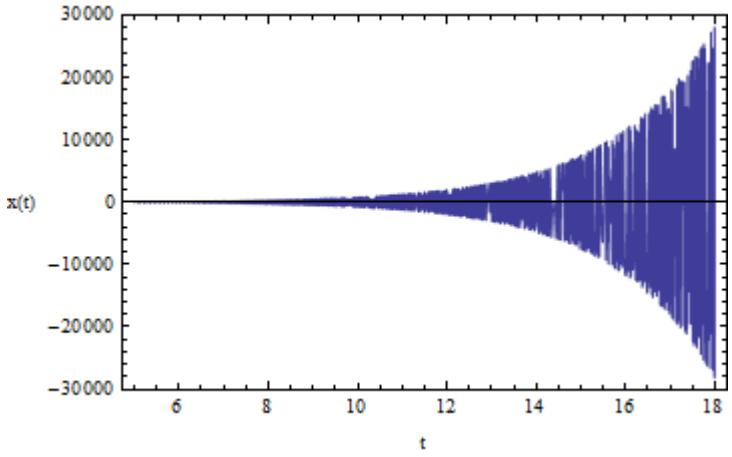

Figure 6.2: The function $x(t)$ versus time for equation 6.2.0.1 for $a = 1, b = 4.5, c = 3, d = 10, k = -17.85$.

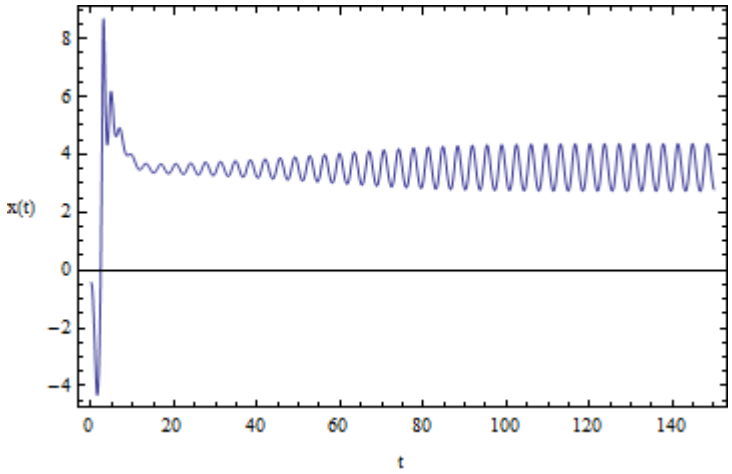

Figure 6.3: The function $x(t)$ versus time for equation 6.2.0.1 for $a = 2, b = 15, c = 2, d = 1, k = -3.5$. Note the stable periodic oscillations on the limit cycle

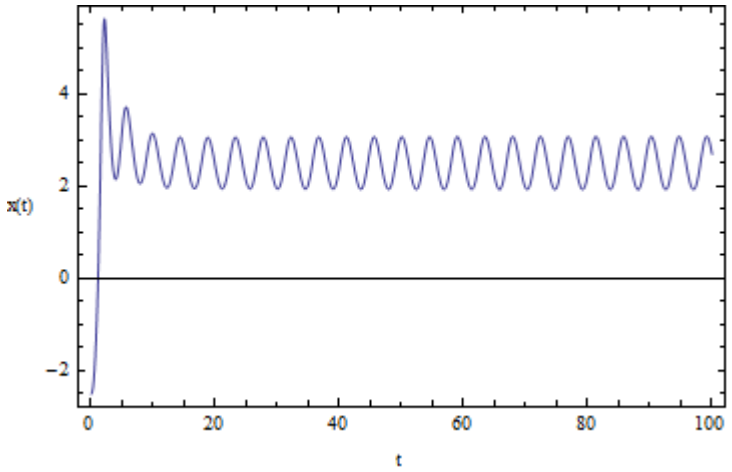

Figure 6.4: The function $x(t)$ versus time for equation 6.2.0.1 for $a = 1, b = 10, c = 1, d = 1, k = -2.48$. Note the stable periodic oscillations on the limit cycle

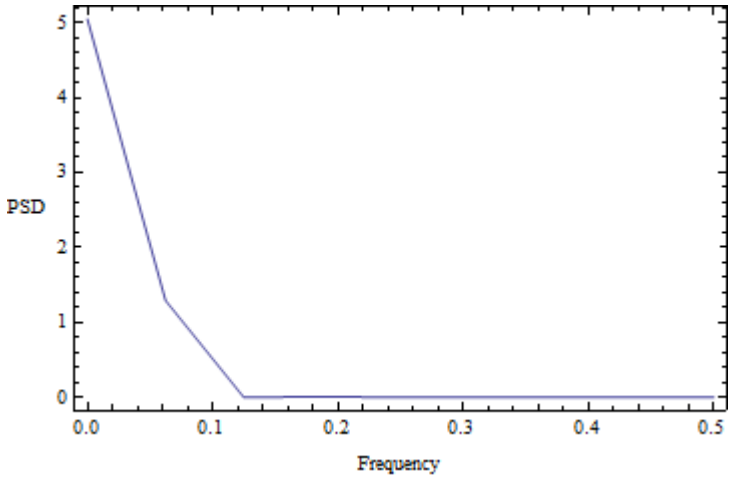

Figure 6.5: Power spectral density as a function of frequency of the numerical time-series of Fig. 6.1. Notice the apparently "broad" peak, indicative of randomness.

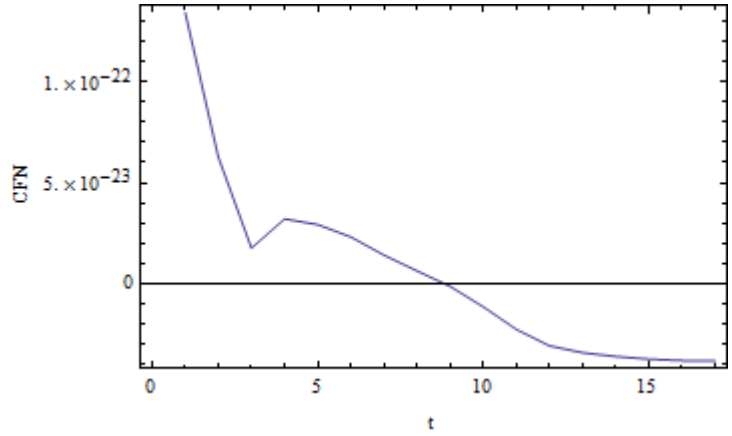

Figure 6.6: The auto-correlation function as a function of time of the numerical time-series of Fig. 6.1. Note the envelope of the oscillations gradually tending to zero. The first zero is at $t_c \sim 9$.

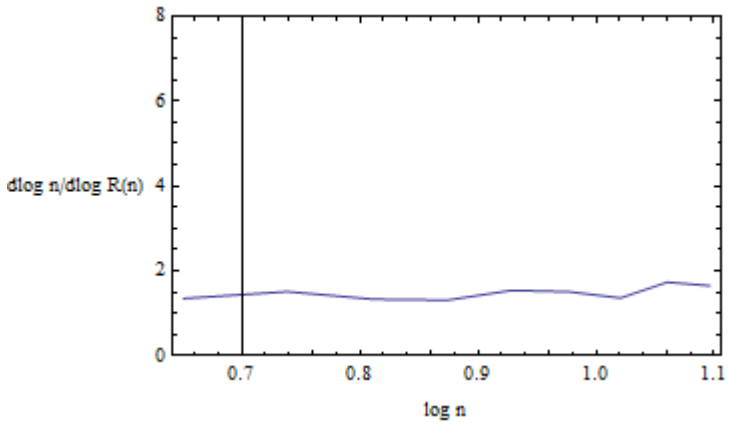

Figure 6.7: Plot of $d\log n/d\log R(n)$ versus $\log n$ from cluster dimension calculation for the numerical time series of Fig. 6.1. The embedding dimension is $E = 3$, and the delay is $\tau = t_c = 9$ of Fig. 6.6. The cluster dimension is approximately $D \approx 107$.

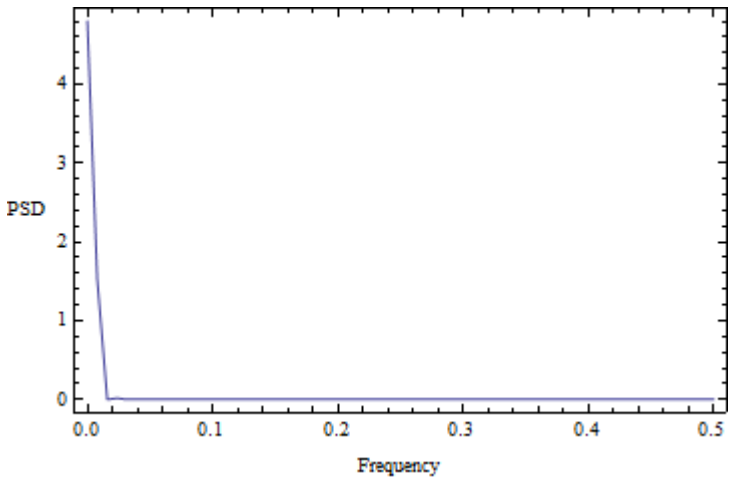

Figure 6.8: Power spectral density as a function of frequency of the numerical time-series of Fig. 6.3. Notice the single narrow peak indicative of periodicity.

The model is next integrated for the various parameter sets using an L-stable composite backward-Euler/trapezoidal rule scheme. The initial conditions are chosen to be close to the fixed point in each case. For the first set of parameters above $a = 1, b = 4, c = 2.2, d = 40, k = -11$, having chosen k_2 slightly negative as required in the normal form for a real periodic

orbit, the time behavior of x is shown in Figure 1. Note that, as anticipated and predicted by the normal form, there is no stable fixed point or limit cycle attractor and we first observe aperiodic behavior. In fact, the behavior is intermittent, with occasional chaotic bursts, as the orbits try to settle to the weakly unstable periodic attractor in the post-subcritical-Hopf regime, but are repelled and then re-injected by the weak dissipation in the system. However, not unexpectedly given the small negative value of the trace of the Jacobian matrix at the fixed point, the orbits eventually fly off to infinity (a finite-time, movable, initial-condition dependent singularity). Similar behavior occurs, as expected from the normal form predictions, for the second set of parameters $a = 1, b = 4.5, c = 3, d = 10, k = -17.85$ (once again choosing k_2 slightly negative as required in the normal form for a real periodic orbit). The time behavior of x is once again shown in Figure 6.2. Note that, as anticipated and predicted by the normal form, there is no stable fixed point or limit cycle attractor and we first observe aperiodic behavior. In fact, the behavior is again intermittent, with occasional chaotic bursts, as the orbits try to settle to the weakly unstable periodic attractor in the post-subcritical-Hopf regime, but are repelled and then re-injected by the weak dissipation in the system. However, not unexpectedly given the even smaller negative value of the trace of the Jacobian matrix at the fixed point (than for Fig. 6.1), the orbits eventually fly off to infinity (a finite-time, movable, initial-condition dependent singularity). For both the above cases, one could characterize the chaotic bursts in the pre-blow-up phase using diagnostics, such as power spectral density, fractal dimensions, or Lyapunov exponents [12, 52, 78]. However, the weak dissipation leading to relatively rapid blow-up makes the time-series in this phase

somewhat short, and hence the numerical diagnostics have greater error than in a genuine bounded chaotic regime. By contrast, Figures 6.3 and 6.4 show the periodic behavior on stable periodic orbits (limit cycles) in the post-supercritical regimes for the third and fourth parameter sets discussed above. This is in agreement with the normal form predictions in these cases. In conclusion, we have comprehensively analyzed the possible, standard local bifurcations of the fixed points of the modified Chen system in this work, as part of delineating its transition to the hyperchaotic regime. Future work will map out the remainder of the possible routes into the chaotic regimes, including: a. direct transition to bounded hyperchaos in post-subcritical Hopf regimes with strong dissipation, b. further bifurcations of the post-supercritical Hopf limit cycle attractors, c. double Hopf bifurcations, leading into periodic, two-period quasiperiodic, or aperiodic (bounded or unbounded) dynamics, and d. secondary bifurcations of two-periodic quasiperiodic attractors.

LIST OF REFERENCES

[1] Lauren Austin, Xiong Liu, and Qun Huo. An immunoassay for monomclonal antibody typing and quality analysis using gold nanoparticle probes and dynamic light scattering. *American Biotechnology Laboratory*, 28(3):8–12, March/April 2010.

[2] J.E. Bailey. Complex biology with no parameters. *Nature Biotechnology*, 19(6):503–504, 2001.

[3] Murad Banaji and Gheorghe Craciun. Graph-theoretic approaches to injectivity and multiple equilibria in systems of interacting elements. *Commun. Math. Sci.*, 7(4):867–900, 2009.

[4] Murad Banaji and Gheorghe Craciun. Graph-theoretic criteria for injectivity and unique equilibria in general chemical reaction systems. *Adv. in Appl. Math.*, 44(2):168–184, 2010.

[5] N. Barkai and S. Leibler. Robustness in simple biochemical networks. *Nature*, 387(6636):913–917, 1997.

[6] Anna Bigatti and Lorenzo Robbiano. Toric ideals. *Mat. Contemp.*, 21:1–25, 2001. 16th School of Algebra, Part II (Portuguese) (Brasília, 2000).

[7] S. Boccaletti, J. Kurths, G. Osipov, D.L. Valladares, and C.S. Zhou. The synchronization of chaotic systems. *Physics Reports*, 366(1-2):1–101, 2002.

[8] Joseph Brennan and Teng Chen. A stoichiometric model of the kinetics of nanoparticle clusterings mediated by antigen-antibody interactions. *Journal of Computational and Theoretical Nanoscience*, To appear.

[9] Richard A. Brualdi and Herbert J. Ryser. *Combinatorial matrix theory*, volume 39 of *Encyclopedia of Mathematics and its Applications*. Cambridge University Press, Cambridge, 1991.

[10] Madalena Cabral Ferreira Chaves. *Observer design for a class of nonlinear systems, with applications to biochemical networks*. ProQuest LLC, Ann Arbor, MI, 2003. Thesis (Ph.D.)–Rutgers The State University of New Jersey - New Brunswick.

[11] Teng Chen and Roy Choudhury. Bifurcations and Chaos in a Modied Driven Chens System. Submitted.

[12] S.Roy Choudhury. On bifurcations and chaos in predator-prey models with delay. *Chaos, Solitons and Fractals*, 2(4):393 – 409, 1992.

[13] B.L. Clarke. Complete set of steady states for the general stoichiometric dynamical system. *J. Chem. Phys.*, 75:4970, 1981.

[14] B.L. Clarke. Stoichiometric network analysis. *Cell Biochemistry and Biophysics*, 12(1):237–253, 1988.

[15] B.L. Clarke and W. Jiang. Method for deriving Hopf and saddle-node bifurcation hypersurfaces and application to a model of the Belousov–Zhabotinskii system. *J. Chem. Phys.*, 99:4464, 1993.

[16] Bruce L. Clarke. Stability of complex reaction networks. *Adv. Chem. Phys.*, 43, 1980.

[17] Bruce L. Clarke. Qualitative dynamics and stability of chemical reaction networks. In *Chemical applications of topology and graph theory (Athens, Ga., 1983)*, volume 28 of *Stud. Phys. Theoret. Chem.*, pages 322–357. Elsevier, Amsterdam, 1983.

[18] Miriam Colombo, Silvia Ronchi, Diego Monti, Fabio Corsi, Emilio Trabucchi, and Davide Prosperi. Femtomolar detection of autoantibodies by magnetic relaxation nanosensors. *Anal. Biochem.*, 392(1):96–102, Sep 1 2009.

[19] C. Conradi, D. Flockerzi, J. Raisch, and J. Stelling. Subnetwork analysis reveals dynamic features of complex (bio) chemical networks. *Proceedings of the National Academy of Sciences*, 104(49):19175, 2007.

[20] C. Conradi, J. Saez-Rodriguez, E. Gilles, and J. Raisch. Using chemical reaction network theory to discard a kinetic mechanism hypothesis. *Systems biology*, 152(4):243, 2005.

[21] Carsten Conradi, Dietrich Flockerzi, and Jörg Raisch. Multistationarity in the activation of a MAPK: parametrizing the relevant region in parameter space. *Math. Biosci.*, 211(1):105–131, 2008.

[22] A. Cornish-Bowden. *Fundamentals of enzyme kinetics*. Portland Press London, 2004.

[23] D. Cox, J. Little, and H. Schenck. Toric varieties. *American Mathematical Society*, 2011.

[24] David Cox. What is a toric variety? In *Topics in algebraic geometry and geometric modeling*, volume 334 of *Contemp. Math.*, pages 203–223. Amer. Math. Soc., Providence, RI, 2003.

[25] David Cox, John Little, and Donal O'Shea. *Ideals, varieties, and algorithms*. Undergraduate Texts in Mathematics. Springer, New York, third edition, 2007. An introduction to computational algebraic geometry and commutative algebra.

[26] David A. Cox, John Little, and Donal O'Shea. *Using algebraic geometry*, volume 185 of *Graduate Texts in Mathematics*. Springer, New York, second edition, 2005.

[27] Gheorghe Craciun, Alicia Dickenstein, Anne Shiu, and Bernd Sturmfels. Toric dynamical systems. *J. Symbolic Comput.*, 44(11):1551–1565, 2009.

[28] Gheorghe Craciun and Martin Feinberg. Multiple equilibria in complex chemical reaction networks. II. The species-reaction graph. *SIAM J. Appl. Math.*, 66(4):1321–1338, 2006.

[29] Gheorghe Craciun, J. William Helton, and Ruth J. Williams. Homotopy methods for counting reaction network equilibria. *Math. Biosci.*, 216(2):140–149, 2008.

[30] S.G. Dan, G. Erich, and S. Gregory. The capacity for multistability in small gene regulatory networks. *BMC Systems Biology*, 3.

[31] Phillipp Raymond Ellison. *The advanced deficiency algorithm and its applications to mechanism discrimination*. ProQuest LLC, Ann Arbor, MI, 1998. Thesis (Ph.D.)–University of Rochester.

[32] P. Érdi and J. Tóth. *Mathematical models of chemical reactions*. Nonlinear Science: Theory and Applications. Princeton University Press, Princeton, NJ, 1989.

[33] M. Feinberg. Chemical reaction network structure and the stability of complex isothermal reactors–I. The deficiency zero and deficiency one theorems. *Chemical Engineering Science*, 42(10):2229–2268, 1987.

[34] Martin Feinberg. On chemical kinetics of a certain class. *Arch. Rational Mech. Anal.*, 46:1–41, 1972.

[35] Martin Feinberg. Complex balancing in general kinetic systems. *Arch. Rational Mech. Anal.*, 49:187–194, 1972/73.

[36] Martin Feinberg. Lectures on chemical reaction networks. 1979. `http://www.che.eng.ohio-state.edu/~FEINBERG/LecturesOnReactionNetworks/`.

[37] Martin Feinberg. Chemical oscillations, multiple equilibria, and reaction network structure. In *Dynamics and modelling of reactive systems (Proc. Adv. Sem., Math. Res. Center, Univ. Wisconsin, Madison, Wis., 1979)*, volume 44 of *Publ. Math. Res. Center Univ. Wisconsin*, pages 59–130. Academic Press, New York, 1980.

[38] Martin Feinberg. Some recent results in chemical reaction network theory. In *Patterns and dynamics in reactive media (Minneapolis, MN, 1989)*, volume 37 of *IMA Vol. Math. Appl.*, pages 43–70. Springer, New York, 1991.

[39] Martin Feinberg. The existence and uniqueness of steady states for a class of chemical reaction networks. *Arch. Rational Mech. Anal.*, 132(4):311–370, 1995.

[40] Martin Feinberg. Multiple steady states for chemical reaction networks of deficiency one. *Arch. Rational. Mech. Anal.*, 132(4):371–406, 1995.

[41] Martin Feinberg and F. J. M. Horn. Chemical mechanism structure and the coincidence of the stoichiometric and kinetic subspaces. *Arch. Rational. Mech. Anal.*, 66(1):83–97, 1977.

[42] F.Horn and R.Jackson. General mass action kinetics. *Arch. Rational. Mech. Anal.*, 47(2), 1972.

[43] R.J. Field and H.D. Foersterling. On the oxybromine chemistry rate constants with cerium ions in the Field-Koeroes-Noyes mechanism of the Belousov-Zhabotinskii reaction: the equilibrium HBrO2+ BrO3-+ H+. dblharw. 2BrO. ovrhdot. 2+ H2O'. *J. Phys. Chem.*, 90(21):5400–5407, 1986.

[44] R.J. Field, E. Koros, and R.M. Noyes. Oscillations in chemical systems. II. Thorough analysis of temporal oscillation in the bromate-cerium-malonic acid system. *Journal of the American Chemical Society*, 94(25):8649–8664, 1972.

[45] William Fulton. *Introduction to toric varieties*, volume 131 of *Annals of Mathematics Studies*. Princeton University Press, Princeton, NJ, 1993. The William H. Roever Lectures in Geometry.

[46] T. Gao, Z. Chen, Z. Yuan, and G. Chen. A hyperchaos generated from Chen's system. *International Journal of Modern Physics C*, 17:471–478, 2006.

[47] Karin Gatermann. Counting stable solutions of sparse polynomial systems in chemistry. In *Symbolic computation: solving equations in algebra, geometry,and engineering (South Hadley, MA, 2000)*, volume 286 of *Contemp. Math.*, pages 53–69. Amer. Math. Soc., Providence, RI, 2001.

[48] Karin Gatermann, Markus Eiswirth, and Anke Sensse. Toric ideals and graph theory to analyze Hopf bifurcations in mass action systems. *J. Symbolic Comput.*, 40(6):1361–1382, 2005.

[49] Karin Gatermann and Birkett Huber. A family of sparse polynomial systems arising in chemical reaction systems. *J. Symbolic Comput.*, 33(3):275–305, 2002.

[50] Karin Gatermann and Matthias Wolfrum. Bernstein's second theorem and Viro's method for sparse polynomial systems in chemistry. *Adv. in Appl. Math.*, 34(2):252–294, 2005.

[51] Ewgenij Gawrilow and Michael Joswig. polymake: a framework for analyzing convex polytopes. In Gil Kalai and Günter M. Ziegler, editors, *Polytopes — Combinatorics and Computation*, pages 43–74. Birkhäuser, 2000.

[52] P. Glendinning. *Stability, instability, and chaos: An introduction to the theory of nonlinear differential equations*. Cambridge Univ Pr, 1994.

[53] Martin Golubitsky and David G. Schaeffer. *Singularities and groups in bifurcation theory. Vol. I*, volume 51 of *Applied Mathematical Sciences*. Springer-Verlag, New York, 1985.

[54] Martin Golubitsky, Ian Stewart, and David G. Schaeffer. *Singularities and groups in bifurcation theory. Vol. II*, volume 69 of *Applied Mathematical Sciences*. Springer-Verlag, New York, 1988.

[55] Robert Gross, Martin L. Yarmush, John W. Kennedy, and Louis V. Quintas. Antigenesis: a cascade-theoretical analysis of the size distributions of antigen-antibody complexes. *Discrete Appl. Math.*, 19(1-3):177–194, 1988. Applications of graphs in chemistry and physics.

[56] John Guckenheimer and Philip Holmes. *Nonlinear oscillations, dynamical systems, and bifurcations of vector fields*, volume 42 of *Applied Mathematical Sciences*. Springer-Verlag, New York, 1990. Revised and corrected reprint of the 1983 original.

[57] John Guckenheimer and Mark Myers. Computing Hopf bifurcations. II. Three examples from neurophysiology. *SIAM J. Sci. Comput.*, 17(6):1275–1301, 1996.

[58] John Guckenheimer, Mark Myers, and Bernd Sturmfels. Computing Hopf bifurcations. I. *SIAM J. Numer. Anal.*, 34(1):1–21, 1997.

[59] Hilde Hans, Xiong Liu, Guido Maes, and Qun Huo. Dynamic light scattering as a powerful tool for gold nanoparticle bioconjugation and biomolecular binding studies. *Anal. Chem.*, 81(22):9425–9432, November 2009.

[60] Hiram E. Hart and Ki-Chuen Chak. Theory of antigen-antibody induced particulate aggregation. I. General assumptions and basic theory. *Bull. Math. Biol.*, 42(1):17–36, 1980.

[61] Hiram E. Hart and Ki-Chuen Chak. Theory of antigen-antibody induced particulate aggregation. II. Theoretical analysis and comparison with experimental results. *Bull. Math. Biol.*, 42(1):37–56, 1980.

[62] Jered B. Haun, Tae-Jong Yoon, Hakho Lee, and Ralph Weissleder. Magnetic nanoparticle biosensors. *Wiley interdisciplinary reviews. Nanomedicine and nanobiotechnology*, 2(3):291–304, May-June 2010.

[63] F. Horn. Necessary and sufficient conditions for complex balancing in chemical kinetics. *Arch. Rational Mech. Anal.*, 49:172–186, 1972/73.

[64] F. Horn. On a connexion between stability and graphs in chemical kinetics. I. Stability and the reaction diagram. *Proc. Roy. Soc. (London) Ser. A*, 334:299–312, 1973.

[65] F. Horn. Stability and complex balancing in mass-action systems with three short complexes. *Proc. Roy. Soc. (London) Ser. A*, 334:331–342, 1973.

[66] F. Horn. The dynamics of open reaction systems. In *Mathematical aspects of chemical and biochemical problems and quantum chemistry (Proc. SIAM-AMS Sympos. Appl. Math., New York, 1974)*, pages 125–137. SIAM–AMS Proceedings, Vol. VIII. Amer. Math. Soc., Providence, R.I., 1974.

[67] Birkett Huber and Bernd Sturmfels. A polyhedral method for solving sparse polynomial systems. *Math. Comp.*, 64(212):1541–1555, 1995.

[68] Nathan Jacobson. *Basic algebra. I.* Dover Publications, Mineola, NY, second edition, 2009.

[69] Isaac Koh, Rid Hong, Ralph Weissleder, and Lee Josephson. Sensitive NMR sensors detect antibodies to influenza. *Angew. Chem. Int. Ed.*, 47(22):4119–4121, 2008.

[70] Isaac Koh, Rui Hong, Ralph Weissleder, and Lee Josephson. Nanoparticle-Target Interactions Parallel Antibody-Protein Interactions. *Anal. Chem.*, 81(9):3618–3622, May 1 2009.

[71] Isaac Koh and Lee Josephson. Magnetic Nanoparticle Sensors. *Sensors*, 9(10):8130–8145, Oct. 2009.

[72] Chuandong Li, Qi Chen, and Tingwen Huang. Coexistence of anti-phase and complete synchronization in coupled Chen system via a single variable. *Chaos, Solitons and Fractals*, 38(2):461 – 464, 2008.

[73] Chuandong Li, Xiaofeng Liao, and Kwok-wo Wong. Lag synchronization of hyperchaos with application to secure communications. *Chaos Solitons and Fractals*, 23(1):183–193, 2005.

[74] Xiong Liu and Qun Huo. A washing-free and amplification-free one-step homogeneous assay for protein detection using gold nanoparticle probes and dynamic light scattering. *Journal of Immunological Methods*, 349(1-2):38–44, September 2009.

[75] M. Mazzotti, M. Morbidelli, and G. Serravalle. Bifurcation analysis of the Oregonator model in the 3-D space bromate/malonic acid/stoichiometric coefficient. *The Journal of Physical Chemistry*, 99(13):4501–4511, 1995.

[76] H. Melenk, H.M. Möller, and W. Neun. *On Gröbner bases computation on a supercomputer using REDUCE.* Citeseer, 1988.

[77] L. Michaelis and M. L. Menten. Die kinetik der invertinwirkung. *Biochem. Z*, 49(333-369):352, 1913.

[78] A.H. Nayfeh and B. Balachandran. *Applied nonlinear dynamics*, volume 2. Wiley Online Library, 1995.

[79] Lior Pachter and Bernd Sturmfels, editors. *Algebraic statistics for computational biology*. Cambridge University Press, New York, 2005.

[80] Louis M. Pecora and Thomas L. Carroll. Synchronization in chaotic systems. *Phys. Rev. Lett.*, 64(8):821–824, Feb 1990.

[81] K. Pyragas. Weak and strong synchronization of chaos. *Phys. Rev. E*, 54(5):R4508–R4511, Nov 1996.

[82] J. Reidl, P. Borowski, A. Sensse, J. Starke, M. Zapotocky, and M. Eiswirth. Model of calcium oscillations due to negative feedback in olfactory cilia. *Biophysical journal*, 90(4):1147–1155, 2006.

[83] Michael G. Rosenblum, Arkady S. Pikovsky, and Jürgen Kurths. Phase synchronization of chaotic oscillators. *Phys. Rev. Lett.*, 76(11):1804–1807, Mar 1996.

[84] S. Schuster, S. Klamt, W. Weckwerth, F. Moldenhauer, and T. Pfeiffer. Use of network analysis of metabolic systems in bioengineering. *Bioprocess and Biosystems Engineering*, 24(6):363–372, 2002.

[85] A. Sensse and M. Eiswirth. Feedback loops for chaos in activator-inhibitor systems. *J. Chem. Phys.*, 122:044516, 2005.

[86] A. Sensse, M.J.B. Hauser, and M. Eiswirth. Feedback loops for Shilnikov chaos: The peroxidase-oxidase reaction. *J. Chem. Phys.*, 125:014901, 2006.

[87] L. D. Shiau. A systematic analysis of average molecular weights and gelation conditions for branched immune complexes: The interaction between a multivalent antigen with distinct epitopes and many different types of bivalent antibodies. *Journal of Immunological Methods*, 178(2):267–275, January 1995.

[88] L. D. Shiau. A systematic analysis of average molecular weights and gelation conditions for branched immune complexes: The interaction between a multivalent antigen with distinct epitopes and many different types of bivalent antibodies. *Biopolymers*, 39(3):445–454, September 1996.

[89] Anne Shiu. *Algebraic methods for biochemical reaction network theory*. Dissertation, University of California,Berkeley, 2010.

[90] Silicon Kinetics. Kinetic characterization of antibody/antigen interactions. http://www.siliconkinetics.com/pages/pdf%20files/application_notes/08Antibody%20Characterization.pdf.

[91] Eduardo D. Sontag. Structure and stability of certain chemical networks and applications to the kinetic proofreading model of T-cell receptor signal transduction. *IEEE Trans. Automat. Control*, 46(7):1028–1047, 2001.

[92] Bernd Sturmfels. *Gröbner bases and convex polytopes*, volume 8 of *University Lecture Series*. American Mathematical Society, Providence, RI, 1996.

[93] Bernd Sturmfels. *Solving systems of polynomial equations*, volume 97 of *CBMS Regional Conference Series in Mathematics*. Published for the Conference Board of the Mathematical Sciences, Washington, DC, 2002.

[94] William J. Terrell. *Stability and stabilization*. Princeton University Press, Princeton, NJ, 2009. An introduction.

[95] M. Thomson and J. Gunawardena. Unlimited multistability in multisite phosphorylation systems. *Nature*, 460(7252):274–277, 2009.

[96] John J. Tyson. "oscillations, bistability, and echo waves in models of the belousov-zhabotinskii reaction". *Ann. N.Y. Acad. Sci.*, 1979.

[97] P. Waage and CM Gulberg. Studies concerning affinity. *J. Chem. Educ.*, 63(12):1044, 1986.

[98] A.T. Winfree. The prehistory of the Belousov-Zhabotinsky oscillator. *J. Chem. Educ.*, 61(8):661, 1984.

[99] Wolfram Research, Inc. Mathematica edition: Version 7.0.

[100] H. Xiang and G. Li. A constructional method for generalized synchronization of coupled time-delay chaotic systems. *Chaos, Solitons and Fractals*, 41(4):1849–1853, 2009.

[101] Ping Zhang and Hai-Jun Wang. Monte carlo simulation on growth of antibody-antigen complexes: the role of unequal activity. *Chin. Phys. Lett.*, 27(3):038701–1–038701–5, 2010.

[102] Ping Zhang and Hai-Jun Wang. Statistics and thermodynamics in the growth of antigen-antibody complexes. *Chinese J. Physics*, 48(2):277–293, 2010.

[103] W. Zhu, D. Xu, and Y. Huang. Global impulsive exponential synchronization of time-delayed coupled chaotic systems. *Chaos, Solitons and Fractals*, 35(5):904–912, 2008.